

Investigating the protein quality control pathways that prevent protein aggregation in the social amoeba *Dictyostelium discoideum*.

by

Holly Noelle Haver

Department of Molecular Genetics and Microbiology  
Duke University

Date: \_\_\_\_\_

Approved:

\_\_\_\_\_  
Matthew Scaglione, Supervisor

\_\_\_\_\_  
Douglas Marchuk

\_\_\_\_\_  
Beth Sullivan

\_\_\_\_\_  
Dennis Ko

\_\_\_\_\_  
Laurie Sanders

Dissertation submitted in partial fulfillment of the requirements  
for the degree of Doctor of Philosophy in the Department of Molecular  
Genetics and Microbiology in the Graduate School of Duke University

2023

ABSTRACT

Investigating the protein quality control pathways that prevent protein aggregation in the social amoeba *Dictyostelium discoideum*.

by

Holly Noelle Haver

Department of Molecular Genetics and Microbiology  
Duke University

Date: \_\_\_\_\_

Approved:

\_\_\_\_\_  
Matthew Scaglione, Supervisor

\_\_\_\_\_  
Douglas Marchuk

\_\_\_\_\_  
Beth Sullivan

\_\_\_\_\_  
Dennis Ko

\_\_\_\_\_  
Laurie Sanders

An abstract of a dissertation submitted in partial fulfillment of the requirements for the degree of Doctor of Philosophy in the Department of Molecular Genetics and Microbiology in the Graduate School of Duke University

2023

Copyright by  
Holly Noelle Haver  
2023

## Abstract

A major hallmark of many neurodegenerative diseases is protein aggregation. Protein aggregation occurs in part due to failure of protein quality control pathways. A better understanding of these pathways could allow us to improve therapies to help control protein aggregation. Here, I investigated molecular chaperones of the social amoeba, *Dictyostelium discoideum*, an organism resistant to polyglutamine (polyQ) protein aggregation and whose proteostasis pathways have not been intensively studied. Serine-rich chaperone protein 1 (SRCP1), a *Dictyostelium*-specific chaperone, was previously found to prevent aggregation of exon 1 of the mutant huntingtin protein (Htt) in both *Dictyostelium* and human cells. I discovered that a region within its C-terminus, residues 61-80 (SRCP1<sup>61-80</sup>), were sufficient to suppress Htt aggregation *in vitro* and in human cells. While I was unable to purify recombinant protein for structural studies, we utilized computational and experimental approaches to show that SRCP1 is predicted to be a mainly disordered protein with residues 61-80 structured in a  $\beta$ -hairpin conformation. Additionally, I found that a peptide of residues 61-70 were the minimal sequence required for SRCP1 to suppress aggregation, and a tandem repeat peptide of this sequence increased its potency. Kinetic analysis revealed that SRCP1<sup>61-80</sup> inhibits aggregation of mutant Htt at the secondary nucleation step, and I demonstrated that SRCP1<sup>61-80</sup> does not inhibit pure polyglutamine (polyQ) aggregation, suggesting it interacts with another part

of the Htt protein. Finally, I show that SRCP1<sup>61-80</sup> is also sufficient to suppress aggregation of another polyQ protein, mutant ataxin-3, confirming that SRCP1<sup>61-80</sup> can generally inhibit aggregation. Together, these data give a clearer image of both SRCP1's structure and function and could help develop therapies for neurodegenerative diseases.

Another *Dictyostelium* protein proposed to prevent polyQ aggregation is heat shock protein 101 (Hsp101). Hsp101 was previously shown to act as a protein disaggregase of heat-induced polyQ foci. To further investigate Hsp101 as a polyQ disaggregase, I generated Hsp101 knockout *Dictyostelium* strains and found that Hsp101 knockout did not cause the accumulation of mutant Htt or prion aggregates under heat stress, suggesting that Hsp101 does not regulate protein aggregation. I instead turned to determine the biological role of Hsp101 in *Dictyostelium*. I showed that the only Hsp101 knockout phenotype was an axenic growth defect, which could be rescued by Hsp101 overexpression. I also used mass spectrometry of Hsp101 pulldowns to reveal high fold enrichments for proteins involved in the Skp1-Cullin-F-box (SCF) ubiquitin ligase pathway. These results suggest that Hsp101 may play a role in the SCF pathway, and could uncover novel roles for Hsp100-type chaperones.

# Contents

Abstract .....	iv
List of Tables .....	ix
List of Figures .....	x
List of Abbreviations .....	xiii
Acknowledgements .....	xvi
1. Introduction .....	1
1.1 Protein aggregation in neurodegenerative diseases .....	1
1.2 The protein quality control network and the role of molecular chaperones .....	3
1.3 Dictyostelium discoideum as a model organism for neurodegenerative diseases .....	7
1.3.1 <i>Dictyostelium</i> as a model for Alzheimer's disease .....	9
1.3.2 <i>Dictyostelium</i> as a model for Parkinson's disease .....	11
1.3.3 <i>Dictyostelium</i> as a model for polyQ diseases .....	13
1.4 The Dictyostelium-specific chaperone serine-rich chaperone protein 1 .....	16
1.5 Research objectives .....	17
2. A C-terminal region of SRCP1 suppresses polyglutamine aggregation .....	20
2.1 A peptide of SRCP1 is sufficient to suppress polyQ aggregation in vitro .....	23
2.2 Discussion .....	27
2.3 Materials and Methods .....	28
3. Elucidating structural properties and mechanisms of SRCP1 .....	32
3.1 Recombinant SRCP1 is insoluble and cannot be purified .....	33

3.1.1 <i>Dictyostelium</i> purification method.....	34
3.1.2 Bacterial purification method .....	35
3.1.3 Cell-free purification method .....	38
3.1.4 Insect cell purification method .....	40
3.2 Mechanistic insight into the suppression of polyglutamine aggregation by SRCP1 .....	44
3.2.1 Generating a structural model of SRCP1. ....	44
3.2.2 Experimental evaluation and selection of SRCP1 models. ....	48
3.2.3 SRCP1 <sup>61-70</sup> is the minimal sequence necessary for function. ....	53
3.2.4 SRCP1 <sup>61-80</sup> inhibits secondary nucleation of Htt <sup>ex1Q46</sup> and inhibits aggregation independent of the polyQ region. ....	56
3.2.5 SRCP1 <sup>61-80</sup> is sufficient to suppress polyQ aggregation in human cells .....	62
3.2.6 SRCP1 <sup>61-80</sup> suppresses aggregation of another polyQ protein, ataxin-3 <sup>Q55</sup> . ....	63
3.3 Discussion.....	64
3.4 Materials and Methods .....	69
4. Determining the biological function of the <i>Dictyostelium</i> disaggregase Hsp101 .....	82
4.1 Characterization of <i>Dictyostelium</i> Hsp101 knockout cells.....	86
4.2 Hsp101 does not act as a disaggregase in <i>Dictyostelium</i> 's heat stress response...	90
4.3 Hsp101 is linked to many cellular pathways in <i>Dictyostelium</i> .....	92
4.4 Discussion.....	93
4.5 Materials and Methods .....	97
5. Conclusion .....	107
5.1 Determining the role of other SRCP1 domains and SRCP1-like proteins .....	108

5.2 Elucidating Hsp101's function as an ATPase and a chaperone .....	111
5.2 Conclusions .....	113
Appendix – Contributions to other projects.....	115
References .....	120
Biography.....	152

## List of Tables

Table 1: <i>in silico</i> mutagenesis scanning predicted mutants and Rosetta score change prediction. ....	48
Table 2: Modified peptides of SRCP1 <sup>61-70</sup> or SRCP1 <sup>61-80</sup> tested in polyQ aggregation assays. ....	54
Table 3: Primers used for sgRNA cloning into pTM1285.....	98
Table 4: Primers used for screening of indel generation by CRISPR-Cas9 .....	100
Table 5: SRCP1-like genes are upregulated during development. ....	111

## List of Figures

Figure 1: Schematic of the protein aggregation process.....	2
Figure 2: Description of the protein quality control network.....	4
Figure 3: <i>Dictyostelium's</i> developmental cycle.....	8
Figure 4: <i>Dictyostelium</i> is naturally resistant to aggregation from a human pathogenic polyQ protein. ....	15
Figure 5: SRCP1 knockout causes <sup>GFP</sup> Htt <sup>ex1Q103</sup> aggregation in <i>Dictyostelium</i> . ....	16
Figure 6: SRCP1's C-terminus contains a region predicted to form amyloid. ....	20
Figure 7: Amino acids 61–70 are essential for suppressing <sup>GFP</sup> Htt <sup>ex1Q74</sup> aggregation. ....	21
Figure 8: Amino acids V65 and I69 are essential for suppressing <sup>GFP</sup> Htt <sup>ex1Q74</sup> aggregation. ....	22
Figure 9: A peptide of SRCP1's C-terminal domain suppresses huntingtin aggregation <i>in vitro</i> .....	24
Figure 10: SRCP1 peptide delays but does not prevent Htt <sup>Q46</sup> aggregation. ....	26
Figure 11: A peptide mimicking SRCP1 <sup>61-70</sup> suppresses polyQ aggregation. ....	27
Figure 12: SRCP1 is not pulled down from <i>Dictyostelium</i> lysates. ....	34
Figure 13: <sup>6xHis</sup> SRCP1 <sup>SUMO</sup> is insoluble in <i>E. coli</i> . ....	36
Figure 14: GST-SRCP1 is insoluble in <i>E. coli</i> .....	37
Figure 15: Buffer additives do not increase solubility of <sup>GST</sup> SRCP1. ....	38
Figure 16: SRCP1 does not express in a cell-free <i>E. coli</i> system.....	39
Figure 17: SRCP1-like proteins can be expressed in SF9 cells. ....	40
Figure 18: Sequence alignment of SRCP1 and SRCP1-like proteins. ....	41
Figure 19: GST-H3c-SRCP1-like proteins express in SF9 cells.....	41

Figure 20: GST-H3c-SRCPB is unable to bind to beads due to competing GBPs.....	42
Figure 21: 6x-His-GST-H3c-SRCP1-like proteins express in SF9 cells. ....	43
Figure 22: 6x-His-GST-H3c-SRCP1 is insoluble under denaturing conditions.....	43
Figure 23: AlphaFold predicts SRCP1 structure with low confidence. ....	45
Figure 24: A C-terminal region of SRCP1 is predicted to be structured and have a propensity to self-aggregate. ....	45
Figure 25: Computational modeling of SRCP1 predicts a largely disordered N-terminal region and a $\beta$ -sheet rich C-terminal region. ....	46
Figure 26: SRCP1 models are predicted to form a $\beta$ -hairpin at residues 61-80.....	47
Figure 27: Experimental evaluation of the SRCP1 model. ....	50
Figure 28: NMR analysis of SRCP1 <sup>61-80</sup> .....	52
Figure 29: Amino acids 61-70 are the minimal sequence required for SRCP1 peptide function.....	55
Figure 30: SRCP1 inhibits the secondary nucleation pathway of Htt <sup>ex1Q46</sup> aggregation....	58
Figure 31: SRCP1 <sup>61-80</sup> inhibits huntingtin but not polyQ aggregation.....	59
Figure 32: SRCP1 <sup>61-80</sup> does not disaggregate pre-formed Htt <sup>ex146Q</sup> fibrils.....	60
Figure 33: A truncated form of SRCP1 is sufficient to suppress polyglutamine aggregation in human cells.....	61
Figure 34: SRCP1 <sup>61-80</sup> suppresses aggregation of recombinant ataxin-3 <sup>Q55</sup> . ....	63
Figure 35: Comparison of yeast Hsp104 and <i>Dictyostelium</i> Hsp101. ....	83
Figure 36: Hsp101 knockout cells have an axenic growth defect.....	88
Figure 37: Overexpression of Hsp101 rescues the axenic growth defect. ....	89
Figure 38: Polyglutamine does not aggregate in Hsp101 KO cells, but eRF3 forms SDS-insoluble aggregates in WT and Hsp101 KO cells. ....	91

Figure 39: Hsp101 is associated with components of the SCF E3 ubiquitin ligase pathway.....	93
Figure 40: Increased concentrations of an E2 ubiquitinating enzyme and substrate bypasses the need for and E3 ubiquitin ligase for <i>in vitro</i> ubiquitination assays. ....	116
Figure 41: Ube2w and UbcH5 retain substrate residue selectivity in the absence of CHIP. ....	117
Figure 42: UbcH5, but not other E2s, ubiquitinates the JD of ATXN3 in the absence of CHIP. ....	118

## List of Abbreviations

A $\beta$	Amyloid- $\beta$ protein
AD	Alzheimer's disease
ALS	Amyotrophic Lateral Sclerosis
APP	Amyloid precursor protein
ATXN3	Ataxin-3
Cas9	CRISPR-associated protein 9
CRISPR	Clustered regularly interspaced short palindromic repeats
CTD	C-terminal domain
DLS	Dynamic light scattering
GFP	Green fluorescent protein
GST	Glutathione-S-transferase
h	Hour(s)
H3c	Human Rhinovirus (HRV) 3C Protease
HEK293	Human embryonic kidney 293 cells
His	Histidine
Hsp	Heat-shock protein
Htt	Huntingtin
IPTG	Isopropyl- $\beta$ -D-1-thiogalactopyranoside

kDa	Kilodalton
KO	Knockout
LRRK2	Leucine-rich repeat kinase 2
M	Molar
MD	Middle domain
min	Minute(s)
mL	Milliliter
mM	Millimolar
$\mu$ L	Microliter
$\mu$ M	Micromolar
NBD	Nucleotide binding domain
ns	Nanosecond
NTD	N-terminal domain
PAM	Protospacer adjacent motif
PD	Parkinson's disease
PolyQ	Polyglutamine
PQC	Protein quality control
PSEN	Presenilin
RFP	Red fluorescent protein
s	Second

SCF	Skp1-Cullin-F-box
sgRNA	small guide RNA
SRCP1	Serine-rich chaperone protein 1
SRCPB	SRCP1-like protein B
SRCP C	SRCP1-like protein C
TEM	Transmission electron microscopy
ThT	Thioflavin-T
UPS	Ubiquitin-proteasome system
WT	Wildtype

## Acknowledgements

First and foremost, I want to thank the Scaglione lab. Thanks to Matt Scaglione for all the mentorship and support you have provided me over the years. Thanks to my senior students, Adam Kanack and Stephanie Santarriaga for your mentorship and friendship when I was just starting graduate school. Thanks to Jamie Scaglione, Madeline Brunner, and Samantha Chou for helping me survive the move to Duke, and to the current lab members for your friendship and support: Ran Ming, Felicia Williams, Anna Umamo, Ryan Rodriguez, Graham Wallace, Kanasha Travis, and Yumei Wu.

I want to thank my thesis committee: Doug Marchuk, Beth Sullivan, Dennis Ko, and Laurie Sanders, for their mentorship and constructive feedback on my projects over the years and for the support they have offered.

I need to thank important people from the very beginning of my graduate school journey from the Medical College of Wisconsin: Julie Arthur, Austin Schoen, and other administration from the graduate school and Biochemistry Department for being supportive in my first year of graduate education; and also John Corbett and Daisy Sahoo, who continue to offer me mentorship.

I also want to thank everyone who helped me with my science along this journey. Thanks to Clive Wells at the Medical College of Wisconsin for performing transmission electron microscopy for me. I also want to thank the Volkman lab, especially Mike

Wedemeyer, for collaborating with me on the SRCP1 project and helping out with the computational modeling. I truly appreciate all the effort you put into this project over the years. Thank you to Francis Peterson and Brian Volkman as well for performing and analyzing NMR spectra of the SRCP1 peptide. I also want to acknowledge Duke Shared Materials and Instrumentation Facilities (SMIF) for use of their sample preparation lab, chemicals, and transmission electron microscope. Thank you to the Duke Proteomics and Metabolomics Core Facility and Eric Soderblom for performing and analyzing Hsp101 knockout samples.

Lastly I need to thank my amazing support network: my parents, Andy and Deanna, for encouraging me through the good and the difficult times; my siblings, Natalie, Heidi, and Mitchell, for keeping me loving and laughing through this process; my aunts, uncles, cousins, and grandparents for their interest and support throughout the years; my many friends including Jamie, Johann, Megan, Jacob, Caroline, and Kelly, who I left behind in the Midwest, and who have endlessly supported me and been so empathetic; my friend Akshay, who I met in the lab next door at Duke and who gave me friendship when I needed it most; and finally the two most important beings in my life, my dog Arlo and my boyfriend James, for the unconditional love and support even when I was struggling the most. I love you all and would not be writing this document if it hadn't been for you!

# 1. Introduction

## *1.1 Protein aggregation in neurodegenerative diseases*

Neurodegenerative diseases are debilitating disorders characterized by neuronal dysfunction and degeneration. They arise by either sporadic or genetic causes, affect different types of neurons, and present with diverse pathology. One major hallmark of many neurodegenerative diseases is protein aggregation, which presents in Alzheimer's disease (AD), Parkinson's disease (PD), amyotrophic lateral sclerosis (ALS), the polyglutamine (polyQ) diseases, and others (Ross & Poirier, 2004). In these diseases, specific proteins misfold to have toxic  $\beta$ -sheet-rich conformations called amyloid (Ross & Poirier, 2004). Amyloid conformations tend to be glycine rich and highly hydrophobic, allowing amyloidogenic proteins to easily accumulate into soluble oligomers that eventually become large, insoluble aggregates (Figure 1) (Kelly, 1996, 1997; Sunde et al., 1997; Wetzel, 1994). The current theory is that the toxic species are the soluble oligomers while the larger aggregates seem to be more stable and protective, but there is still a lack of evidence to support this theory (Arrasate et al., 2004; Cascella et al., 2022; Cecchi & Stefani, 2013; Diogenes et al., 2012; Karpinar et al., 2009; Winner et al., 2011). It is known, however, that the process of aggregation does play a role in disease pathogenesis (Klein et al., 2001; Lambert et al., 1998; Lue et al., 1999; McLean et al., 2001; Poirier et al., 2002; Sanchez et al., 2003; Terry et al., 1991; Volles et al., 2001; Walsh et al., 2002).

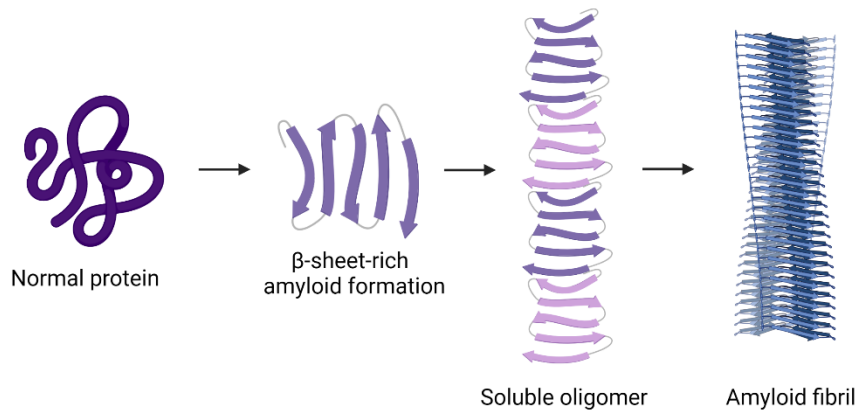


**Figure 1: Schematic of the protein aggregation process.**

Protein aggregation occurs when normally folded proteins adopt a  $\beta$ -sheet-rich conformation called amyloid. Proteins that have formed amyloid readily accumulate with other amyloid, leading to the formation of soluble oligomers and eventually insoluble amyloid fibrils. (Created with BioRender.)

One class of neurodegenerative diseases that I focused on is the polyQ diseases. This class consists of nine neurodegenerative diseases that are caused by the expansion of a CAG trinucleotide repeat in the coding region of specific genes (Williams & Paulson, 2008). CAG encodes for glutamine, and therefore the polyQ tracts in the proteins are expanded. PolyQ lengths vary by protein, but expansions of these tracts cause proteins to be prone to misfolding and aggregation, leading to neuronal loss and disease (Williams & Paulson, 2008). The most common polyQ disease is Huntington's disease (HD), which is caused by a polyQ expansion in exon 1 of the huntingtin (Htt) protein. HD is an autosomal dominant genetic disease that presents with both physical and mental deterioration

(NINDS, 2017). There is no cure for HD, and current therapies only relieve some symptoms (NINDS, 2017; Ross & Tabrizi, 2011).

While neurodegenerative diseases are incurable, it is thought that many can be treated by preventing protein aggregation. One way to accomplish this would be by enhancing pathways of the protein quality control network. Therefore, it is important to understand these cellular pathways in the context of neurodegenerative diseases.

## ***1.2 The protein quality control network and the role of molecular chaperones***

The protein quality control (PQC) network consists of pathways that regulate protein translation, folding, and degradation (Kaushik & Cuervo, 2015; Labbadia & Morimoto, 2015). Three major pathways that specifically regulate protein folding and degradation include the molecular chaperones, the ubiquitin-proteasome system (UPS), and autophagy (Figure 2). Molecular chaperones are central to PQC because they can recognize and refold misfolded proteins. Chaperones can also recruit machinery for protein degradation by the UPS (Chen et al., 2011; Hartl & Hayer-Hartl, 2002; McClellan et al., 2005). The two protein degradation systems, the UPS and autophagy, contribute to PQC by degrading misfolded proteins that cannot be refolded by chaperones. The UPS utilizes a series of three ubiquitinating enzymes to tag proteins with ubiquitin (Ciechanover, 1994; Kwon & Ciechanover, 2017). Misfolded proteins are tagged with a

## The Protein Quality Control Network

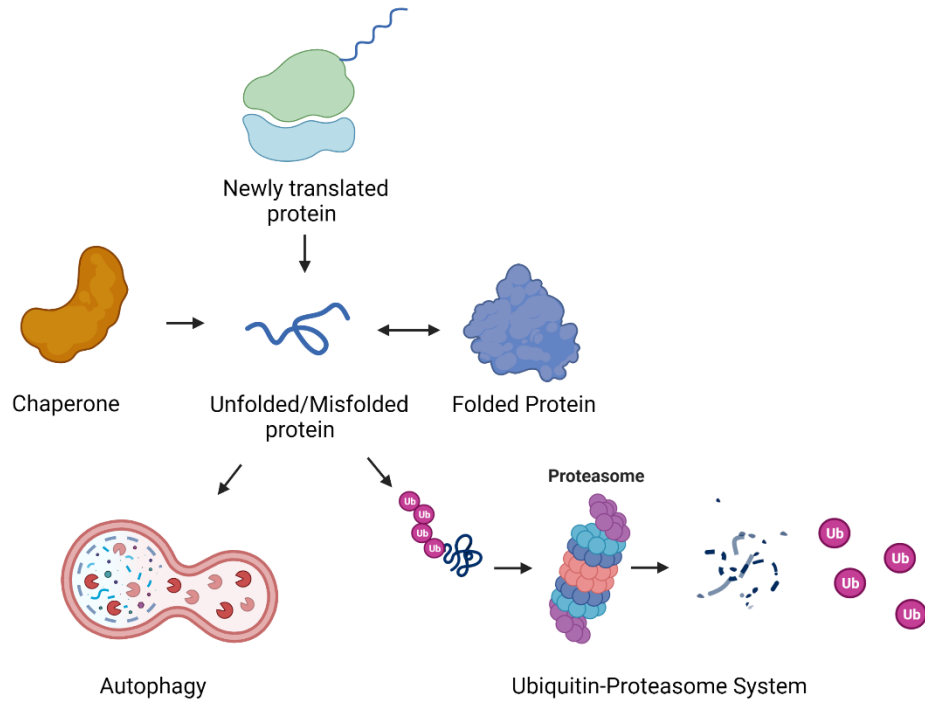


**Figure 2: Description of the protein quality control network.**

Newly translated proteins and natively folded proteins that have become misfolded are refolded with the help of molecular chaperones. When misfolded proteins cannot be refolded with chaperones, they will be targeted for degradation either via the lysosome in autophagy or the proteasome in the ubiquitin-proteasome system. (Created with BioRender.)

specific ubiquitin chain which serves as a signal for the protein to be degraded by the proteasome (Ciechanover, 1994; Kwon & Ciechanover, 2017; Tanaka & Matsuda, 2014).

Misfolded proteins can alternatively be degraded by autophagy. Protein degradation by autophagy can be either non-selective, where large cellular debris is engulfed by the autophagosome, or more selective, such as chaperone-mediated autophagy where

chaperones shuttle debris directly to the lysosome (Cuervo & Wong, 2014; Kaushik & Cuervo, 2018; Kroemer et al., 2010; Kwon & Ciechanover, 2017; Tanaka & Matsuda, 2014). While all the PQC pathways are important in the context of misfolded proteins and neurodegenerative disease, my research focuses on novel molecular chaperones.

Molecular chaperones are a diverse family of proteins with three main classes. The first class of chaperone proteins is the holdases, which include small heat shock proteins (sHsps). Holdases bind to misfolded proteins and prevent them from aggregating (Bakthisaran et al., 2015; Haslbeck, 2002; Jakob et al., 1993; Sun & MacRae, 2005; Taylor & Benjamin, 2005). The second class is the foldases, which includes Hsp70 and Hsp90 proteins. These chaperones utilize ATP to fold newly translated proteins and refold misfolded proteins to their native conformations (Hartl et al., 2011; Kim et al., 2013; Mayer & Bukau, 2005; Pearl, 2016; Saibil, 2013). Finally, there are disaggregases including the human Hsp40-Hsp70-Hsp110 chaperone complex and the newly characterized Skd3 (human CLPB), which can extract and refold monomeric proteins from larger aggregates in an ATP-dependent manner (Cupo & Shorter, 2020; Franco et al., 2021; Gao et al., 2015). These three types of chaperones work together to maintain protein homeostasis in cells by binding, disaggregating, and refolding proteins.

There are instances in which aggregation-prone proteins escape PQC pathways and aggregate, eventually causing disease. It is thought that preventing protein

aggregation is one way to treat neurodegenerative diseases. One potential therapeutic approach is to prevent protein aggregation by upregulating the molecular chaperone network. This could be accomplished by using small molecules to directly or indirectly induce transcription of heat shock factor 1, the master regulator of chaperone gene transcription, to upregulate sHsps and Hsp70 chaperones. (Bakthisaran et al., 2015; Ebrahimi-Fakhari et al., 2013; Kalia et al., 2010; Labbadia & Morimoto, 2015; Sinnige et al., 2020; Voisine et al., 2010; Yu et al., 2019). Additionally, chemical chaperones could be used to enhance protein folding and stability (Ebrahimi-Fakhari et al., 2013). Another strategy that is commonly employed to prevent protein aggregation is the use of peptides specifically designed to mimic amyloid. These peptide sequences are often derived from known amyloid forming sequences of aggregation-prone proteins, such as amyloid- $\beta$  or  $\alpha$ -synuclein, and directly interact with amyloid to prevent aggregation (Austen et al., 2008; Bett et al., 2010; Cheng et al., 2012; Eskici & Gur, 2013; Gazit, 2005; Henning-Knetchel et al., 2020; Neddenriep et al., 2011; Orner et al., 2006; Sato et al., 2006; Yamin et al., 2009). However, these treatment options need to be investigated more thoroughly in an *in vivo* system before further drug development can be pursued.

### ***1.3 Dictyostelium discoideum as a model organism for neurodegenerative diseases<sup>1</sup>***

Due to the lack of curative treatments for neurodegenerative diseases, it is important to understand molecular mechanisms that drive neurodegenerative diseases to develop therapies. A powerful way to investigate pathogenic mechanisms is by utilizing model organisms. Neurodegenerative diseases have been studied in a wide variety of models ranging from yeast to non-human primates (Andrews et al., 2016; Dawson et al., 2018; Emborg, 2017; Gama Sosa et al., 2012; Lopes et al., 2017; Miller-Fleming et al., 2008; Slanzi et al., 2020; Suresh et al., 2018; van Ham et al., 2009). One model organism that is emerging as a model for neurodegenerative diseases is the social amoeba *Dictyostelium discoideum* (*Dictyostelium*). *Dictyostelium* is a simple eukaryote that usually exists in the soil as a unicellular amoeba. However, under stress conditions like starvation, *Dictyostelium* undergoes a developmental cycle where it transitions from a unicellular state to a multicellular fruiting body (Figure 3) (Chisholm & Firtel, 2004; Kessin, 2001). This developmental process makes *Dictyostelium* an ideal organism for studying cellular processes such as chemotaxis, cell motility, and cell differentiation (Bozzaro et al., 2008;

---

<sup>1</sup> Section 1.3 is adapted with permission from the published review: Haver, HN and Scaglione, KM (2021). *Dictyostelium discoideum* as a Model for Investigating Neurodegenerative Diseases. *Front. Cell. Neurosci.* 15:759532. <https://doi.org/10.3389/fncel.2021.759532>.

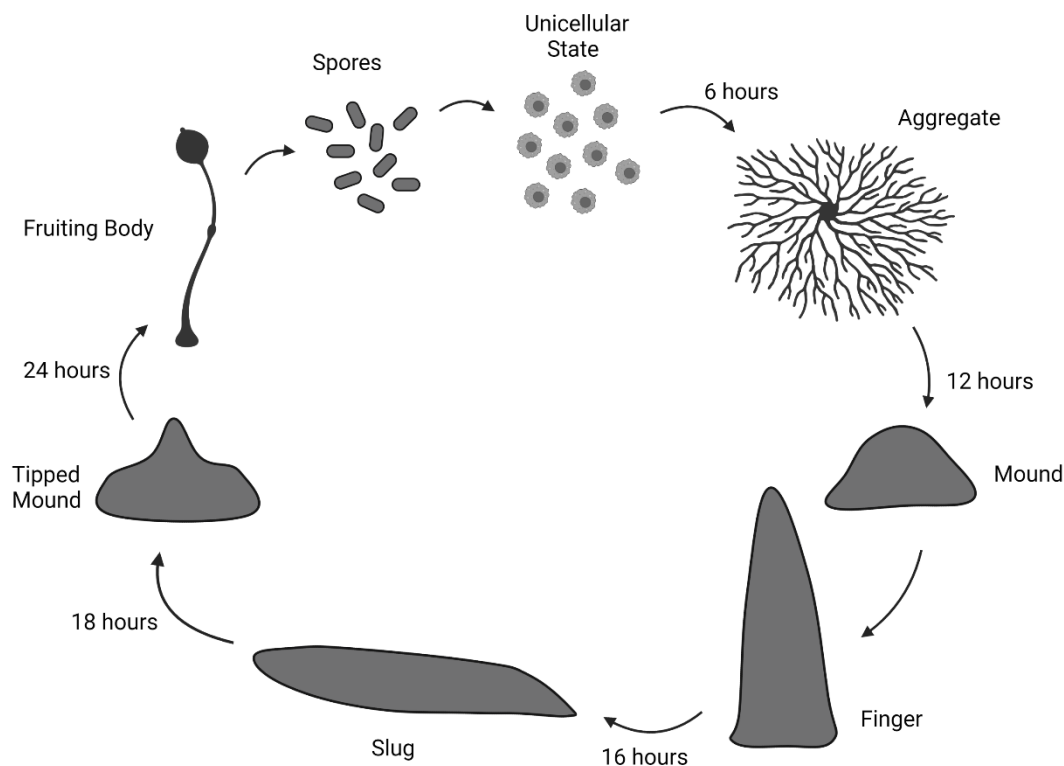


**Figure 3: *Dictyostelium's* developmental cycle.**

Under stress conditions such as starvation, unicellular *Dictyostelium* undergoes a 24-hour developmental cycle. After 6 hours, individual cells culminate to form aggregates. The aggregates begin to form mounds after 12 hours, which turn into finger/slug structures around 16 hours. The slug carries the *Dictyostelium* cells to the top of the forest floor where it forms a tipped mound around 18 hours. After 24 hours, a fruiting body consisting of a spore filled sorus is lifted by a stalk. Fruiting bodies are then carried off by wildlife where spores can germinate and propagate elsewhere. (Created with BioRender.)

Cai & Devreotes, 2011; Chattwood & Thompson, 2011; Giusti et al., 2008; Harwood, 2008; Maniak, 2003; Rivero, 2008; Surcel et al., 2010; Swaney et al., 2010; Y. Wang et al., 2011; Williams, 2006). In addition, *Dictyostelium's* simplicity makes it useful as a model to investigate disease-causing mechanisms in human diseases. Compared to yeast, another

single-cell model organism, *Dictyostelium* has a larger genome that contains more human disease gene orthologs, including more neurodegenerative disease-causing genes (Eichinger et al., 2005). This, coupled with its numerous technical advantages, including its genetic tractability, makes *Dictyostelium* a relevant model for identifying both the normal function of neurodegenerative disease genes and how gene mutations may disrupt function.

### **1.3.1 *Dictyostelium* as a model for Alzheimer's disease**

AD is the most common neurodegenerative disease. One major pathological hallmark of AD is the accumulation of extracellular amyloid- $\beta$  ( $A\beta$ ) plaques. These plaques arise due to abnormal cleavage of the amyloid precursor protein (APP) (O'Brien & Wong, 2011). Under normal conditions, the N-terminus of APP is initially cleaved by a  $\beta$ -secretase (O'Brien & Wong, 2011). Then the  $\gamma$ -secretase complex cleaves the C-terminal region into either  $A\beta_{40}$  or  $A\beta_{42}$  peptides (O'Brien & Wong, 2011). Both of these C-terminal fragments are present, with  $A\beta_{40}$  being nontoxic and  $A\beta_{42}$  being more toxic and prone to misfolding (O'Brien & Wong, 2011). Normally,  $A\beta_{40}$  is the most abundant  $A\beta$  fragment, with very little of the toxic  $A\beta_{42}$  fragment present. However, in AD there is an alteration of APP cleavage leading to an increased  $A\beta_{42}/A\beta_{40}$  ratio which results in  $A\beta$  aggregation and eventually plaque formation (O'Brien & Wong, 2011).

Mutations in the presenilin (*PSEN*) genes are one cause for abnormal A $\beta$  cleavage (Hutton & Hardy, 1997; O'Brien & Wong, 2011). The PSEN proteins serve as the catalytic subunit of  $\gamma$ -secretase complexes and are involved in APP processing into A $\beta$  peptides (De Strooper et al., 1999; De Strooper et al., 1998; Esler et al., 2000; Li et al., 2000; Struhl & Greenwald, 1999; Wolfe et al., 1999b). Over 150 missense mutations in PSEN1/2 have been linked to AD pathogenesis, and a large amount of research has investigated the function of the  $\gamma$ -secretase complex in the context of AD (De Strooper et al., 2012; Haass et al., 2012; Mucke, 2012). Interestingly, while *Dictyostelium* does not encode for a  $\beta$ -secretase or APP, it does express an orthologous  $\gamma$ -secretase complex, which includes orthologs for PSEN1 and 2. Research utilizing *Dictyostelium* found roles for PSEN1 in phagocytosis and for PSEN2 in cell differentiation, confirming that different PSEN/ $\gamma$ -secretase complexes serve different biological functions (Gu et al., 2004; McMains et al., 2010; Myre, 2012).

In addition to identifying the role of the  $\gamma$ -secretase complex in *Dictyostelium* biology, it was also found that wildtype (WT) *Dictyostelium* cells expressing human APP process APP in a similar manner as human cells, producing both A $\beta$ 40 and A $\beta$ 42 fragments (McMains et al., 2010). This process is dependent on the  $\gamma$ -secretase complex, but does not require a  $\beta$ -secretase for initial cleavage (McMains et al., 2010). Therefore, *Dictyostelium* can initiate APP processing either without N-terminal cleavage or by another unknown enzyme. Identifying how *Dictyostelium* initiates APP cleavage could

provide new insight into currently unknown roles of the  $\gamma$ -secretase complex in AD. Additionally, *Dictyostelium* could be a powerful model organism for identifying novel modulators of APP processing.

### 1.3.2 *Dictyostelium* as a model for Parkinson's disease

Parkinson's disease (PD) is caused by the loss of dopaminergic neurons due in part to the formation and accumulation of protein aggregates in the cytoplasm called Lewy bodies. In PD, neurons have numerous problems including oxidative stress, mitochondrial dysfunction, synaptic dysfunction, and inhibition of protein quality control pathways (Cook et al., 2012; Dias et al., 2013; Park et al., 2018; Picconi et al., 2012). There are many proteins that have been implicated in PD pathogenesis, but only  $\alpha$ -synuclein, DJ-1, and LRRK2 have been investigated in *Dictyostelium*.

The  $\alpha$ -synuclein protein is one of the main proteins found in Lewy body aggregates and several mutations are associated with familial cases of PD (Stefanis, 2012). While *Dictyostelium* does not encode for  $\alpha$ -synuclein, it was utilized as a model to determine the normal function of human  $\alpha$ -synuclein. Both WT and mutant  $\alpha$ -synuclein expressed in *Dictyostelium* caused defects in photo- and thermotaxis, altered fruiting body morphology, and decreased rate of phagocytosis, suggesting that this protein imparts toxicity to *Dictyostelium* (Fernando et al., 2020). These phenotypes encompass some, but not all, of the well-established *Dictyostelium* phenotypes of mitochondrial dysfunction

(Fernando et al., 2020; Francione et al., 2011). Because mitochondrial dysfunction is a common problem in PD, this makes *Dictyostelium* a valuable model for studying the function of  $\alpha$ -synuclein. Furthermore, because  $\alpha$ -synuclein expression in *Dictyostelium* only causes a subset of mitochondrial dysfunction phenotypes, this suggests that *Dictyostelium* may have mechanisms of suppressing mitochondrial toxicity induced by  $\alpha$ -synuclein.

Another protein that has many PD-associated mutations is DJ-1 (Gorner et al., 2007; Malgieri & Eliezer, 2008; Ramsey & Giasson, 2010; Wilson et al., 2003). DJ-1 functions to protect cells from oxidative stress as well as acting as a chaperone to modulate the toxicity and misfolding of  $\alpha$ -synuclein (Batelli et al., 2008; Batelli et al., 2015; Catazaro et al., 2018; Chunna & Pu, 2017; Eberhard & Lammert, 2017; Jain et al., 2012; Kawate et al., 2017; Kim et al., 2005; Kinumi et al., 2004; Kiss et al., 2017; Meulener et al., 2005; Ottolini et al., 2013; Sajjad et al., 2014; Smith & Wilson, 2017; Taira et al., 2004; Wagenfeld et al., 1998; Z. Wang et al., 2011; Wilson, 2011; Zondler et al., 2014). *Dictyostelium* has an ortholog of *DJ-1* that when deleted results in growth defects under normal conditions, suggesting a non-mitochondrial role for DJ-1 (Chen et al., 2017). Under oxidative conditions however, loss of DJ-1 results in worsened mitochondrial respiration, defects in phagocytosis, phototaxis, morphogenesis, and growth, suggesting that the oxidized form of DJ-1 is protective against oxidative stress and could play a mitochondrial role (Chen et al., 2021).

Finally, leucine-rich repeat kinase 2 (LRRK2) is another commonly mutated protein associated with PD. It is part of the family of Roco proteins, which were originally discovered in *Dictyostelium* (Bosgraaf et al., 2002; Bosgraaf & van Haastert, 2003; Rui et al., 2018). *Dictyostelium*'s Roco4 protein has the same domain architecture as LRRK2 and has been used for comparative studies (Kortholt et al., 2012). PD-related mutations in Roco4 behave the same in *Dictyostelium* as the corresponding LRRK2 mutations in human cells, suggesting similar functions between the proteins (Jaleel et al., 2007; Kortholt et al., 2012; Ohta et al., 2010). Deletion of Roco4 in *Dictyostelium* also indirectly leads to mitochondrial dysfunction, similar to deletion of LRRK2 in human macrophages (Rosenbusch et al., 2021). This suggests Roco4 plays a similar role to LRRK2 and could be a potential candidate for investigating the normal physiological role of LRRK2 in a simple model organism.

### **1.3.3 *Dictyostelium* as a model for polyQ diseases**

As mentioned above, the polyQ diseases are a class of nine neurodegenerative diseases caused by the expansion of a polyQ tract in specific proteins, leading to protein misfolding and aggregation. The most common polyQ disease is HD, where the polyQ tract within the Htt protein expands beyond the disease threshold of ~35 glutamines and leads to nuclear inclusions. Interestingly, *Dictyostelium* encodes for an ortholog of Htt (Chisholm et al., 2006; Myre, 2012). Unlike human Htt, however, *Dictyostelium* Htt does

not possess a polyQ tract within exon 1 (Insall, 2005; Myre et al., 2011). Deletion of the *Htt* gene from *Dictyostelium* causes a number of subtle defects including processes involved in actin remodeling, cyclic AMP relay, and cell differentiation during development (Myre et al., 2011). These data suggest a multipurpose role for Htt in *Dictyostelium*.

One unique aspect of *Dictyostelium* is that its genome naturally has over 10,000 single-sequence repeats, with many of these repeats appearing within protein-coding regions (Eichinger et al., 2005). Surprisingly, polyasparagine (polyN) and polyQ tracts are the two most abundant homopolymeric repeats within *Dictyostelium's* proteome, with many of these repeats extending beyond the human pathogenic threshold (Eichinger et al., 2005; Santarriaga et al., 2015). This is remarkable since polyQ/N tracts are considered to be prion-like, where proteins can transmit their misfolded versions to infect healthy cells, and long polyQ tracts are pathogenic in humans (Bolton & Bendheim, 2007; Cohen et al., 1994; Come et al., 1993; Gajdusek, 1996; Harris, 1999; Hope et al., 1986; Malinowska et al., 2015; Santarriaga et al., 2015). This suggests that *Dictyostelium* utilizes these repeats in its normal biology.

Because *Dictyostelium* encodes for so many long homopolymeric repeats, an important question to ask is: Is *Dictyostelium* naturally resistant to polyQ/N aggregation? To date, only two studies have been performed examining human pathogenic prion or polyQ in *Dictyostelium*. The Scaglione lab and others have found that expressing either

human pathogenic Htt exon 1 with 103 glutamines (Htt<sup>ex1Q103</sup>) or prion in WT *Dictyostelium* results in soluble proteins diffuse throughout the cells (Figure 4, performed by Stephanie Santarriaga) (Malinovska et al., 2015; Santarriaga et al., 2015). This resistance to aggregation has not been observed in any other model organism. This observation is very important because we can utilize *Dictyostelium* as a model to investigate how nature can overcome the obstacle of protein aggregation.

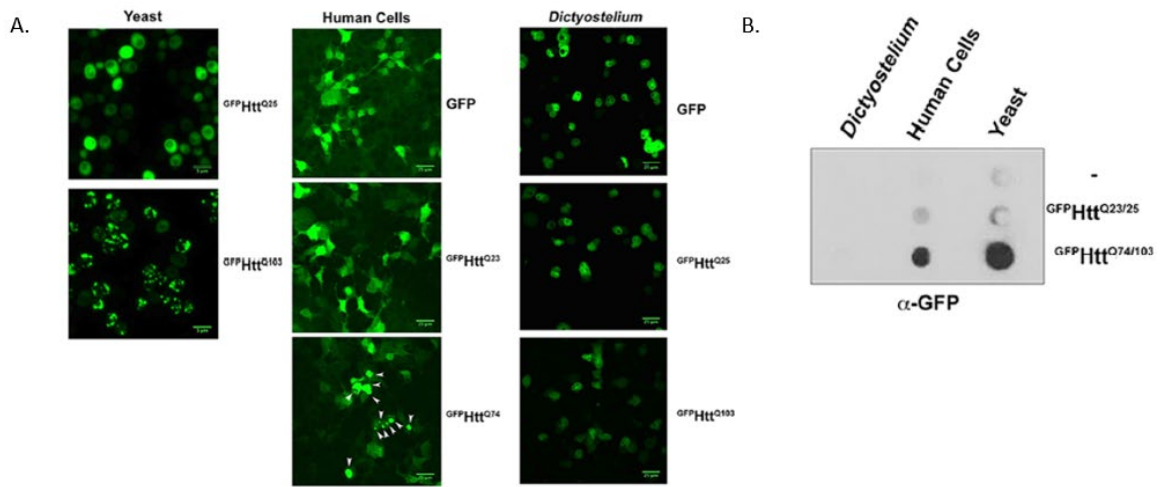


**Figure 4: *Dictyostelium* is naturally resistant to aggregation from a human pathogenic polyQ protein.**

(A) GFP-expanded Htt exon 1 aggregates in yeast and human cells in a polyglutamine length-dependent manner but remain soluble in *Dictyostelium*. All cell types were imaged using confocal microscopy. White arrows indicate aggregates. (B) Filter trap analysis of *Dictyostelium* expressing GFP-Htt<sup>Q103</sup> fails to detect aggregates. Aggregation of normal and expanded polyglutamine Htt exon 1 was compared in yeast, HEK293 cells, and *Dictyostelium* by filter trap analysis. (Santarriaga et al., 2015)

## 1.4 The *Dictyostelium*-specific chaperone serine-rich chaperone protein 1

We wanted to further investigate how *Dictyostelium* is resistant to polyQ aggregation. We performed a forward genetic screen called restriction enzyme-mediated integration (REMI) to disrupt random genes within the genome of *Dictyostelium* cells expressing  $\text{GFP}^{\text{Htt}^{\text{ex1Q103}}}$  to identify genes that suppress polyQ aggregation (Guerin & Larochelle, 2002; Kuspa, 2006). From this screen we were able to identify one gene that, when disrupted, causes *Dictyostelium* cells to form Htt aggregates (Figure 5, performed by Stephanie Santarriaga) (Santarriaga et al., 2018). This gene encodes for an 88-amino acid protein that we named serine-rich chaperone protein 1 (SRCP1). Further work validated that SRCP1 is both necessary and sufficient to impart resistance of mutant Htt aggregation to *Dictyostelium* and other cell types including human cells (Santarriaga et al., 2018).

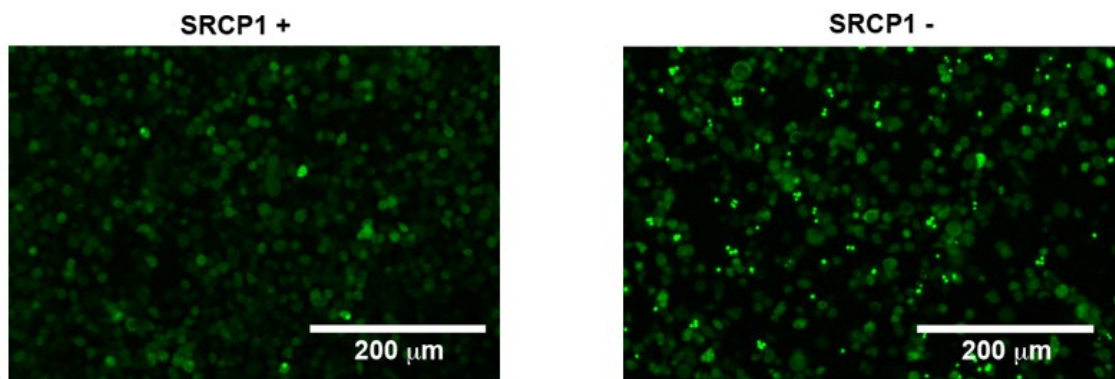


**Figure 5: SRCP1 knockout causes  $\text{GFP}^{\text{Htt}^{\text{ex1Q103}}}$  aggregation in *Dictyostelium*.**

WT (left) and SRCP1 knockout (right) cells were transfected with  $\text{GFP}^{\text{Htt}^{\text{ex1Q103}}}$ , selected with G-418, and imaged by fluorescent microscopy.  $\text{GFP}^{\text{Htt}^{\text{ex1Q103}}}$  puncta only form in SRCP1 knockout cells (Santarriaga et al., 2018)

The discovery of SRCP1 has opened a door in therapeutic developments for neurodegenerative diseases. SRCP1 has been found to suppress a non-polyQ protein, superoxide dismutase 1 (SOD1), an aggregation-prone protein in ALS. Additionally, when SRCP1 was packaged into adeno-associated virus 9 (AAV9) and injected into the brain of an ALS mouse model, SOD1 aggregation was significantly reduced, although the lifespan was not extended (Luecke et al., 2021). This suggests that SRCP1 could potentially serve as a therapeutic to prevent protein aggregation in neurodegenerative diseases. It is therefore critical that we understand SRCP1's mechanism to suppress aggregation as well as deliver SRCP1 to affected neuronal populations and assess its neuroprotective ability.

### ***1.5 Research objectives***

*Dictyostelium* is naturally resistant to polyQ aggregation due, at least in part, to the presence of the *Dictyostelium*-specific chaperone SRCP1. SRCP1 is also sufficient to impart resistance to polyQ aggregation to other organisms. However, its mechanism for suppressing polyQ aggregation is unknown. Here, I aimed to further investigate the structure and function of SRCP1 and *Dictyostelium*'s PQC network.

First, I wanted to elucidate how SRCP1 is able to suppress polyQ aggregation. I began by showing that SRCP1's C-terminus is sufficient *in vitro* to suppress aggregation of a recombinant mutant Htt protein. I hypothesized that SRCP1's C-terminus forms an amyloid-like  $\beta$ -hairpin structure to bind polyQ and prevent further aggregation. While I

was unable to generate recombinant SRCP1, I was successful in utilizing computational and experimental approaches to show that SRCP1 does form a  $\beta$ -hairpin around amino acid residues 61-80. I also determined that a peptide of these residues (SRCP1<sup>61-80</sup>) suppresses mutant Htt aggregation at the secondary nucleation pathway, and it does not bind specifically to the polyQ tract *in vitro*. I was able to show that SRCP1<sup>61-80</sup> is also sufficient to suppress aggregation of another polyQ protein, ataxin-3, suggesting that SRCP1 is not specific in its ability to suppress polyQ aggregation.

In addition to SRCP1, I wanted to further examine another *Dictyostelium* chaperone protein suggested to regulate polyQ aggregation, heat shock protein 101 (Hsp101). Hsp101 shares high sequence homology to the yeast disaggregase Hsp104 and has previously been shown to protect *Dictyostelium* cells from protein aggregation under heat stress (Malinovska et al., 2015). There is currently no data available on Hsp101's function in *Dictyostelium*. I wanted to verify its ability to prevent polyQ aggregation and examine its biological function in *Dictyostelium*. I generated a Hsp101 knockout strain and found that loss of Hsp101 resulted in reduced axenic growth, which was rescued by Hsp101 overexpression. I also discovered that loss of Hsp101 did not result in aggregation of either polyQ or a *Dictyostelium* prion protein with or without heat stress. To probe more into Hsp101's interactome, I performed a Hsp101 pulldown and used mass spectrometry to identify potential interactors. The highest fold enrichment in protein domains that

interact with Hsp101 were multiple components of the Skp1-Cullin-F-box (SCF) complex ubiquitin ligase machinery, suggesting a role for Hsp101 in this pathway.

Together, my dissertation work has brought more understanding into *Dictyostelium's* PQC network by giving new insight into SRCP1's mechanism and by providing more evidence into the biological role of Hsp101. This work also shows that *Dictyostelium* is a simple model system that is useful for learning more about PQC pathways and can help us understand how to overcome the obstacle of protein aggregation.

## 2. A C-terminal region of SRCP1 suppresses polyglutamine aggregation<sup>1</sup>

SRCP1 is a novel molecular chaperone protein that is native to *Dictyostelium*. While we know that it is essential for suppressing polyQ aggregation in both *Dictyostelium* and human cells, its mechanism is currently unknown. Previous data from our lab showed that mutating all of the serine and threonine residues in the N-terminus of SRCP1 (~40% of the N-terminus) still resulted in suppression of polyQ aggregation in cells (Santarriaga et al., 2018). We next turned to the C-terminus of SRCP1 to determine if a region within it was responsible for SRCP1's function. Initial analysis of SRCP1's amino acid sequence revealed that the C-terminus is glycine-rich and highly

```
AmylPred2:          *****
FISH Amyloid:      *****
Tango:             *****
FoldAmyloid:       *****
PASTA 2.0:         *****
                   40-GGWGGFGGPKGGSFNVDIAGNLIWGVYGFIRGGVGLVKWRGLQKGCKQP-88
```

**Figure 6: SRCP1's C-terminus contains a region predicted to form amyloid.**

Schematic of SRCP1's C-terminal amino acid sequence is shown. Multiple *in silico* programs predict an amyloid-forming region in SRCP1. Asterisks indicate amino acids that are predicted to form amyloid. (Santarriaga et al., 2018)

---

<sup>1</sup> Chapter 2 is adapted with permission from the published article: Santarriaga, S, Haver, HN, Kanack, AJ, Fikejs, AS, Sison, SL, Egner, JM, Bostrom, JR, Seminary, ER, Hill, RB, Link, BA, Ebert, AD, and Scaglione, KM. (2018). SRCP1 Conveys Resistance to Polyglutamine Aggregation. *Mol. Cell.* 71:216-228. <https://doi.org/10.1016/j.molcel.2018.07.008>

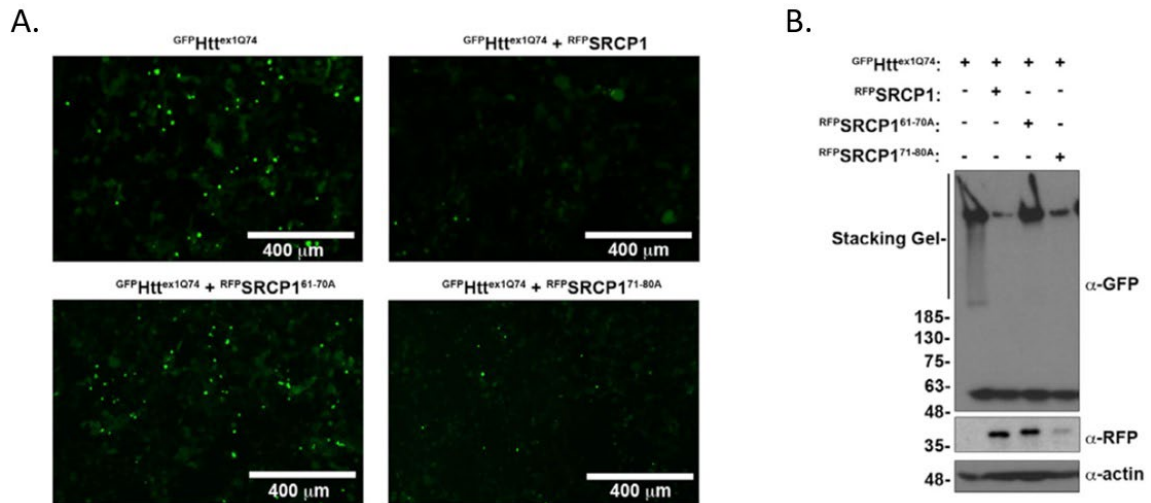


**Figure 7: Amino acids 61–70 are essential for suppressing GFPHtt<sup>ex1Q74</sup> aggregation.**

(A) HEK293 cells were transfected with GFPHtt<sup>ex1Q74</sup>, GFPHtt<sup>ex1Q74</sup> and RFP-SRCP1, GFPHtt<sup>ex1Q74</sup> and RFP-SRCP1<sup>61-70A</sup>, or GFPHtt<sup>ex1Q74</sup> and RFP-SRCP1<sup>71-80A</sup>. Cells were imaged 48 h post-transfection by fluorescent microscopy. (B) Samples from (A) were collected 48 h post-transfection and analyzed by western blot (n = 7). (Santarriaga et al., 2018)

hydrophobic, closely resembling amyloid-forming sequences. A sequence within this region (amino acid residues 61-80) was predicted to form amyloid by multiple amyloid-predicting programs (Figure 6, created by Matt Scaglione). We hypothesized that SRCP1's C-terminus utilizes an amyloid-forming domain to suppress polyQ aggregation.

To determine whether this region is required for suppressing polyQ aggregation, we initially mutated either residues 61-70 or 71-80 to alanine (RFP-SRCP1<sup>61-70A</sup> and RFP-SRCP1<sup>71-80A</sup>, respectively). We expressed these constructs in HEK293 cells alongside a mutant huntingtin exon-1 fragment with 74 glutamines (GFPHtt<sup>ex1Q74</sup>) and assessed their ability to suppress GFPHtt<sup>ex1Q74</sup> aggregation via fluorescence microscopy and western blot.

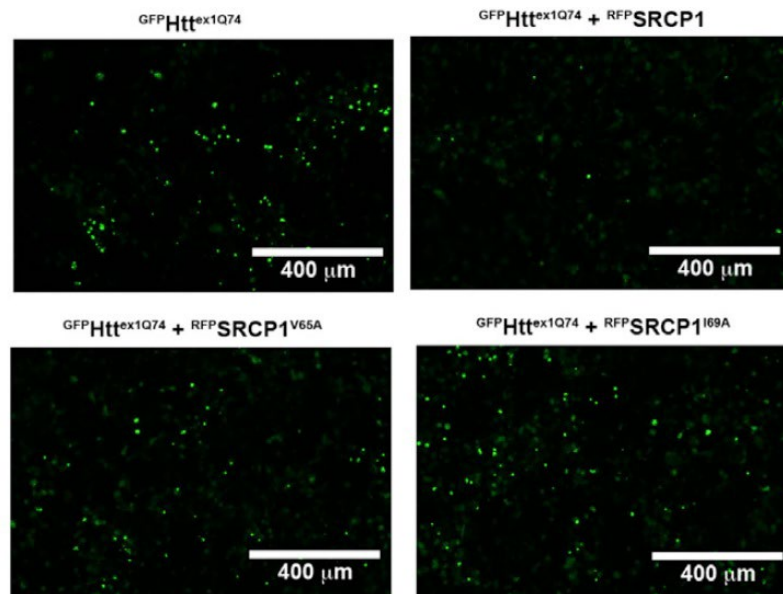


**Figure 8: Amino acids V65 and I69 are essential for suppressing  $\text{GFP}^{\text{Htt}^{\text{ex1Q74}}}$  aggregation.**

HEK293 cells were transfected with  $\text{GFP}^{\text{Htt}^{\text{ex1Q74}}}$ , with  $\text{GFP}^{\text{Htt}^{\text{ex1Q74}}}$  and  $\text{RFP}^{\text{SRCP1}}$ , with  $\text{GFP}^{\text{Htt}^{\text{ex1Q74}}}$  and  $\text{RFP}^{\text{SRCP1}^{\text{V65A}}}$ , or with  $\text{GFP}^{\text{Htt}^{\text{ex1Q74}}}$  and  $\text{RFP}^{\text{SRCP1}^{\text{I69A}}}$ . Cells were imaged 48 h post-transfection by fluorescent microscopy. (Santarriaga et al., 2018)

From this, we found that co-transfection of  $\text{GFP}^{\text{Htt}^{\text{ex1Q74}}}$  with  $\text{RFP}^{\text{SRCP1}^{\text{61-70A}}}$  resulted in more fluorescent puncta compared to  $\text{GFP}^{\text{Htt}^{\text{ex1Q74}}}$  with WT  $\text{RFP}^{\text{SRCP1}}$ , consistent with a loss in SRCP1's ability to suppress  $\text{GFP}^{\text{Htt}^{\text{ex1Q74}}}$  aggregation (Figure 7, A and B, experiment and image by Stephanie Santarriaga).  $\text{RFP}^{\text{SRCP1}^{\text{71-80A}}}$ , however, maintained WT function (Figure 7, A and B). This suggests that SRCP1 residues 61-70 are critical for suppressing polyQ aggregation. To gain more detailed insight into residues important for SRCP1 function, we next mutated individual amino acid residues within  $\text{SRCP1}^{\text{61-70}}$  to alanine and determined their ability to suppress  $\text{GFP}^{\text{Htt}^{\text{ex1Q74}}}$  aggregation via fluorescence microscopy. Two individual mutants,  $\text{SRCP1}^{\text{V65A}}$  and  $\text{SRCP1}^{\text{I69A}}$ , resulted in loss of

function, consistent with these residues playing an important role in SRCP1's ability to suppress polyQ aggregation (Figure 8, experiment and image by Stephanie Santarriaga). From these data, we have shown that SRCP1<sup>61-70</sup> is necessary for SRCP1's ability to suppress polyQ aggregation.

These data led us to hypothesize that SRCP1<sup>61-70</sup> is also sufficient for function. I further investigated the role of SRCP1's C-terminus and show that the predicted amyloid-forming domain alone is sufficient to suppress polyQ aggregation *in vitro*. I also found that this region only delays rather than prevents amyloid formation.

## ***2.1 A peptide of SRCP1 is sufficient to suppress polyQ aggregation in vitro***

To investigate if SRCP1's predicted amyloid-forming domain is sufficient to suppress polyQ aggregation, I asked if SRCP1 could directly suppress mutant huntingtin aggregation *in vitro*. We were unable to generate soluble recombinant SRCP1 protein for these experiments, so we synthesized a 20-amino-acid peptide containing residues 61-80 that mimics SRCP1's C-terminal amyloid-forming region (SRCP1<sup>61-80</sup>). I first utilized thioflavin-T (ThT) to measure aggregation of mutant huntingtin with 46 glutamines (Htt<sup>Q46</sup>) in the presence of this peptide. I found that SRCP1<sup>61-80</sup> was sufficient to suppress aggregation of Htt<sup>Q46</sup> *in vitro* in a dose-dependent manner (Figure 9A).

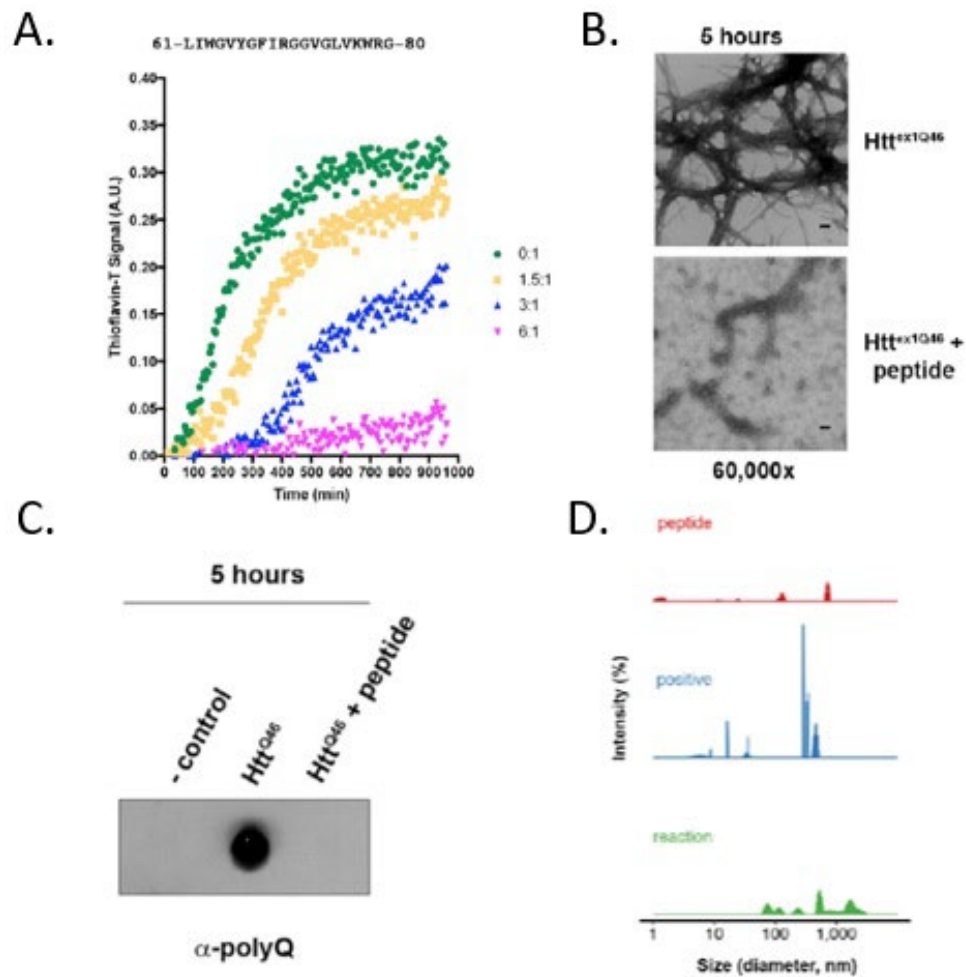


**Figure 9: A peptide of SRCP1's C-terminal domain suppresses huntingtin aggregation *in vitro*.**

(A) *In vitro* Htt<sup>Q46</sup> aggregation assays were performed in the absence or presence of increasing ratios of SRCP1<sup>61-80</sup> to Htt<sup>Q46</sup>. A representative image is shown (n = 5). (B) *In vitro* Htt<sup>Q46</sup> aggregation assays were performed with Htt<sup>Q46</sup> and SRCP1<sup>61-80</sup> peptide (3:1 peptide to Htt<sup>Q46</sup>) for 5 h and imaged by EM. (C) *In vitro* Htt<sup>Q46</sup> aggregation assays were performed with Htt<sup>Q46</sup> and SRCP1<sup>61-80</sup> peptide for 5 h (3:1 peptide to Htt<sup>Q46</sup>). Samples were prepared with SDS, subjected to filter-trap assay, and analyzed via western blot for polyQ. (D) *In vitro* Htt<sup>Q46</sup> aggregation assays were performed with Htt<sup>Q46</sup> and SRCP1<sup>61-80</sup> peptide for 5 h (3:1 peptide to Htt<sup>Q46</sup>). Samples were analyzed by DLS (performed by John Egnér). (Santarriaga et al., 2018)

I next wanted to confirm that SRCP1<sup>61-80</sup> was inhibiting Htt<sup>Q46</sup> aggregation and not disrupting the binding of ThT to Htt<sup>Q46</sup> aggregates. To accomplish this, I analyzed Htt<sup>Q46</sup> aggregate formation after a 5-h incubation with or without SRCP1<sup>61-80</sup> by transmission electron microscopy (TEM). I found that the addition of the SRCP1 peptide decreased Htt<sup>Q46</sup> fibril formation and led to the appearance of spherical structures similar to previously described soluble oligomers (Tsigelny et al., 2008) (Figure 9B, images taken by Clive Wells). I confirmed this data by filter-trap assay, where fewer aggregates were present with SRCP1<sup>61-80</sup>, and dynamic light scattering (DLS), which showed an increase in smaller species over time with SRCP1<sup>61-80</sup> (Figures 9C and D, DLS performed by John Egner). Together, these data show that SRCP1<sup>61-80</sup> is sufficient to suppress polyQ aggregation. The observation that the 1.5:1 and 3:1 molar ratios of peptide to Htt<sup>Q46</sup> resulted in a delay of Htt<sup>Q46</sup> aggregation led us to hypothesize that the SRCP1 peptide delays rather than prevents Htt<sup>Q46</sup> aggregation (Figure 9A). To test this hypothesis, I analyzed Htt<sup>Q46</sup> aggregation in the presence or absence of SRCP1<sup>61-80</sup> after a 72-h incubation. Consistent with SRCP1<sup>61-80</sup> delaying aggregation, Htt<sup>Q46</sup> aggregates were detected by TEM and filter-trap analysis after 72 h (Figures 10A and B, TEM images taken by Clive Wells). Additionally, the smaller species observed via DLS at 5 h were no longer detectable at 72 h (Figure 10C, DLS performed by John Egner). These data confirm that SRCP1<sup>61-80</sup> does delay Htt<sup>Q46</sup> aggregation but does not prevent it completely.

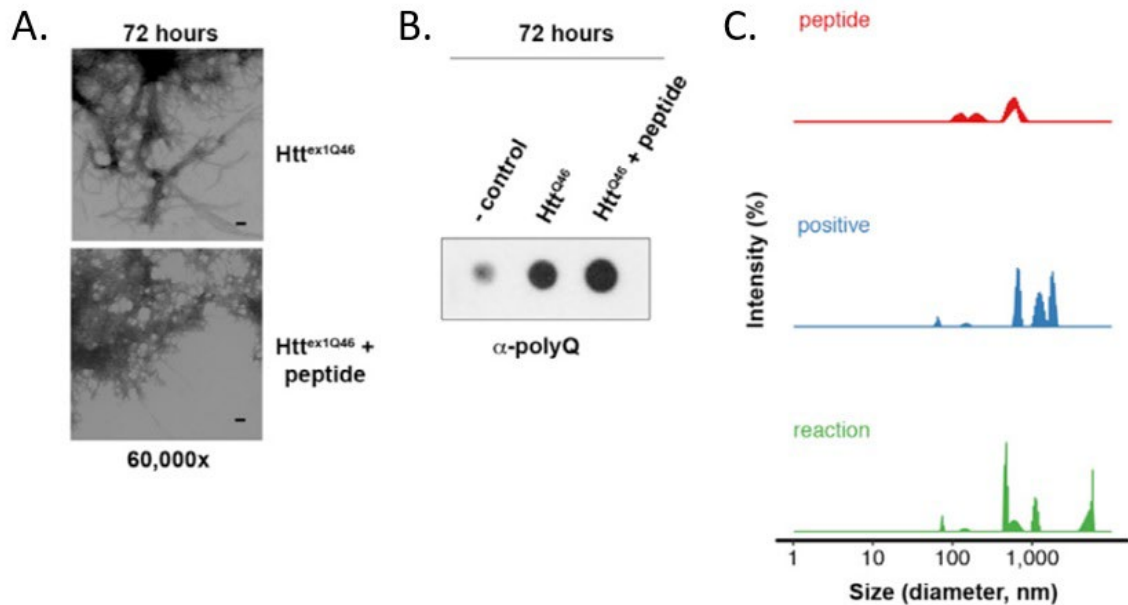


**Figure 10: SRCP1 peptide delays but does not prevent Htt<sup>Q46</sup> aggregation.**

(A) *In vitro* Htt<sup>Q46</sup> aggregation assays were performed with Htt<sup>Q46</sup> and SRCP1<sup>61–80</sup> peptide (3:1 peptide to Htt<sup>Q46</sup>) for 72 h and imaged by EM. (B) *In vitro* Htt<sup>Q46</sup> aggregation assays were performed with Htt<sup>Q46</sup> and SRCP1<sup>61–80</sup> peptide for 72 h (3:1 peptide to Htt<sup>Q46</sup>). Samples were prepared with SDS, subjected to filter-trap assay, and analyzed via western blot for polyQ. (C) *In vitro* Htt<sup>Q46</sup> aggregation assays were performed with Htt<sup>Q46</sup> and SRCP1<sup>61–80</sup> peptide for 72 h (3:1 peptide to Htt<sup>Q46</sup>). Samples were analyzed by DLS (performed by John Egner). (Santarriaga et al., 2018)

To further analyze SRCP1's amyloid-forming domain *in vitro* and confirm our in cell data, we tested peptides of the two predicted amyloid-forming domains (amino acids 61–70 or 71–80) within SRCP1. Consistent with our in cell data, SRCP1<sup>61–70</sup> was also sufficient to suppress Htt<sup>Q46</sup> aggregation *in vitro*, whereas SRCP1<sup>71–80</sup> was not (Figure 11A). Similarly, a peptide consisting of amino acids 61–70 with V65 and I69 mutated to alanine resulted in a loss in activity, similar to the fluorescent microscopy data in cells (Figure

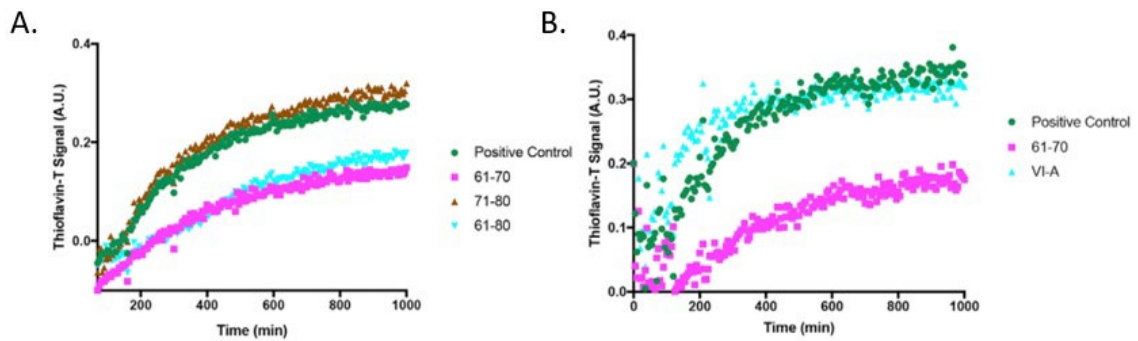


**Figure 11: A peptide mimicking SRCP1<sup>61-70</sup> suppresses polyQ aggregation.**

(A) *In vitro* Htt<sup>Q46</sup> aggregation assays were performed with Htt<sup>Q46</sup> and either SRCP1<sup>61-80</sup>, SRCP1<sup>61-70</sup> or SRCP1<sup>71-80</sup> (3:1 peptide to Htt<sup>Q46</sup>). Htt<sup>Q46</sup> alone was used as a positive control. A representative image is shown (n = 3). (B) *In vitro* Htt<sup>Q46</sup> aggregation assays were performed with Htt<sup>Q46</sup> and either SRCP1<sup>61-70</sup> or SRCP1<sup>61-70</sup> with amino acids V65 and I69 mutated to alanine (VI-A) (3:1 peptide to Htt<sup>Q46</sup>). Htt<sup>Q46</sup> alone was used as a positive control. A representative image is shown (n = 3). (Santarriaga et al., 2018)

11B). Together, these data support a role for SRCP1's C-terminal amyloid-forming region in contributing to SRCP1's ability to suppress polyQ aggregation both in cells and *in vitro*.

## 2.2 Discussion

Here, we identified the amyloid-like C-terminal region of SRCP1 to be responsible for suppressing polyQ aggregation *in vitro*. I found that a synthetic peptide of this C-terminal region was sufficient for suppressing Htt<sup>Q46</sup> aggregation in a dose-dependent manner (Figure 9A). This was confirmed by TEM, filter trap assay, and DLS (Figure 9B-D). Additionally, I show that SRCP1<sup>61-80</sup> delays Htt<sup>Q46</sup> aggregation rather than completely prevents it (Figure 10). Finally, I demonstrated that other peptides mimicking individual domains of SRCP1 confirm our in cell data (Figure 11).

While SRCP1 does not have any canonical chaperone domains, it nonetheless suppresses polyQ aggregation. We identified that its C-terminus is glycine-rich and hydrophobic, similar to amyloid-forming domains of known amyloid-forming proteins (Balbirnie et al., 2001; Giasson et al., 2001; Halverson et al., 1990; von Bergen et al., 2000). We found that a region within the C-terminus is predicted to form amyloid, and I show that this amyloid-forming sequence is sufficient to suppress polyQ aggregation and alters the rate of amyloid formation. Previous work from others has described that peptides resembling amyloid in sequence can integrate into pathogenic amyloid fibrils, forming mixed amyloid and serving as potent inhibitors of amyloid formation (Cheng et al., 2012; Eskici & Gur, 2013; Sato et al., 2006). My *in vitro* data suggest that SRCP1<sup>61-80</sup> directly interacts with Htt<sup>Q46</sup> *in vitro* to inhibit amyloid fibril formation. Additionally, I discovered that SRCP1<sup>61-80</sup> decreases the rate of Htt<sup>Q46</sup> amyloid formation, but amyloid fibrils still form after 72 h *in vitro*. However, the morphology of fibrils at 72 h is noticeably different with or without peptide (Figure 10A). This observation may be a result of SRCP1<sup>61-80</sup> integrating into the fibrils and forming mixed amyloid.

## ***2.3 Materials and Methods***

### **Huntingtin Exon-1 46Q Purification**

Thioredoxin-tagged huntingtin exon-1 with 46 glutamines (Htt<sup>Q46</sup>) in pET-32 was obtained from Addgene (Plasmid #11515). Htt<sup>Q46</sup> was grown in BL21 cells at 37°C to an OD<sub>600</sub> of 0.6 and induced with IPTG at 1 mM overnight at 16°C. After induction, cells were

spun down at 7,000 rpm for 5 min and resuspended in resuspension buffer (15 mM Tris-HCl buffer, pH 8.0). For lysis, lysozyme was added and cells were incubated at 4°C for 45 min. To obtain soluble fraction, lysates were spun down at 12,000 rpm for 10 min, after which supernatant was added to 3 mL of nickel beads (GoldBio) per 100 mL of lysate and tumbled for 4 h at 4°C. Beads were then washed three times with resuspension buffer and then washed three more times with wash buffer (50 mM Tris-HCl pH 8.0, 150 mM NaCl, 1 mM PMSF, 1 mM EDTA). Protein was then eluted off beads by tumbling overnight at 4°C in 25 mL of wash buffer with 250 mM imidazole.

#### **Thioflavin T Aggregation Assay**

Aggregation assays were performed as previously described (Kakkar et al., 2016). Briefly, 15  $\mu$ M Htt<sup>46Q</sup> was mixed with indicated molar ratios of SRCP1 peptide (GenScript; 1:6, 1:3, 1:1.5 ratios) and 10  $\mu$ M Thioflavin-T (Sigma-Aldrich). All samples were prepared on ice in buffer containing 20 mM Tris-HCl pH 8.0, 50 mM NaCl, 2 mM CaCl<sub>2</sub>. Enterokinase (New England BioLabs) was added at 1.6 units/50  $\mu$ L sample to initiate aggregation. All samples were prepared on ice and 50  $\mu$ L aliquots were transferred to a flat, black 384-well plate and allowed to aggregate at 37°C for 16–18 hr. Fluorescence was measured with the excitation at 440 nm and emission at 480 nm every 5 min using a Tecan Spark plate reader.

### **Filter-Trap Assay**

For filter-trap assays, Htt<sup>46Q</sup> was used at a concentration of 15  $\mu$ M alone or with 90  $\mu$ M of SRCP1 peptide. Peptide alone was used at 50  $\mu$ M. All samples were prepared on ice in buffer containing 20 mM Tris-HCl pH 8.0, 50 mM NaCl, 2 mM CaCl<sub>2</sub>. Enterokinase at 1.6 units/50  $\mu$ L sample was added to initiate the reactions and samples were allowed to aggregate at 37°C for 5 and 72 h. Approximately 40  $\mu$ g of protein sample were then used for filter-trap assay. Protein was diluted up to 90  $\mu$ L with NETN. Ten  $\mu$ L of 10% SDS was added to sample and diluted to 1 mL with 1% SDS in 1X PBS and filtered through a 0.2 mm cellulose acetate membrane filter (Sterlitech) using a DHM-48 filter-trap hybridization manifold. Membrane was then washed with 1 mL of 1% SDS in 1X PBS and analyzed by western blotting (Scherzinger et al., 1999; Wanker et al., 1999).

### **Dynamic Light Scattering (DLS)**

For dynamic light scattering (DLS) measurements, Htt<sup>46Q</sup> was used at a concentration of 15  $\mu$ M alone or with 90  $\mu$ M of SRCP1 peptide. Peptide alone was used at 50  $\mu$ M. All samples were prepared on ice in buffer containing 20 mM Tris-HCl pH 8.0, 50 mM NaCl, 2 mM CaCl<sub>2</sub>. Enterokinase at 1.6 units/50  $\mu$ L sample was added to initiate the reactions and samples were allowed to aggregate at 37°C for 5 and 72 hr. Following aggregation, 10  $\mu$ L of sample was loaded into a Hellma Analytics QC High Precision Cell Quartz Suprasil Cuvette (cuvette model #ZMV1002, light path of 1.25  $\times$  1.25 mm). DLS measurements were collected at 25°C by using a Malvern Zetasizer  $\mu$ V with a 50 mW laser

at 830 nm, using a detector angle of 90°. The laser power was set to 30% power and integration time was set to 100 s. Each measurement consisted of 50–60 collections and are representative of  $n = 2$ , where each  $n$  consisted of at least 2 technical replicates. DLS spectra were analyzed and visualized in R (Team, 2016) by using the tidyverse (Wickham, 2017), scales (Wickham, 2016), and direct labels (Hocking, 2017) packages.

### **Electron Microscopy (EM)**

For EM, samples were prepared on ice in buffer containing 20 mM Tris-HCl pH 8.0, 50 mM NaCl, 2 mM CaCl<sub>2</sub>. Htt<sup>46Q</sup> was used at a concentration of 30  $\mu$ M alone or with 174  $\mu$ M of SRCP1 peptide. Peptide alone was used at 50  $\mu$ M. Enterokinase at 2.2 units/sample was added to initiate the reactions and samples were allowed to aggregate at 37°C for 5 and 72 hr.

Following aggregation assays, freshly ionized 400mesh Formvar/carbon coated copper grids were floated onto 10  $\mu$ L droplets of sample for 2 min to allow adsorption of the sample to the grid. After adsorption, the sample was then wicked away from the edge of grid surface and the grid was immediately floated on the droplet of negative stain (2% aqueous uranyl acetate) for 1 min. The stain was wicked away from the edge of the grid and the grid was then allowed to air dry. Samples were examined by a Hitachi H600 TEM.

### 3. Elucidating structural properties and mechanisms of SRCP1

SRCP1's C-terminal domain of amino acids 61-70 is essential for its ability to suppress polyQ aggregation (Santarriaga et al., 2018). But how SRCP1 suppresses polyQ aggregation through this domain is not understood. We have been unable to identify SRCP1 homologs in other organisms, suggesting it may be a *Dictyostelium*-specific inhibitor of polyQ aggregation. Additionally, no information exists about the structure of SRCP1, and delineating its structure would provide information about its mechanism of suppressing polyQ aggregation.

I wanted to investigate both SRCP1's structure and mechanism to inhibit polyQ aggregation. I first attempted to solve SRCP1's structure to better understand its function. Unfortunately, I was unable to purify recombinant protein for structural studies because SRCP1 was insoluble in multiple systems. Instead, I turned to computational protein modeling in tandem with experimental approaches to gain insight into SRCP1's structural layout. From this, we generated an ensemble of *de novo* models that predict SRCP1's C-terminus to form a  $\beta$ -hairpin structure while the serine-rich N-terminus is highly dynamic. To determine if this  $\beta$ -hairpin region is important, I generated a series of peptides mimicking this C-terminal region and demonstrated that amino acids 61-70 comprise the minimal active sequence that is sufficient to suppress polyQ aggregation. Additionally, expression of a truncated version of SRCP1 containing only the predicted

$\beta$ -hairpin region is sufficient to suppress polyQ aggregation in human cells. Finally, to demonstrate that this peptide is not restricted to suppressing mutant Htt, I found that this region is sufficient to suppress another polyQ-expanded protein, ataxin-3 (ATXN3). Together, these data give structural and functional information for SRCP1 and may provide insight towards developing therapeutics to treat neurodegenerative diseases.

### ***3.1 Recombinant SRCP1 is insoluble and cannot be purified***

In order to understand a protein's function, it is critical to learn about its structure. The most accurate method of structure determination is by purification of recombinant protein and subjecting the purified protein to techniques such as X-ray crystallography, nuclear magnetic resonance (NMR) spectroscopy, or cryo-TEM. The main caveat to these techniques is the necessity of very pure, soluble recombinant protein at a high concentration.

The first step I took to determine SRCP1's structure was to purify recombinant SRCP1 protein for structural studies. I used multiple protein purification systems, including *Dictyostelium*, *E. coli*, cell-free expression systems, and insect cells, to attempt SRCP1 purification. Here, I show that despite repeated attempts in multiple systems, I was unable to recover any soluble SRCP1 protein and therefore was unable to perform structural analysis.

### 3.1.1 *Dictyostelium* purification method

SRCP1 is a unique chaperone that is specific to *Dictyostelium*. Because of this specificity, we first wanted to determine if SRCP1 could be purified directly from *Dictyostelium*. Protein purification from *Dictyostelium* has not been widely performed in the field. Attempts at SRCP1 purification from *Dictyostelium* had been made by previous lab members with no positive results (data not shown). I decided to proceed with small-scale pulldowns using either a GFP- or FLAG-tagged version of SRCP1 being overexpressed in *Dictyostelium* AX4 cells. The elutions (E1 and E2) and boiled beads from

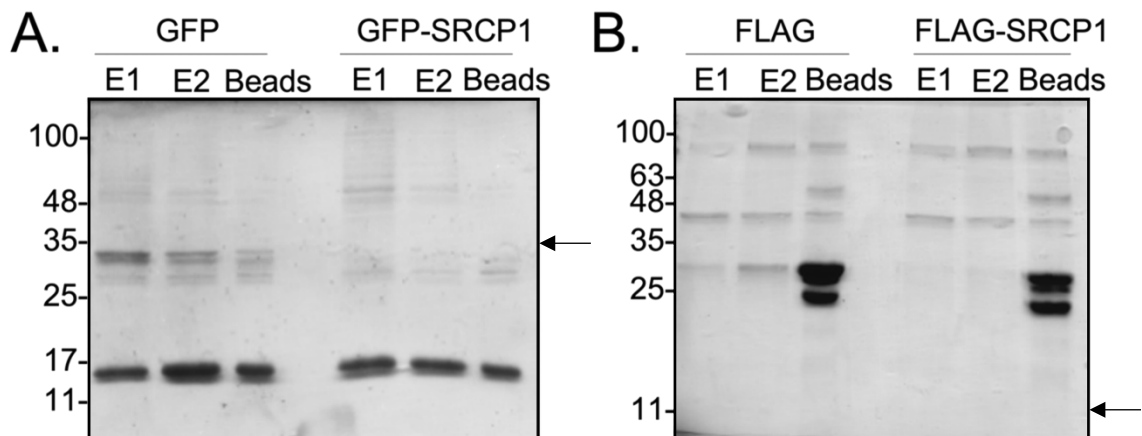


**Figure 12: SRCP1 is not pulled down from *Dictyostelium* lysates.**

(A) 8xHis-GFP or 8xHis-GFP-SRCP1 were expressed in AX4 cells. Cells were collected, lysed, and subjected to pulldown on Nickel beads. Protein was eluted twice with imidazole (E1 and E2) and beads were then boiled in 1X Laemmli buffer and ran on an SDS-PAGE gel. Coomassie stains are shown. Arrow indicates expected size of GFP SRCP1. (B) FLAG or FLAG-SRCP1 were expressed in AX4 cells. Cells were collected, lysed, and subjected to pulldown on FLAG-epitope beads. Protein was eluted twice with 3X-FLAG peptide (E1 and E2) and beads were then boiled in 1X Laemmli buffer and ran on an SDS-PAGE gel. Coomassie stains are shown. Arrow indicates expected size of FLAG-SRCP1.

the pulldowns of both the controls (GFP or FLAG) and SRCP1 samples resulted in similar banding patterns, with no bands corresponding to either GFP-SRCP1 (35 kDa) or FLAG-SRCP1 (11 kDa) (Figure 12). This suggests that SRCP1 was either not present or not visible on the gel. These results are not surprising since we determined that SRCP1 is rapidly degraded by the proteasome, and bands the size of GFP- or FLAG-SRCP1 may not be visible due to their rapid proteosomal degradation in *Dictyostelium* (Santarriaga et al., 2018). If SRCP1 is being degraded too quickly for detection, the purification would have to proceed under proteasome inhibition. Extended periods of proteasome inhibition is toxic to cells and would make it difficult to obtain high concentrations of protein due to cell death. Alternatively, recombinant SRCP1 could be cleaved by the many proteases naturally present in *Dictyostelium* cells, making it difficult to purify. Therefore, I turned to other methods of protein purification.

### **3.1.2 Bacterial purification method**

One of the most common ways to express recombinant protein is in a bacterial system such as *E. coli*. This is done by cloning a gene of interest into a bacterial expression vector with a lactose operon to control protein expression. Protein expression is induced by either lactose or the non-hydrolysable lactose analog, isopropyl- $\beta$ -D-1-thiogalactopyranoside (IPTG). After induction, cells can then be lysed and protein collected and purified. Limitations to this method include a lack of post-translational

modifications, such as glycosylation, and the possibility of the recombinant protein going into inclusion bodies.

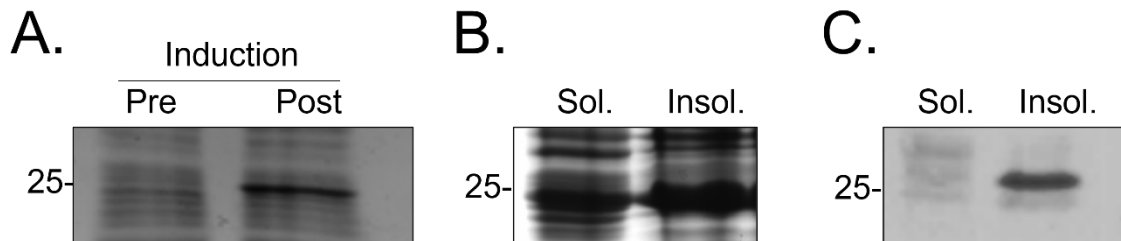


**Figure 13:**  $6xHisSRCP1^{SUMO}$  is insoluble in *E. coli*.

(A) Rosetta *E. coli* expressing  $6xHisSRCP1^{SUMO}$  were induced for 1.5 h with 1 mM IPTG prior to collection. Pre- and post-induction are shown via Coomassie stain. (B) Coomassie stain of soluble (Sol.) and insoluble (Insol.) fractions of  $6xHisSRCP1^{SUMO}$ . SRCP1 is present mainly in the insoluble fraction. (C) Western blot against the 6x-His tag confirms that SRCP1 is in the insoluble fraction of the cell lysate.

Previous lab members had attempted SRCP1 expression in *E. coli* with no positive results (data not shown). I chose to clone SRCP1 into multiple bacterial expression vectors with purification different tags. I first decided to use was a construct of SRCP1 with an N-terminal 6x-Histidine (His) tag for purification and a C-terminal SUMO tag to aid in detection and solubility. Because SRCP1 contains a predicted amyloid-forming domain, I wanted to determine if SRCP1 induced in bacteria would be soluble. I separated the soluble and insoluble fractions of the cell lysate and performed SDS-PAGE. Coomassie staining clearly shows the majority of SRCP1 generated in *E. coli* is present in the insoluble fraction, presumably in inclusion bodies (Figure 13).

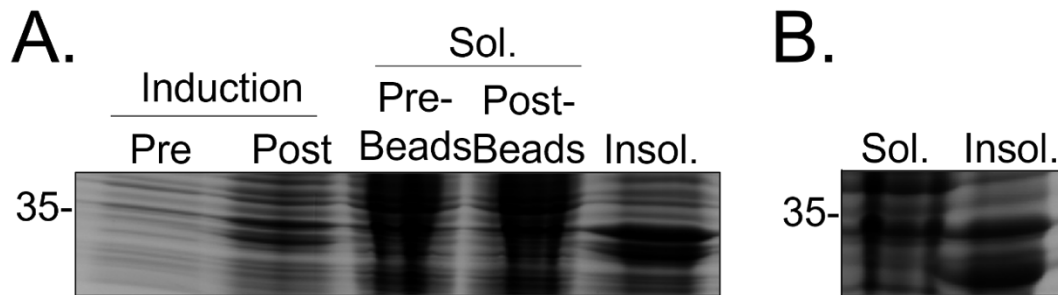


**Figure 14: GST-SRCP1 is insoluble in *E. coli*.**

(A) BL21 *E. coli* cells expressing <sup>GST</sup>SRCP1 were induced for 6 h with 0.01 mM IPTG. Cells were collected, lysed, and fractionated under normal GST-purification conditions, were subjected to SDS-PAGE, and Coomassie stained. SRCP1 is mainly present in the insoluble fraction. (B) BL21 *E. coli* cells expressing <sup>GST</sup>SRCP1 were induced for 6 h with 0.01 mM IPTG. Cells were collected, lysed, and fractionated under denaturing conditions, were subjected to SDS-PAGE, and Coomassie stained. SRCP1 is again primarily present in the insoluble fraction.

To improve solubility, I utilized a glutathione-S-transferase (GST) fusion version of SRCP1. This larger purification tag is very stable and can aid in solubility of proteins. I lysed and fractionated the cells after induction and found that <sup>GST</sup>SRCP1 also was sequestered to inclusion bodies (Figure 14A). To see if SRCP1 could be solubilized by a denaturant, I lysed cells in the presence of 8 M urea and separated the soluble and insoluble cell fractions. Unfortunately, even 8 M urea was not able to solubilize <sup>GST</sup>SRCP1 (Figure 14B).

One way to improve and maintain protein solubility of a protein is by utilizing certain buffer additives (Churion & Bondos, 2012). To potentially improve solubility of <sup>GST</sup>SRCP1 in the crude cell lysate, I followed a previously published protocol describing the determination and optimization of additives appropriate for a protein of interest

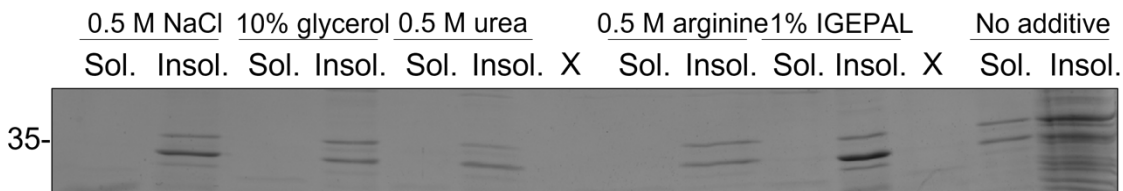


**Figure 15: Buffer additives do not increase solubility of <sup>GST</sup>SRCP1.**

Crude cell lysates were incubated with either 0.5 M NaCl, 10% glycerol, 0.5 M urea, 0.5 M arginine, or 1% IGEPAL and run through a centrifugal filter to separate soluble and insoluble fractions. Fractions were subjected to SDS-PAGE and Coomassie staining. SRCP1 remained in the insoluble fraction for all additives. “X” denotes a skipped lane.

(Churion & Bondos, 2012). Initially, I wanted to identify a buffer additive that would improve <sup>GST</sup>SRCP1 solubility. I tested the following additives: high concentration of NaCl, glycerol, urea, arginine, or IGEPAL. After incubating crude lysates expressing <sup>GST</sup>SRCP1 with the different additives, I filtered the lysate via centrifugation to separate the soluble and insoluble fractions. Coomassie staining showed that none of the additives were sufficient to keep <sup>GST</sup>SRCP1 soluble (Figure 15). It was unlikely at this point that I would obtain soluble SRCP1 from bacteria, so I decided to use other protein purification methods.

### 3.1.3 Cell-free purification method

Cell-free protein purification methods can be useful if a protein of interest does not behave in a foreign cell system. This includes the formation of inclusion bodies in bacterial cell systems or if protein function depends on post-translational modifications. There are several types of cell-free systems including plant, mammalian, and bacterial

lysates. Unfortunately, cell-free kits are expensive and protein purification from these expression systems is normally done on a small scale, generating only small amounts of pure protein.

I used an *E. coli* cell-free kit to perform a small-scale expression of SRCP1 as well as a control. Compared to the negative control, expression of the control protein expressed clearly (Figure 16, yellow arrow). For SRCP1, I added three vectors with SRCP1 cloned in to separate lysates. Both pQE30 and pET47b(+) SRCP1 were expected to express at ~25 kDa, while pGEX-6P1 SRCP1 was expected to be ~35 kDa. For each of these samples, there was not a clear expression band that appeared. I therefore did not pursue this expression method.

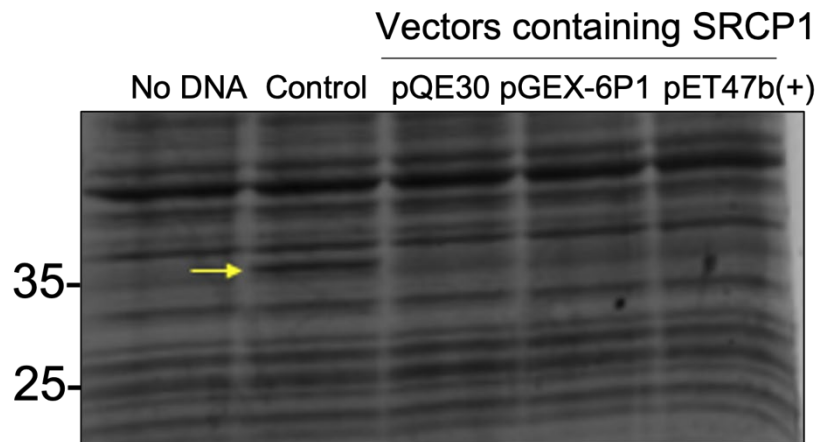


**Figure 16: SRCP1 does not express in a cell-free *E. coli* system.**

*E. coli* cell lysates were incubated with no DNA, control DNA, or SRCP1 DNA in either pQE30 (25 kDa), pGEX-6P1 (35 kDa), or pET47b(+) (25 kDa) vectors. Only the control protein expressed (yellow arrow).

### 3.1.4 Insect cell purification method

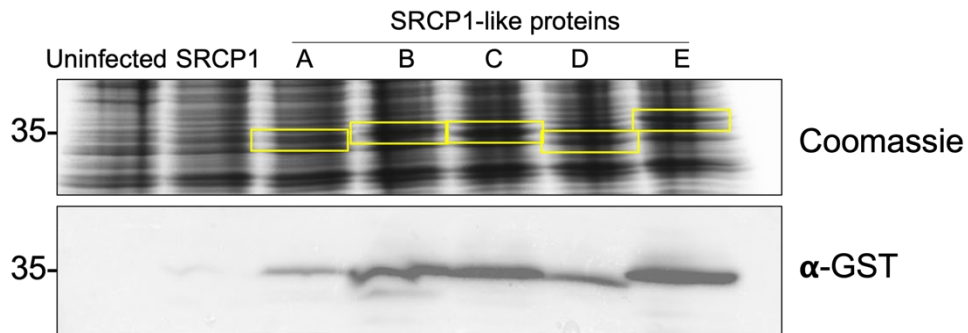


**Figure 17: SRCP1-like proteins can be expressed in SF9 cells.**

SF9 cells were infected with baculovirus containing SRCP1 or SRCP1-like proteins (A-E). All SRCP1-like proteins were detectable by Coomassie stain (top, yellow boxes) and western blot (bottom). SRCP1 was undetectable in both cases.

The final system I utilized to express and purify SRCP1 was SF9 insect cells. Insect cells are useful in that they can glycosylate proteins (similar to mammalian systems) and they are more likely to keep proteins soluble and functional, with no risk of inclusion body formation.

I cloned SRCP1 and five other SRCP1-like proteins (SRCPA-E) from *Dictyostelium* into the baculovirus vector GST-pFastBac1. I produced baculovirus for all of the SRCP1-like proteins and they expressed well, with the exception of SRCP1 (Figure 17). From these data, I focused my efforts on the SRCP1-like proteins since their sequences are highly similar to SRCP1 (Figure 18). In order to purify these proteins for structural studies, I cloned an H3c site into the GST vector to cleave the GST tag and produced baculovirus for expression. Two of the proteins, SRCP1-like B and C (SRCPB and SRCP C,

```

SRCP1 1  MTLSTFTSFNSPP-KLNKSSFSSSTGSLSMGSN---SFAW-GGWGGFGGPKGG-----SFNVDIAGNLI 62
SRCPA 1  MTLASISSIGNVK-SISKSNFSSLSNSSLQSSN---SIQC-GG-CGGGSPLIgTVGnlvGGVLVGTGIIVGTVVGTVN 74
SRCPB 1  MSILSALTSISNPM-KSSKSSVANGG-GRLSMGSN---SVAC-GS-CGGGSSSSGTINnadGSKTTYTYTSPiYTYNYS 73
SRCPC 1  MTLFSSISSISNPM-TSSKSSIASFG-SGTSMGSN---SIAC-GGCGGSDGILGL----GL----GLSLGLGLNLNT 65
SRCPD 1  MSLLSALTSISKPMnTSSKSSVSSKNVSGLSMGSN---SIAC-GS-CGGSYGYPGA-----GLLAIVDLNVNIDIDINLS 70
SRCPE 1  MTIFNSISSITNST-HSNRSLIAISNQGLVNVNnnnSITCfDGCCGS----GNTN-----INIDIDIDKL 64

SRCP1 63  WGVY---GFIRGGVGL--VKWRGLQKGCKQP* 89
SRCPA 75  GVVGgLLSGPNCGCH*----- 90
SRCPB 74  YSYsSGSSSCGCH*----- 89
SRCPC 66  -----GSSRSRGGCGGsnGSMGGNGSCCGI* 92
SRCPD 71  -----ATRSYSCGCN*----- 81
SRCPE 65  PTSM-MTtTnIDIKInnIYVSTSTTIKST* 95

```

**Figure 18: Sequence alignment of SRCP1 and SRCP1-like proteins.**

Sequence alignment of SRCP1 and five SRCP1-like proteins (SRCPA-E) was performed in NCBI COBALT with a 2-bit relative entropy threshold (Papadopoulos & Agarwala, 2007). Columns with no gaps are colored in either red, to indicate highly conserved columns, or blue, to indicate less conserved columns.

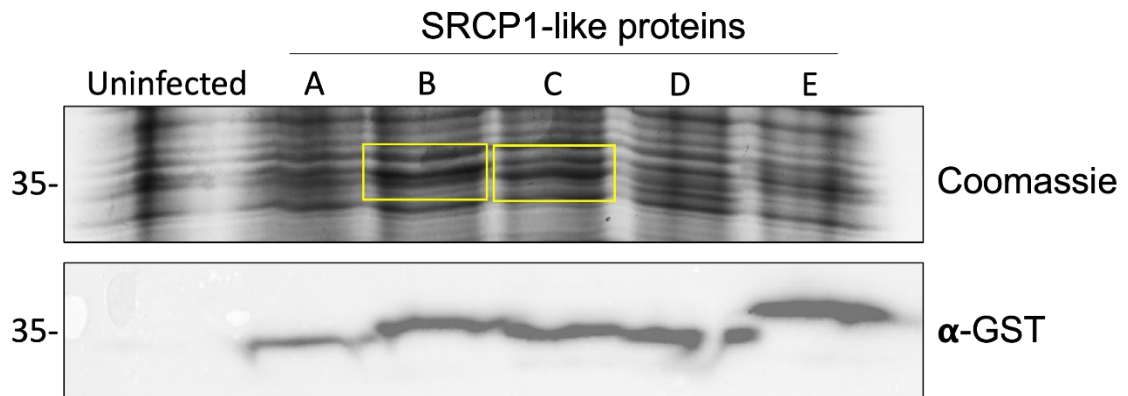


**Figure 19: GST-H3c-SRCP1-like proteins express in SF9 cells.**

SF9 cells were infected with baculovirus containing SRCP1-like proteins A-E. SRCPB and C were detectable by Coomassie stain (top, yellow boxes), while all were detectable by western blot (bottom). SRCPB was chosen for purification.

respectively), expressed better than the other three and were visible by Coomassie stain (Figure 19). For purification experiments, I used the protein that expressed the best, SRCPB (Figure 19, lane 3). My initial GST-purification revealed that SRCPB did not bind

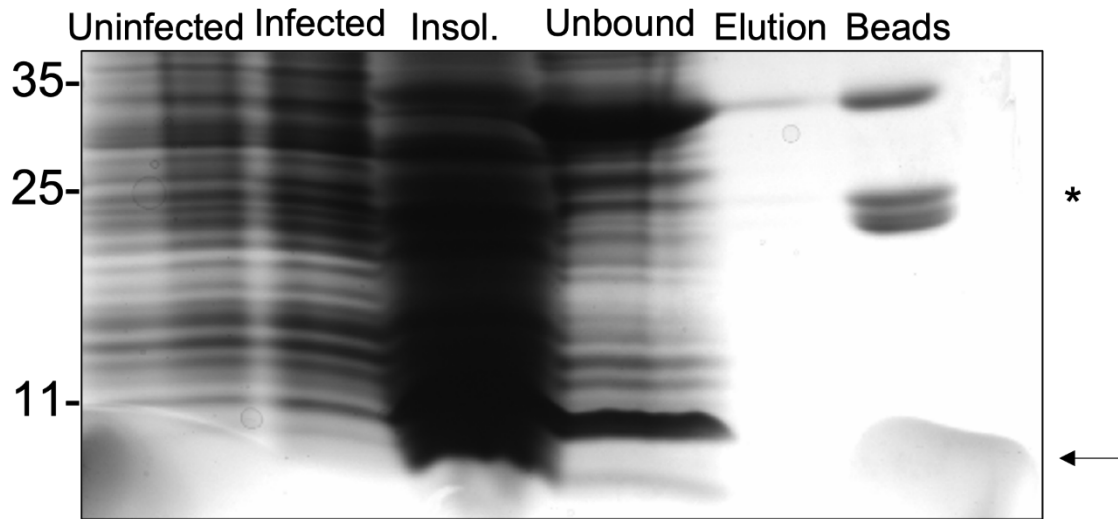


**Figure 20: GST-H3c-SRCPB is unable to bind to beads due to competing GBPs.**

SF9 cells were infected with baculovirus containing SRCPB and lyates were subjected to GST purification. The majority of SRCPB remained unbound (~35 kDa). There was no detection of H3c-cleaved SRCPB in the elution, but there was a smear in the boiled beads around the correct size (~10 kDa, denoted by arrow). Endogenous GBPs present in SF9 cells were pulled down by the GST beads (denoted by asterisk), outcompeting SRCPB.

to the beads (band at ~35 kDa), and elution via H3c cleavage did not result in a band of the correct size (~10 kDa) in the elution lane (Figure 20). There is a smear ~11 kDa detectable by Coomassie stain in the boiled beads lane that could be SRCPB, but that observation suggests that the protein that was cleaved had precipitated upon cleavage (Figure 20, lane 6, denoted by arrow). In addition, a doublet was present in the boiled beads lane ~25 kDa in size (Figure 20, lane 6, denoted by asterisk). These bands are glutathione-binding proteins (GBPs) that are endogenous to insect cell lines (Bichet et al., 2000). GBPs have been reported to be GST-like enzymes with high affinity for GST beads and will outcompete the GST fusion protein (Bichet et al., 2000). I was unable to remove

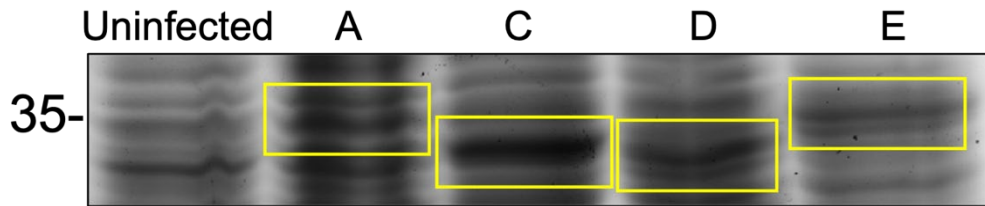


**Figure 21: 6x-His-GST-H3c-SRCP1-like proteins express in SF9 cells.**

SF9 cells were infected with baculovirus containing SRCP1-like proteins A, C, D, or E. All were detectable by Coomassie stain (yellow boxes). SRCPC was chosen for purification.

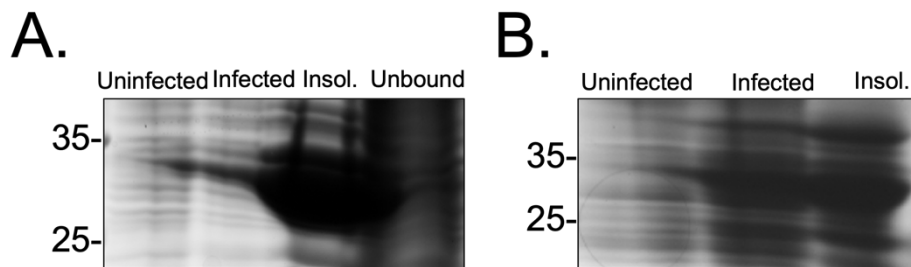


**Figure 22: 6x-His-GST-H3c-SRCPC is insoluble under denaturing conditions.**

(A) SF9 cells were infected with baculovirus containing SRCPC and underwent nickel purification. SRCPC was present in the insoluble fraction (Insol.) after lysis. (B) SF9 lysate expressing SRCPC was subjected to 8 M urea to solubilize the protein. SRCPC remained in the insoluble fraction.

the contaminating GBPs, so I cloned a 6x-His tag into the GST vector with each SRCP1-like protein in order to perform a nickel purification and eliminate GBP contaminants. After producing baculovirus for the 6x-His-GST-H3c-SRCP1-like proteins, I found that SRCPC expressed the best (Figure 21). I proceeded with nickel purification of SRCPC. Coomassie staining clearly showed that SRCPC remained insoluble (Figure 22A). I finally wanted to determine if SRCPC could be solubilized by 8 M urea. Unfortunately, it

remained insoluble under denaturing conditions, suggesting that this protein cannot be purified (Figure 22B).

## ***3.2 Mechanistic insight into the suppression of polyglutamine aggregation by SRCP1<sup>1</sup>***

### **3.2.1 Generating a structural model of SRCP1.**

I was unable to purify recombinant SRCP1 for structural studies, so I turned to computational modeling to generate hypothetical structures of SRCP1. We first analyzed SRCP1's amino acid sequence to predict disordered regions, hydrophobicity, and free energy of aggregation using DisEMBL, PASTA2, PrDOS, and Expasy programs. Disorder prediction revealed that residues 52-78 are predicted to be structured, while the rest of the protein has a high probability of being disordered (Figure 23A, prediction performed by Michael Wedemeyer). I next confirmed that residues 59-82 are highly hydrophobic due to their positive hydrophobicity scores (Figure 23B) (Kyte & Doolittle, 1982). Finally, residues 48-81 are predicted to promote SRCP1 self-aggregation (Figure 23C, prediction performed by Michael Wedemeyer). Notably, the functional sequence of SRCP1, residues 61-80, is within this region.

---

<sup>1</sup> Chapter 3.2 is adapted with permission from the published article:

Haver, HN, Wedemeyer, M, Butcher, E, Peterson, FC, Volkman, BF, and Scaglione, KM. (2023). Mechanistic insight into the suppression of polyglutamine aggregation by SRCP1. *ACS Chem. Biol.* 18(3):549-560. <https://doi.org/10.1021/acscchembio.2c00893>

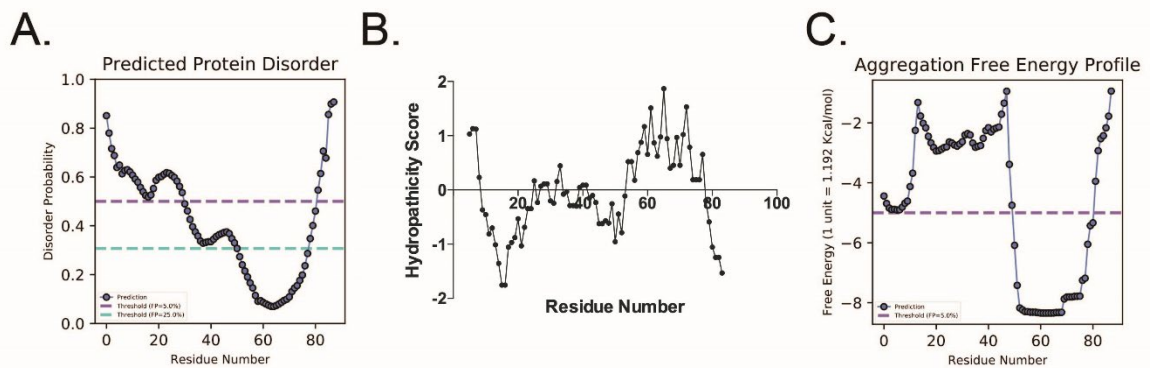


**Figure 24: A C-terminal region of SRCP1 is predicted to be structured and have a propensity to self-aggregate.**

(A) Probability of SRCP1 residues predicted to be disordered (analysis performed by Michael Wedemeyer). (B) Hydrophobicity profile of SRCP1 residues. (C) Calculated free energy for SRCP1 residues predicted in self-aggregation (analysis performed by Michael Wedemeyer). (Haver et al., 2023)

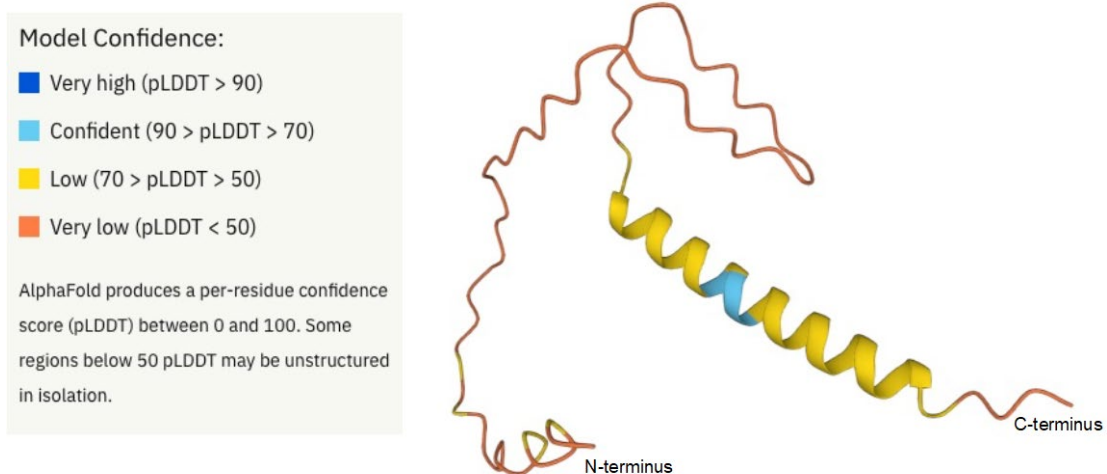


**Figure 23: AlphaFold predicts SRCP1 structure with low confidence.**

Predicted structure of SRCP1 generated by AlphaFold. The model confidence is predicted to be low to very low for the majority of the protein sequence [REF].

I next utilized AlphaFold for structure prediction to initially analyze SRCP1's structure (Jumper et al., 2021; Varadi et al., 2021). However, AlphaFold predicts structure

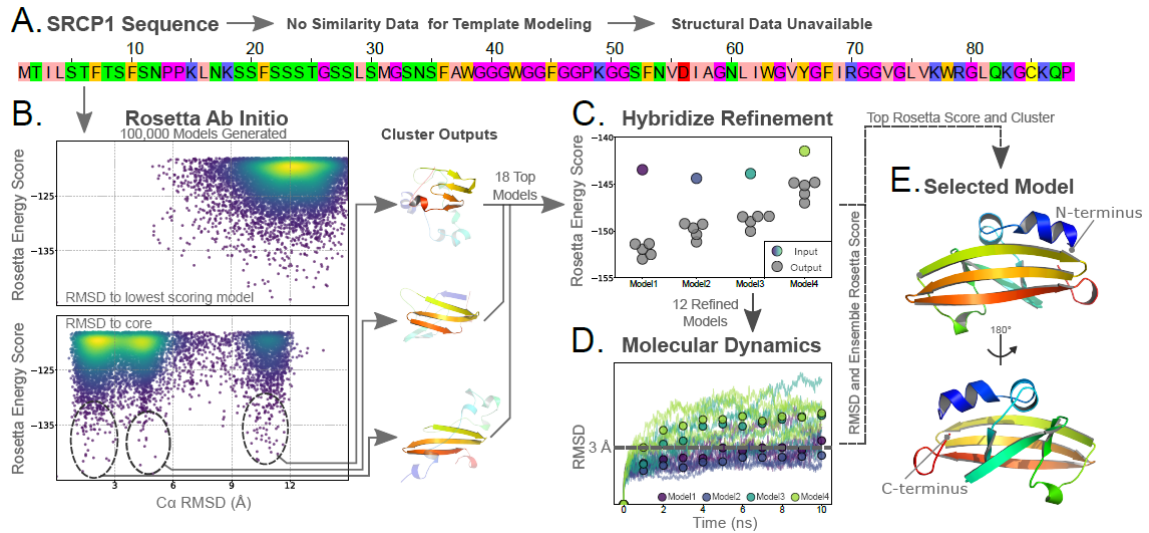


**Figure 25: Computational modeling of SRCP1 predicts a largely disordered N-terminal region and a  $\beta$ -sheet rich C-terminal region.**

(A) SRCP1's amino acid sequence was used for similarity and co-evolutionary analysis. No similar structural data was found to use for template modeling. (B) Rosetta's Ab Initio protocol was utilized to predict de novo protein models from the amino acid sequence in A. Models were plotted as Rosetta energy score vs.  $C\alpha$  RMSD to the lowest scoring model (top) or  $C\alpha$  RMSD to the "core" residues predicted to be structured (bottom). Each dot represents one model. Models were clustered according to similar  $C\alpha$  RMSD and the lowest energy clusters (circled) were chosen for further analysis. (C) The top 18 models were chosen from the clusters and refined through the Rosetta Hybridize protocol. After hybridization, models were in a more relaxed conformation, as denoted by a lower Rosetta energy score. (D) The top 12 refined models from hybridization were chosen for molecular dynamics simulations. Models with lower RMSD over time were predicted to be the most stable models. (E) Initial model selected for experimental validation. (Performed by Michael Wedemeyer.) (Haver et al., 2023)

using sequence similarity and homologous proteins whose structures have been solved.

My AlphaFold-generated model was similar to the one published in the AlphaFold Protein Structure Database and had a large predicted error, with most residues evaluating at low or very low confidence (Figure 24). Because of this, we instead utilized the Rosetta

software suite and molecular dynamic simulations to predict the tertiary structure of SRCP1 (Figure 25, modeling performed by Michael Wedemeyer). We first performed a sequence similarity search and co-evolutionary analysis to identify homologous proteins that could be utilized for comparative modeling. This search found no homologous templates or similar sequences that could guide model production (Figure 25A). Therefore, we began modeling with the Rosetta ab initio protocol to generate structural models from SRCP1's amino acid sequence. We initially generated 100,000 models that were relaxed and clustered via C $\alpha$  root-mean-square deviation (RMSD) (Figure 25B). The best scoring models and clusters were refined using Rosetta hybridization and then further relaxed (Figure 25C). Five independent 10-nanosecond molecular dynamics (MD) simulations were performed with the twelve best-scoring models (Figure 25D). Final scores were assigned using a linear combination of Rosetta energy, size of cluster, RMSD,

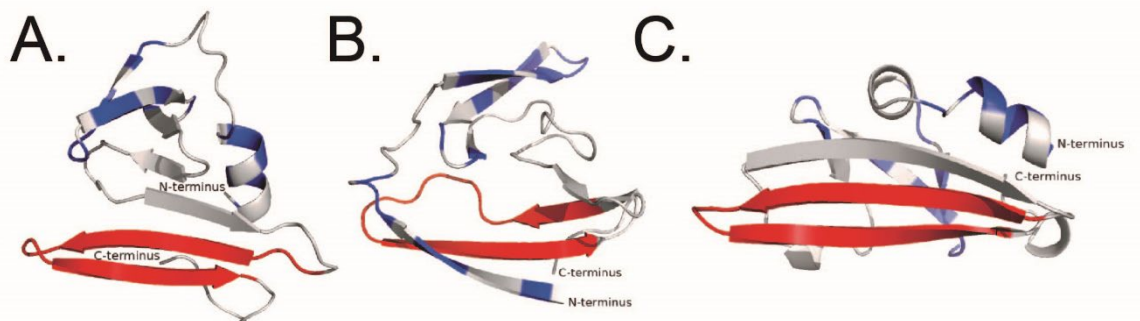


**Figure 26: SRCP1 models are predicted to form a  $\beta$ -hairpin at residues 61-80.**

(A-C) Three of the top predicted models after molecular dynamics-based refinement. Serine and threonine residues (blue) and SRCP1<sup>61-80</sup> (red) are highlighted (Haver et al., 2023).

root-mean-square fluctuation (RMSF), and Rosetta-scored MD ensemble. The final selected model was used for experimental validation (Figure 25E).

Initial models revealed that all top structures have amino acid residues ~61-80 arranged in two antiparallel beta-strands (Figure 26, red). These residues were previously predicted to form an amyloid-like fold, and  $\beta$ -hairpin structures are common precursors to amyloid formation (Baumketner & Shea, 2006; Dupuis et al., 2009; Han & Wu, 2005; Santarriaga et al., 2018; Shim et al., 2009). The N-terminus, however, lacks consistent secondary structure and spatial positioning among models suggesting that it is largely disordered (Figure 25, blue and gray). These models also agree with our initial disorder and self-aggregation analysis (Figure 23). Accordingly, our data suggest that SRCP1 is a partially disordered protein with a  $\beta$ -hairpin in the C-terminal region as the main structural element.

**Table 1: *in silico* mutagenesis scanning predicted mutants and Rosetta score change prediction.**

<b>Mutation</b>	<b>Rosetta Score Change</b>	<b>Structure</b>
G47N	-9.9	Stabilizing
P48W	31.9	Destabilizing
G51I	51.6	Destabilizing
Y66R	25.2	Destabilizing
G67Y	-8.9	Stabilizing
F68K	26.7	Destabilizing
G74L	-6.9	Stabilizing

### **3.2.2 Experimental evaluation and selection of SRCP1 models.**

I next evaluated the SRCP1 models experimentally. I chose to focus experiments on the C-terminus of SRCP1 since both disorder prediction and our models predicted this

region to be structured. Additionally, the C-terminus is responsible for suppressing polyQ aggregation (Santarriaga et al., 2018). To begin validation, point mutations were generated in Rosetta for SRCP1 residues in the selected model (Figure 25E, Figure 26C). Each permutation was scored by Rosetta to predict the change in protein stability from WT (Table 1, scanning mutation analysis performed by Michael Wedemeyer). Mutations that were predicted to be the most stabilizing or destabilizing were selected for evaluation. We have shown that steady-state levels of SRCP1 are destabilized by the proteasome, so I wanted to compare the steady-state levels of SRCP1 mutants to WT in cells (Santarriaga et al., 2018). I transfected WT or mutant RFP-tagged SRCP1 (<sup>RFP</sup>SRCP1) into HEK293 cells to assess how the mutations affected protein stability. Of our mutants, I found that four mutations (P48W, G51I, G67Y, and G74L) led to a significant decrease in SRCP1 stability (Figure 27A).

Because the destabilizing mutations are near (P48W, G51I) or within (G67Y, G74L) SRCP1's functional region, I wanted to determine how these mutations affected SRCP1's ability to suppress polyQ aggregation. I co-transfected HEK293 cells with a GFP-tagged mutant huntingtin exon-1 with 74 glutamines (<sup>GFP</sup>Htt<sup>ex1Q74</sup>) and either WT or mutant <sup>RFP</sup>SRCP1 and analyzed aggregate levels of <sup>GFP</sup>Htt<sup>ex1Q74</sup>. While WT SRCP1 decreases the levels of aggregates present in the stacking gel, all four SRCP1 mutants did not significantly decrease polyQ aggregation (Figure 27B). Due to the amount of variability, I am unable to conclude whether these mutants suppress polyQ aggregation.

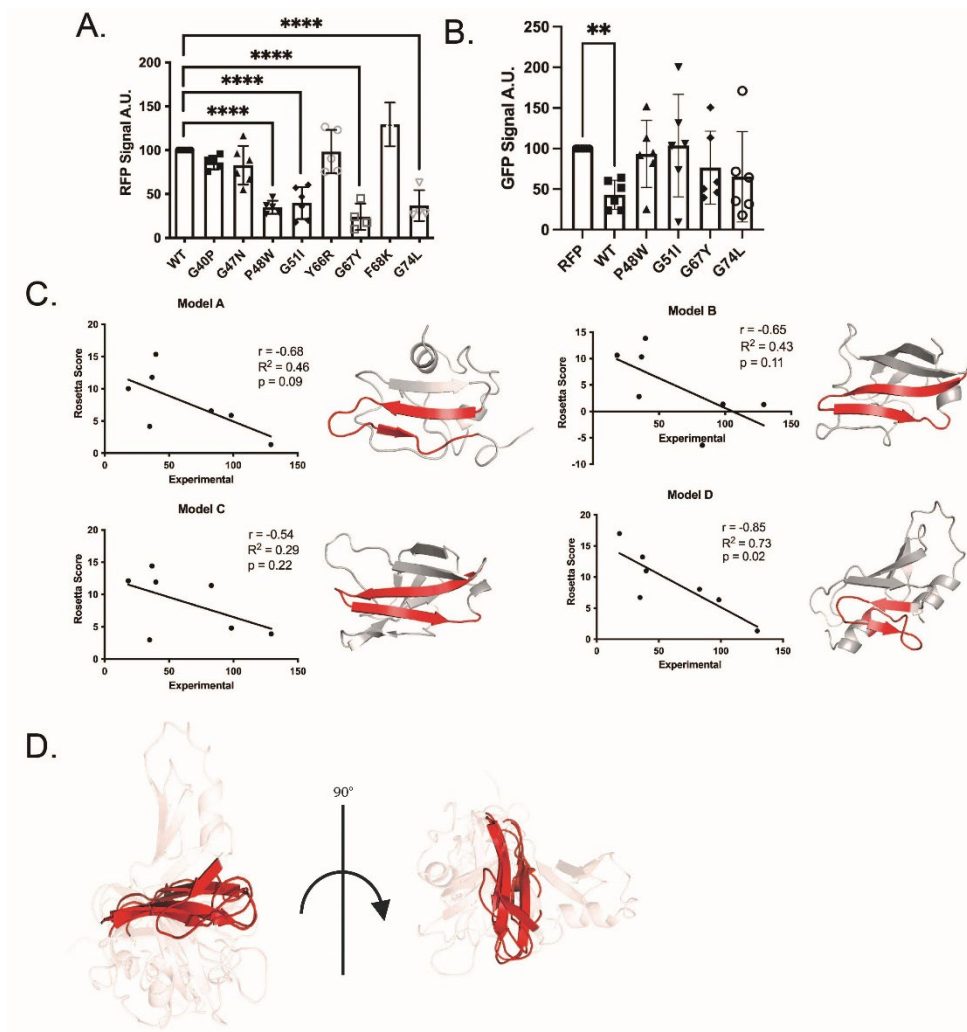


**Figure 27: Experimental evaluation of the SRCP1 model.**

*In silico* scanning mutagenesis was performed on the initial model from Fig 2C to predict key amino acids that would either increase or decrease SRCP1 stability. (A) WT or mutant <sup>RFP</sup>SRCP1 was transfected into HEK293 cells (n = 6). Samples were collected 48 h post-transfection and analyzed by western blot. Quantification of RFP signal is shown (\*\*\*\* $p < 0.0001$ ). (B) WT or mutant <sup>RFP</sup>SRCP1 was co-transfected with <sup>GFP</sup>Htt<sup>ex1Q74</sup> into HEK293 cells (n = 8). Samples were collected 48 h post-transfection and analyzed by western blot. Quantification of GFP signal is shown (\* $p < 0.05$ , \*\* $p < 0.01$ ) (C) Correlation plots showing the correlation between the average mutant signal change from WT SRCP1 and the predicted Rosetta score change for the samples in (A) and their corresponding models. SRCP1<sup>61-80</sup> (red) are highlighted (analysis performed by Michael Wedemeyer). (D) Overlay of the four models in (C), SRCP1<sup>61-80</sup> (red) is predicted to be highly conserved among models as a  $\beta$ -hairpin structure (Haver et al., 2023).

I next wanted to identify which of the models we generated most closely aligned with our experimental data. To accomplish this, we selected 31 candidate models, expanding upon our top 12 refined models to include models from each stage of refinement. We generated seven new models from each of these, each with a single mutation from Table 1. The *in silico* mutagenesis was performed using Rosetta scripts with incorporated flexibility and relaxation. The change in total Rosetta energy score for each mutant was compared to the levels of SRCP1 from our experimental data. Correlation plots were generated to determine the best fit model for the data. Four models had a moderately strong negative correlation between the predicted stability of SRCP1 and its steady-state stability in cells (Figure 27C, correlation data generated by Michael Wedemeyer). The average correlation coefficient ( $r$ ) for these four models was -0.68 with an  $R^2$  of 0.48, with our best fit model having an  $r$  value of -0.85 and a  $R^2$  of 0.73 (Figure 26C). One striking feature of all top models is that residues 61-80 are all predicted to form a  $\beta$ -hairpin (red), consistent with our previous predictions (Figures 25, 26, 27C and D) (Santarriaga et al., 2018).

Finally, we performed two-dimensional nuclear Overhauser effect (NOESY) nuclear magnetic resonance experiments on a peptide of residues 61-80 to see if we could obtain structural data. While long-range contacts defining a  $\beta$ -hairpin were present, the pattern of sequential NOE peak intensities was consistent with extended  $\beta$ -sheet-like segments linked by a turn rather than a helical conformation (Figure 28, experiments

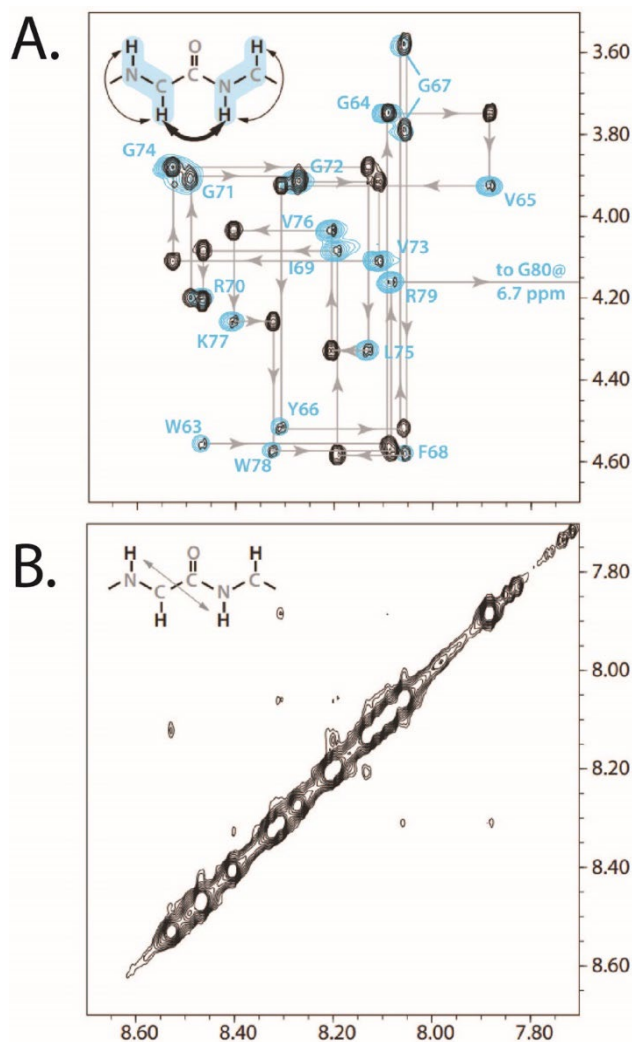


**Figure 28: NMR analysis of SRCP1<sup>61-80</sup>.**

Sequence-specific <sup>1</sup>H chemical shift assignments were deduced from 2D NOESY and TOCSY spectra acquired at 10°C in a 5 mm sample tube at 800 MHz. (A) A segment of polypeptide backbone in an extended conformation shows TOCSY (cyan shading) and NOE (black arrows) connections between HA and HN atoms. The ‘fingerprint’ region of the TOCSY spectrum containing HA-HN crosspeaks (cyan contours) is overlaid with the NOESY spectrum (black contours.) Residue assignments and sequential HA-HN NOE connections are highlighted. Throughout the peptide, the intensity of intra-residue HA-HN NOE peaks is low (black contours on top of cyan contours) in comparison to the sequential (inter-residue) HA-HN NOE peaks (black contours with no corresponding cyan contours.)

(B) The NH-NH region of the NOESY spectrum is plotted at the same contour level of the upper panel. A small number of very weak sequential NH-NH NOE peaks are visible and no strong sequential NH-NH NOEs are present. Taken together, the pattern of weak intra-residue HA-HN NOEs, strong inter-residue (sequential) HA-HN NOEs, and weak sequential NH-NH NOEs throughout the peptide is consistent with an extended (i.e. beta strand-like) conformation with no evidence of helical structure. (Experiment performed by Francis Peterson, analysis performed by Brian Volkman.) (Haver et al., 2023)

---

performed by Francis Peterson, data analysis performed by Brian Volkman). Taken together, modeling and structure-function analysis suggests the C-terminal portion of SRCP1 forms a  $\beta$ -hairpin and this structure is important for SRCP1-mediated suppression of polyQ aggregation (Santarriaga et al., 2018).

### **3.2.3 SRCP1<sup>61-70</sup> is the minimal sequence necessary for function.**

We previously found that amino acids 61-80 were important for SRCP1 function in cells and a peptide mimicking this region was sufficient to suppress aggregation of Htt<sup>ex1Q46</sup> *in vitro*. Additionally, we found that amino acids 61-70 (SRCP1<sup>61-70</sup>) had activity *in vitro* and could suppress polyQ aggregation (Santarriaga et al., 2018). Because the best-fit models of SRCP1 support our previous work with residues 61-80 forming a  $\beta$ -hairpin, I wanted to determine if improved peptides could be developed that were more potent suppressors of polyQ aggregation. To test this, peptides were synthesized that mimicked the  $\beta$ -hairpin of our SRCP1 models to test if they had a more potent effect on Htt<sup>ex1Q46</sup> aggregation (Table 2). These peptides did retain the ability to suppress polyQ aggregation, however they did not improve activity compared to SRCP1<sup>61-80</sup> (Figure 29A and B).

**Table 2: Modified peptides of SRCP1<sup>61-70</sup> or SRCP1<sup>61-80</sup> tested in polyQ aggregation assays.**

Peptide	Design Rationale
SRCP1 <sup>53-78</sup> , SRCP1 <sup>51-79</sup> , SRCP1 <sup>52-70</sup>	Peptides containing predicted $\beta$ -sheet regions from models
Truncated SRCP1 <sup>61-70</sup>	To determine minimal sequence for function
SRCP1 <sup>61-70</sup> D-amino acids	Protease resistance, increased biological potency
SRCP1 <sup>61-70</sup> sequence repeat	A second functional sequence could increase function
Cyclic SRCP1 <sup>61-80</sup>	Maintaining a stable hairpin structure to maximize activity, protease resistance

I next tested modified peptides of SRCP1<sup>61-70</sup> or SRCP1<sup>61-80</sup> to see if modifications could make an improved peptide (Table 2). I first tested peptides that were further truncated at a 6:1 peptide to Htt<sup>ex1Q46</sup> molar ratio. None of these peptides were successful at suppressing Htt<sup>ex1Q46</sup> aggregation, confirming that SRCP1<sup>61-70</sup> is the minimal sequence required for function (Figure 29C). I next tested a peptide utilizing D-amino acids, because D-amino acids are more protease resistant and can make the peptide more biologically potent. Surprisingly, SRCP1<sup>61-70</sup> made with D-amino acids did not efficiently suppress Htt<sup>ex1Q46</sup> aggregation, indicating the amino acid side chain positioning within the peptide is important for function (Figure 29D). Additionally, I tested a peptide with the 61-70 sequence repeated, hypothesizing that an additional functional sequence would more potently suppress polyQ aggregation. This peptide was functional at a 6:1 molar peptide:Htt<sup>ex1Q46</sup> ratio and was more efficient than SRCP1<sup>61-70</sup> at lower ratios (Figure 29E and F). This suggests that having a second functional sequence makes the peptide more efficient at inhibiting mutant Htt<sup>ex1Q46</sup> aggregation. Finally, I tested stapled cyclic peptides

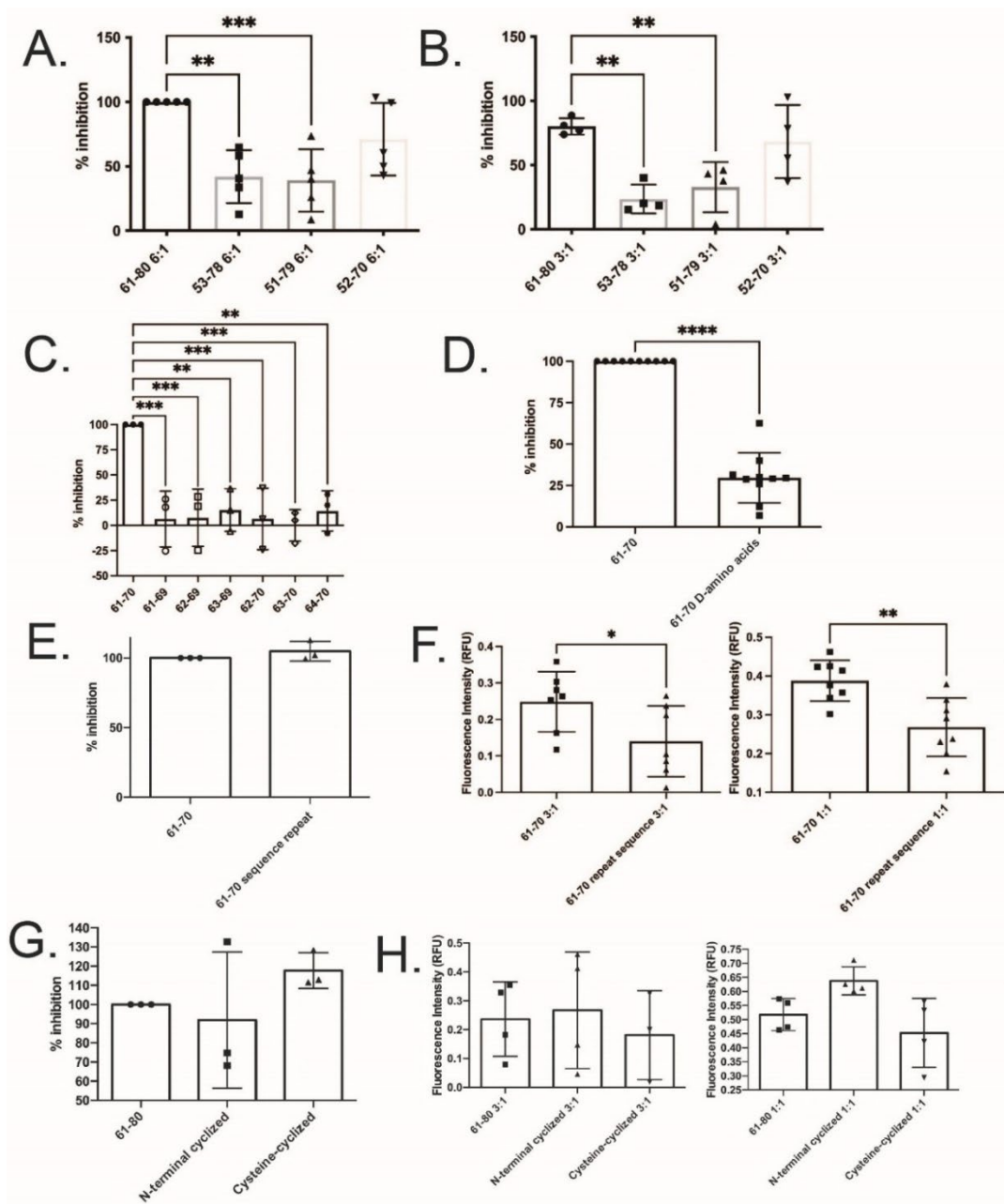


**Figure 29: Amino acids 61-70 are the minimal sequence required for SRCP1 peptide function.**

Thioflavin T (ThT) aggregation assays were carried out with peptides and huntingtin protein (Htt) at a 6:1 molar ratio (peptide:Htt) unless noted. Assays were performed with the following peptides:

(A) SRCP1<sup>61-80</sup> or peptides predicted to form beta sheets. Percent inhibition of each peptide is shown (n = 5). (B) SRCP1<sup>61-80</sup> or peptides predicted to form beta sheets at a 3:1 molar ratio. Percent inhibition of each peptide is shown (n = 4). (C) SRCP1<sup>61-70</sup> or truncated peptides. Percent inhibition of each peptide is shown (n = 3). Negative values correspond to raw fluorescence data that was higher than the control. (D) SRCP1<sup>61-70</sup> or SRCP1<sup>61-70</sup> made with D-amino acids. Percent inhibition of each peptide is shown (n = 9). (E) SRCP1<sup>61-70</sup> or SRCP1<sup>61-70</sup> sequence repeat. Percent inhibition of each peptide is shown (n = 3). (F) SRCP1<sup>61-70</sup> or SRCP1<sup>61-70</sup> repeat sequence peptides at 3:1 (left) or 1:1 (right) molar ratios. Fluorescence intensity comparison is shown here, where decreased signal equals increased inhibition (n = 8). (G) SRCP1<sup>61-80</sup> or cyclic peptides. Percent inhibition of each peptide is shown (n = 3). (H) SRCP1<sup>61-80</sup> or cyclic peptides at 3:1 (left) or 1:1 (right) molar ratio. Fluorescence intensity comparison is shown here, where decreased signal equals increased inhibition (n = 4). \*p<0.05, \*\*p<0.01, \*\*\*p<0.001, \*\*\*\*p<0.0001 (Haver et al., 2023).

---

of SRCP1<sup>61-80</sup> joined either by the N- and C-termini or by disulfide bond via added cysteines at each terminus to lock the peptide in a more stable conformation. The SRCP1<sup>61-80</sup> cyclic peptides also inhibited Htt<sup>ex1Q46</sup> aggregation at a 6:1 molar ratio but did not have significant differences at lower ratios compared to SRCP1<sup>61-80</sup> (Figure 29G and H). From these data, I concluded that the minimal sequence required for function is residues 61-70, and a tandem repeat of this sequence significantly increases the peptide's potency to suppress polyQ aggregation.

### **3.2.4 SRCP1<sup>61-80</sup> inhibits secondary nucleation of Htt<sup>ex1Q46</sup> and inhibits aggregation independent of the polyQ region.**

Now that I knew the minimal sequence necessary for function and had confidence that SRCP1<sup>61-80</sup> forms a  $\beta$ -hairpin, I wanted to determine the mechanism by

which SRCP1 inhibits polyQ aggregation. I examined the kinetic profile of mutant Htt. Amyloid aggregation into fibrils involves a series of processes that includes primary nucleation, fibril elongation, fibril fragmentation, and secondary nucleation, all which are governed by their individual rate constants (Arosio et al., 2014; Cohen et al., 2011). I analyzed the aggregation kinetics of increasing concentrations of Htt<sup>ex1Q46</sup> using AmyloFit (Figure 30A) (Meisl et al., 2016). The calculated rate constants and kinetic profiles generated from this analysis revealed that Htt<sup>ex1Q46</sup> aggregation fits with both nucleation elongation (including primary nucleation and elongation) and secondary nucleation almost equally, with secondary nucleation slightly dominating (Figure 30B and C). This data is consistent with previous findings showing near equal contributions of primary nucleation, elongation, and secondary nucleation to Htt<sup>ex1</sup> aggregation (Boatz et al., 2020; Ceccon et al., 2022; Wagner et al., 2018).

Because Htt<sup>ex1Q46</sup> aggregation involves both nucleation elongation and secondary nucleation pathways, this process is defined by the rate constants for primary nucleation ( $k_n$ ), elongation ( $k_+$ ), and secondary nucleation ( $k_2$ ). To understand the pathway through which SRCP1 inhibits, I again utilized AmyloFit to analyze aggregation data of Htt<sup>ex1Q46</sup> with increasing concentrations of SRCP1<sup>61-80</sup> and fit the kinetic parameters for the combined rate constant of both nucleation elongation ( $k+k_n$ ) and secondary nucleation ( $k+k_2$ ), as done previously in a study using A $\beta$ 42 (Belsare et al., 2022). Fitting both nucleation elongation and secondary nucleation free-fitting parameters resulted in nearly

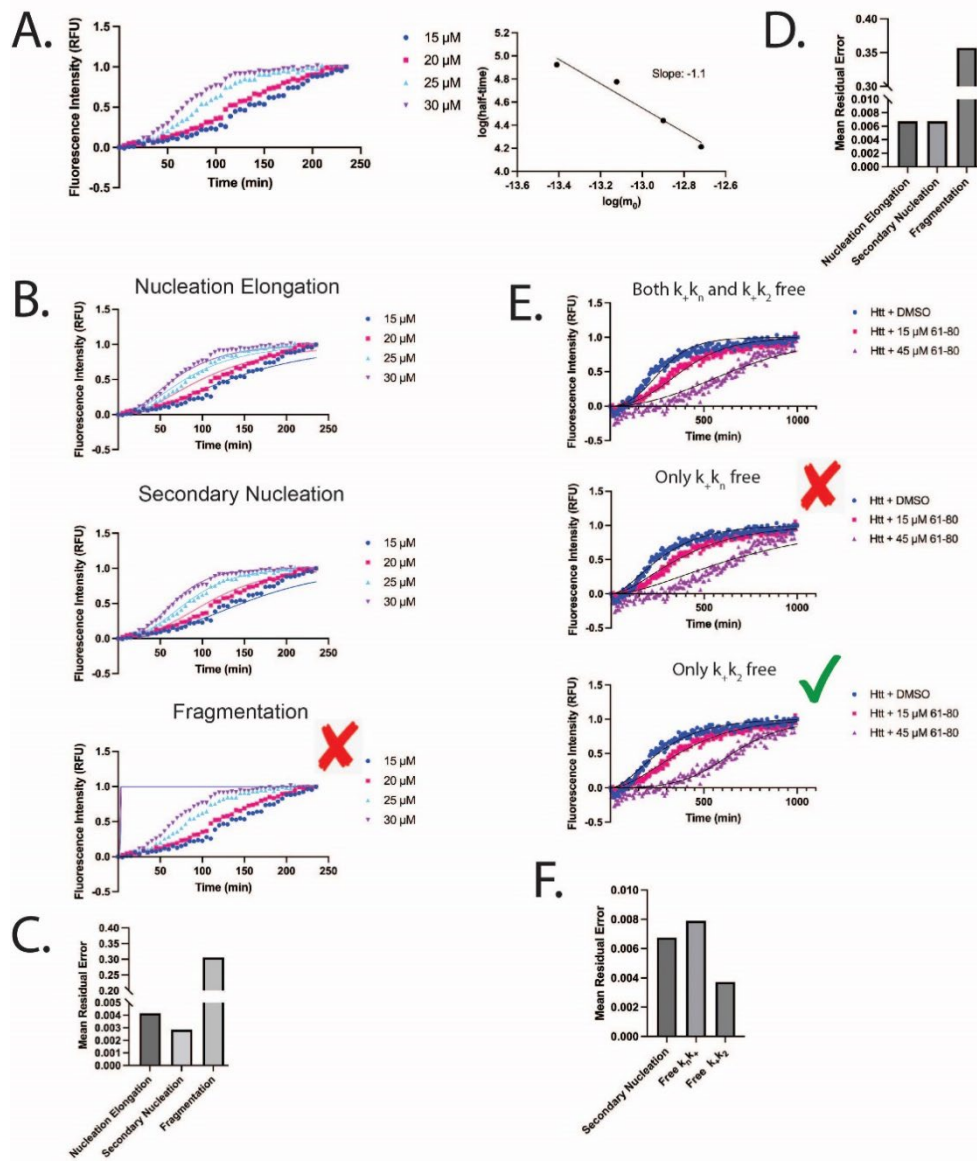


**Figure 30: SRCP1 inhibits the secondary nucleation pathway of Htt<sup>ex1Q46</sup> aggregation.**

(A) Left: Kinetic profiles of Htt<sup>ex1Q46</sup> aggregation at 15, 20, 25, and 30 μM monitored by ThT fluorescence. Right: Scaling of half-time with protein concentration (m<sub>0</sub>). A slope of -1.1 indicates a slight domination of secondary nucleation. (B) Global fitting of data in (A) to either nucleation elongation, secondary nucleation, or fragmentation aggregation models. Dotted lines indicate aggregation profiles, solid lines indicate global fit. Fragmentation has the poorest fit.

(C) Mean residual errors from global fitting in (B). (D) Mean residual errors from global fitting of aggregation profiles of 15  $\mu\text{M}$  Htt<sup>ex1Q46</sup> and increasing concentrations of SRCP1<sup>61-80</sup>. (E) Top: Kinetic profile of 15  $\mu\text{M}$  Htt<sup>ex1Q46</sup> and either 1:1 (15  $\mu\text{M}$ ) or 3:1 (45  $\mu\text{M}$ ) SRCP1<sup>61-80</sup> globally fit (solid lines) to the secondary nucleation model with (top) both  $k_+$  and  $k_n$  and  $k_+$  and  $k_2$ , (Middle) only  $k_+$  and  $k_n$  or (bottom) only  $k_+$  and  $k_2$  set as free-fitting parameters. Free-fitting  $k_+$  and  $k_2$  led to the best fit. (F) Mean residual errors from global fitting in (E) (Haver et al., 2023).

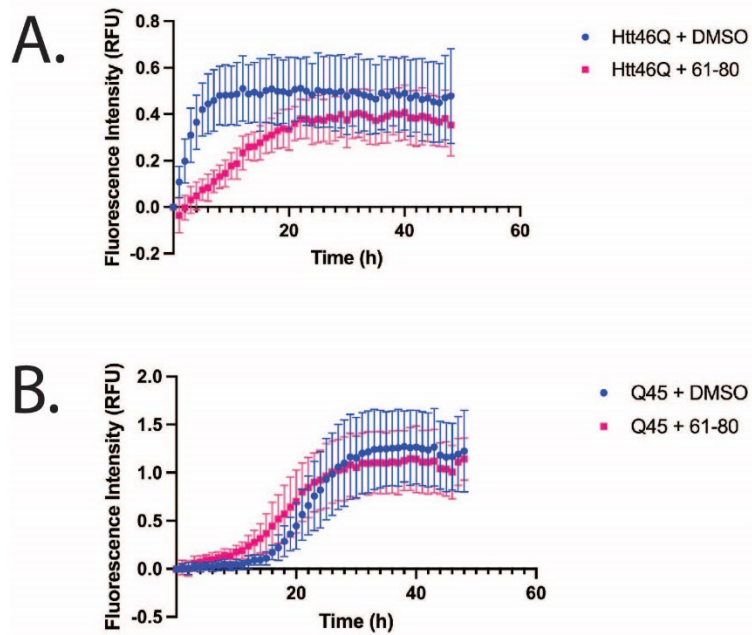


**Figure 31: SRCP1<sup>61-80</sup> inhibits huntingtin but not polyQ aggregation.**

ThT aggregation assays were carried out with peptide and (A) Htt<sup>ex1Q46</sup> or (B) pure poly-Q45 at a 6:1 molar ratio (peptide:protein) or volume equivalent of DMSO ( $n = 7$ ).

equal fits (Figure 30D). Constraining  $k_+$  and  $k_2$  as a global fitting parameter with  $k_+$  and  $k_n$  as a free-fitting parameter resulted in a worse kinetic fit than constraining  $k_+$  and  $k_n$  with  $k_+$  and  $k_2$  as free (Figure 30E and F). This supports SRCP1<sup>61-80</sup> inhibiting Htt<sup>ex1Q46</sup> aggregation at the secondary nucleation pathway rather than nucleation elongation (Belsare et al., 2022).

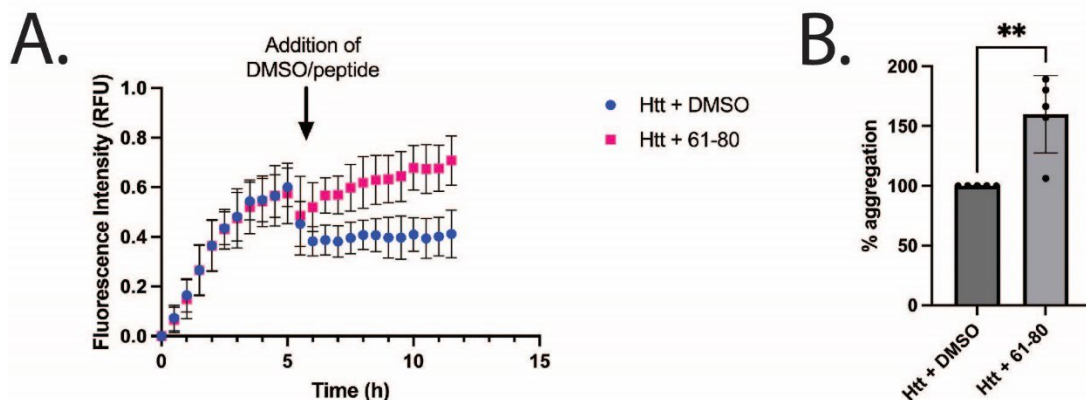


**Figure 32: SRCP1<sup>61-80</sup> does not disaggregate pre-formed Htt<sup>ex146Q</sup> fibrils.**

ThT assays with Htt<sup>ex1Q46</sup> were carried out for 5.5 h prior to addition of either DMSO or 6:1 molar ratio of peptide:protein. Assays were continued for a total of 12 h. (n = 5) (A) Aggregation curves of averaged disaggregation assays, with an arrow denoting addition of DMSO or peptide. Addition of peptide or DMSO resulted in a dip in signal due to disturbance of the sample. (B) Quantification of 12 h time points of disaggregation assays show that SRCP1<sup>61-80</sup> does not cause disaggregation of pre-formed Htt fibrils (Haver et al., 2023).

While I determined that SRCP1<sup>61-80</sup> inhibits aggregation at the secondary nucleation pathway, this does not completely describe SRCP1's mechanism. To further examine its mechanism, I wanted to determine if my peptide binds directly to the polyQ tract of Htt<sup>ex1Q46</sup> or a flanking region of the polyQ tract such as the N-terminus. The N-terminus of Htt<sup>ex1</sup> has been implicated to promote pathogenic aggregation rather than the expanded polyQ tract (Crick et al., 2013; Jayaraman et al., 2012; Liebman & Meredith, 2010; Rockabrand et al., 2007; Tam et al., 2009; Thakur et al., 2009). To investigate whether SRCP1<sup>61-80</sup> inhibits aggregation of a pure polyQ tract, I repeated the ThT assay with either Htt<sup>ex1Q46</sup> or a pure polyglutamine tract of Q45 (polyQ45). SRCP1<sup>61-80</sup> delayed Htt<sup>ex1Q46</sup> over

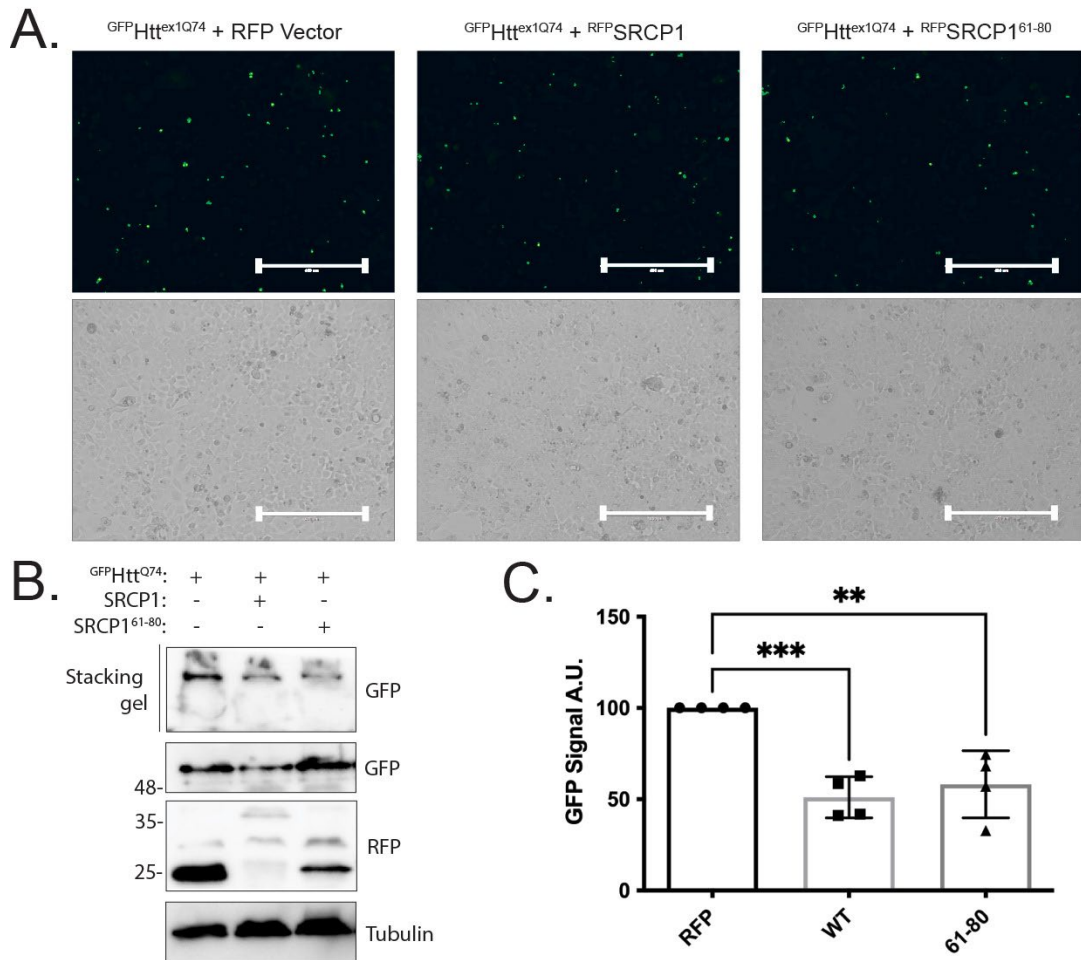


**Figure 33: A truncated form of SRCP1 is sufficient to suppress polyglutamine aggregation in human cells.**

(A) HEK293 cells were transfected with GFP<sup>Htt<sup>ex1Q74</sup></sup> and either RFP vector, RFP<sup>SRCP1</sup>, or RFP<sup>SRCP1<sup>61-80</sup></sup>. Cells were imaged under GFP fluorescence 48 h post-transfection. Scale bar: 400  $\mu$ m (B) HEK293 cells were transfected with GFP<sup>Htt<sup>ex1Q74</sup></sup> and either RFP vector, RFP<sup>SRCP1</sup>, or RFP<sup>SRCP1<sup>61-80</sup></sup>. Cells were collected and analyzed by Western blot (n = 4). (C) Quantification of GFP<sup>Htt<sup>ex1Q74</sup></sup> present in the stacking gel in (B) standardized against the loading control, tubulin (n = 4) (Haver et al., 2023).

48 h as expected (Figure 31A). Surprisingly, the peptide did not have any effect on polyQ45 (Figure 31B). This suggests that SRCP1 does not directly act on the polyQ tract,

but perhaps on a flanking region of the polyQ tract. I also tested the peptide on pre-formed Htt<sup>ex1Q46</sup> fibrils to determine if SRCP1<sup>61-80</sup> has any disaggregation activity; however, SRCP1<sup>61-80</sup> had no effect on fibrils (Figure 32). Together, these data suggest SRCP1 inhibits aggregation at the secondary nucleation pathway and is dependent on the presence of amyloid.

### **3.2.5 SRCP1<sup>61-80</sup> is sufficient to suppress polyQ aggregation in human cells**

Because our modeling data suggest that the C-terminus of SRCP1 has structure, I next tested if SRCP1<sup>61-80</sup> would be able to suppress polyQ aggregation in human cells. Previous work from our lab found that WT SRCP1 was efficient at suppressing aggregation of GFP<sup>Htt<sup>ex1Q74</sup></sup> in human cells (Santarriga et al., 2018). To determine if the C-terminal region was sufficient to suppress polyQ aggregation in cells, I generated a truncated version of SRCP1 containing only the functional region of SRCP1 (RFP<sup>SRCP1<sup>61-80</sup></sup>) and co-expressed it with GFP<sup>Htt<sup>ex1Q74</sup></sup> in HEK293 cells. Fluorescence microscopy revealed a decrease in GFP puncta in cells co-expressing either RFP<sup>SRCP1</sup> or RFP<sup>SRCP1<sup>61-80</sup></sup>, but not RFP vector (Figure 33A, experiments performed by Erin Butcher and me). Consistent with this, western blot analysis on cell lysates showed that the truncated SRCP1<sup>61-80</sup> is sufficient to suppress GFP<sup>Htt<sup>ex1Q74</sup></sup> aggregation (Figure 33B and C, experiments performed by Erin Butcher and me). Together these data are consistent with the C-terminal region of SRCP1 being sufficient to suppress polyQ aggregation.

### 3.2.6 SRCP1<sup>61-80</sup> suppresses aggregation of another polyQ protein, ataxin-3<sup>Q55</sup>.

All of the experiments described above test the effect of SRCP1<sup>61-80</sup> on suppressing the aggregation of a polyQ-expanded huntingtin exon 1 fragment. However, protein context is known to play an important role in the aggregation and toxicity of polyQ-expanded proteins (Adegbuyiro et al., 2017; Bulone et al., 2006; La Spada & Taylor, 2003; McLoughlin et al., 2020; Paulson, 2007; Totzeck et al., 2017). This raises the possibility that SRCP1 may selectively suppress mutant Htt aggregation and may not function with other polyQ proteins. To test this, I performed ThT aggregation assays in the presence or

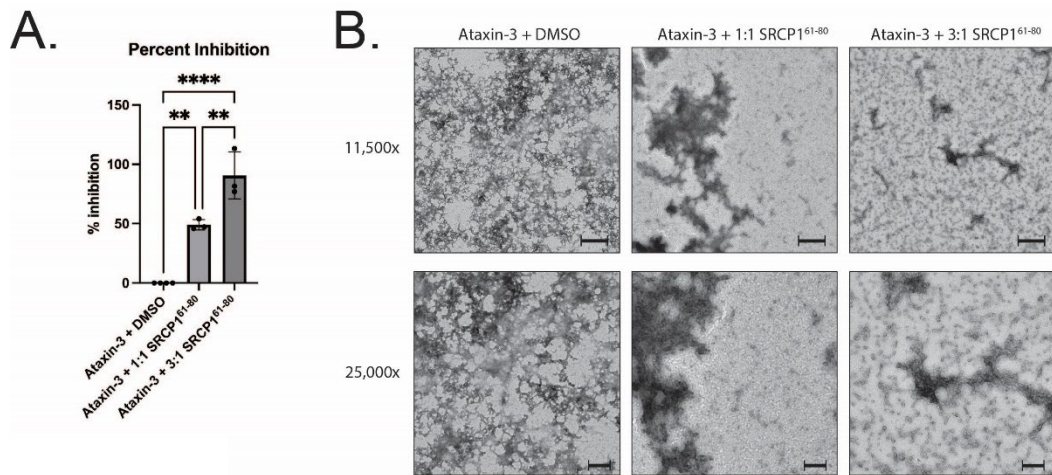


**Figure 34: SRCP1<sup>61-80</sup> suppresses aggregation of recombinant ataxin-3<sup>Q55</sup>.**

(A) ThT aggregation assays were performed with ATXN3<sup>Q55</sup> in the presence of SRCP1<sup>61-80</sup> at 1:1, 3:1, and 6:1 ratios (peptide:protein, n = 3). Percent inhibition was calculated from raw data at the end point. (B) Transmission electron microscopy images were taken of samples containing ATXN3<sup>Q55</sup> with DMSO or with 1:1 or 3:1 ratios of SRCP1<sup>61-80</sup> (peptide:protein). Samples were incubated for 6 h at 37°C prior to negative staining. Scale bars: 11,500x = 500 nm, 25,000x = 200 nm (Haver et al., 2023).

absence of SRCP1<sup>61-80</sup> with another polyQ-expanded protein, ataxin-3 with 55 glutamines (ATXN3<sup>Q55</sup>). ATXN3<sup>Q55</sup> is similar to Htt in that aggregation is initiated independently of the polyQ tract by the Josephin domain (Ellisdon et al., 2007; Gales et al., 2005; Marchal et al., 2003; Masino et al., 2004; Saunders et al., 2011). I observed that SRCP1<sup>61-80</sup> decreased ThT signal induced by ATXN3<sup>Q55</sup> aggregation, consistent with SRCP1 generally inhibiting polyQ aggregation (Figure 34A). To confirm this result, I next performed TEM to visualize ATXN3<sup>Q55</sup> aggregates in the presence and absence of SRCP1<sup>61-80</sup>. Consistent with my ThT data, I found that SRCP1<sup>61-80</sup> efficiently inhibited the aggregation of polyQ-expanded ATXN3<sup>Q55</sup> by TEM (Figure 33B). My data suggest that the SRCP1<sup>61-80</sup> can generally inhibit the aggregation of other polyQ-expanded proteins that aggregate independent of their polyQ tracts.

### ***3.3 Discussion***

Here, we present *de novo* models of SRCP1's structure. Sequence analysis using computational programs strongly predicts structure and self-aggregation propensity around residues 61-80 (Figure 23). Our models consistently predict that SRCP1's functional region at residues 61-80 forms a  $\beta$ -hairpin while the rest of the protein remains highly dynamic (Figures 25-27). Using an array of modified peptides, I also found that SRCP1 residues 61-70 are the minimal sequence necessary to suppress polyQ aggregation and that a tandem repeat of this sequence could more efficiently suppress mutant Htt aggregation (Figure 29). I investigated Htt aggregation kinetics with or without SRCP1<sup>61-</sup>

<sup>80</sup> and discovered that SRCP1 inhibits Htt aggregation at the secondary nucleation step and relies on the presence of amyloid to function (Figures 30 and 31). Consistent with my *in vitro* data, we also found that amino acids 61-80 are sufficient to inhibit GFP<sup>Htt</sup><sup>ex1Q74</sup> aggregation in human cells at a level comparable to the full-length protein (Figure 33). Finally, I tested whether SRCP1 was sufficient to suppress aggregation of other polyQ-expanded proteins and found it could suppress aggregation of ATXN3<sup>Q55</sup>, the protein involved in spinocerebellar ataxia type 3 (SCA3) (Figure 34). Together, our data suggest that SRCP1 residues 61-80 form a  $\beta$ -hairpin, and that this region is sufficient both *in vitro* and in cells to suppress polyQ aggregation.

We originally identified SRCP1<sup>61-80</sup> as being predicted to form amyloid by many computational approaches (Santarriaga et al., 2018). This region is glycine-rich and hydrophobic, consistent with other amyloid forming domains (Santarriaga et al., 2018). Performing *de novo* protein modeling on SRCP1's amino acid sequence suggests that SRCP1<sup>61-80</sup> forms a  $\beta$ -hairpin, consistent with this region having an amyloid-like fold. Importantly,  $\beta$ -hairpins are commonly found to be structural precursors to amyloid formation. Previously, molecular dynamics simulations using amyloid- $\beta$  sequences from Alzheimer's disease uncovered predicted  $\beta$ -hairpin intermediate structures that may contribute to amyloid (Baumketner & Shea, 2006; Han & Wu, 2005). Ion mobility mass spectrometry coupled with MD simulations on another amyloid-forming protein, the human islet amyloid polypeptide, also suggests that this protein exists in equilibrium

between two distinct conformational superfamilies, one containing helix-coil structures and the other having  $\beta$ -hairpin structures which more readily forms amyloid and aggregates (Dupuis et al., 2009). It is therefore possible that SRCP1<sup>61-80</sup> exists as a  $\beta$ -hairpin that interacts with amyloid-forming regions of polyQ proteins to form mixed amyloid. The serine-rich N-terminus, which has previously been shown to be dispensable for function, may be responsible for shielding the  $\beta$ -hairpin region and prevent further amyloid fibrillization (Santarriaga et al., 2018).

Our peptide data also support the idea that SRCP1<sup>61-80</sup> forms a  $\beta$ -hairpin. Amyloid readily interacts with other amyloid-like sequences, therefore the amyloid-like region of SRCP1 may act in a similar manner as an amyloid-inhibiting peptide (Cheng et al., 2012; Santarriaga et al., 2018; Sato et al., 2006). Numerous studies have shown that modified amyloid- $\beta$  peptides inhibit amyloid- $\beta$  aggregation and neurotoxicity (Austen et al., 2008; Bett et al., 2010; Cheng et al., 2012; Fradinger et al., 2008; Li et al., 2010; Orner et al., 2006; Sato et al., 2006). I also have demonstrated that peptides of residues 61-70 and 61-80 inhibit mutant huntingtin aggregation *in vitro* (Santarriaga et al., 2018). Here I found that a peptide consisting of a SRCP1<sup>61-70</sup> sequence repeat inhibits mutant huntingtin aggregation significantly better than amino acids 61-70 (Figure 29E and F), suggesting that a second functional sequence promotes an interaction with amyloid.

Another strategy is to design peptide inhibitors that are locked in a  $\beta$ -hairpin conformation. These peptides have been successfully utilized to inhibit aggregation of

many aggregation-prone proteins including amyloid- $\beta$ , transthyretin, huntingtin, human pancreatic amylin, and  $\alpha$ -synuclein (Hopping et al., 2013; Huggins et al., 2011; Jha et al., 2018; Kar et al., 2017; Li et al., 2010; Yamin et al., 2009). We permanently cyclized SRCP1<sup>61-80</sup> to lock it in a  $\beta$ -hairpin conformation. Our SRCP1<sup>61-80</sup> cyclic peptides were also able to inhibit mutant Htt aggregation, but not significantly better than SRCP1<sup>61-80</sup> (Figure 29G and H). Because the cyclic peptides did not inhibit aggregation better than the WT, our SRCP1<sup>61-80</sup> peptide may already form a  $\beta$ -hairpin structure. From my ThT assays, I have confirmed that residues 61-70 are the minimal sequence necessary to suppress polyQ aggregation and that having a second 61-70 sequence increases the peptide's potency. In addition, our cellular data using SRCP1<sup>61-80</sup> further supports that this region is sufficient to bind mutant Htt and inhibit its aggregation in human cells (Figure 33).

My investigation into SRCP1's mechanism of inhibiting polyQ aggregation found that inhibition occurs through the secondary nucleation pathway of aggregation (Figure 29E and F). This suggests that rather than binding to Htt monomers, our peptide binds to intermediate oligomers of Htt and prevents further fibrillization. Additionally, I discovered that SRCP1<sup>61-80</sup> suppresses Htt aggregation, but not the aggregation of a polyQ45 (Figure 31). This suggests that SRCP1 does not interact with the polyQ tract of mutant, but another domain. Multiple studies have shown that the N-terminal N17 domain dramatically increases the rate of pathogenic Htt aggregation (Crick et al., 2013; Jayaraman et al., 2012; Liebman & Meredith, 2010; Rockabrand et al., 2007; Tam et al.,

2009; Thakur et al., 2009). I also observed that Htt<sup>ex1Q46</sup> aggregates much more rapidly than polyQ45 (Figure 31). Therefore, it is possible that SRCP1 recognizes and binds the N17 domain, reducing Htt amyloid formation and aggregation. Another explanation for this observation could be that our peptide simply incorporates into the polyQ45 fibrils. I previously observed that under long incubation periods, our peptide delays, rather than prevents, the aggregation process (Santarriaga et al., 2018). Because polyQ45 aggregates much more slowly, it is possible that our peptide is not able to suppress aggregation after a certain time and co-aggregates with polyQ45.

Finally, I tested our peptide with another polyQ protein, ATXN3<sup>Q55</sup>, the aggregating protein in SCA3, to verify that SRCP1 is not selective to one polyQ protein. My data from ThT aggregation assays suggest that SRCP1<sup>61-80</sup> does suppress ATXN3<sup>Q55</sup> aggregation (Figure 33A). This data was confirmed by TEM (Figure 33B). ATXN3<sup>Q55</sup> alone yields full fibrils but adding increasing ratios of SRCP1<sup>61-80</sup> yield more spherical species than fibrils. These spherical structures are similar to previously described soluble oligomers, and we observed similar structures with Htt<sup>ex1Q46</sup> (Santarriaga et al., 2018; Tsigelny et al., 2008). The observation of these oligomeric species is also consistent with SRCP1<sup>61-80</sup> interacting with oligomers and inhibiting aggregation at the secondary nucleation pathway (Figure 28).

Here, I provide evidence that our peptide can more generally inhibit polyQ aggregation as it also inhibits ATXN3<sup>Q55</sup>. Our *in vitro* and in cell studies indicate that short

peptides of SRCP1 are sufficient to suppress aggregation of more than one expanded polyQ protein. This suggests that short sequences of SRCP1 like 61-70 or 61-80 could be used as potential therapeutic peptides and could help guide the design of future therapeutic approaches for polyQ diseases.

### ***3.4 Materials and Methods***

#### **Expression Constructs**

<sup>GFP</sup>SRCP1 and <sup>FLAG</sup>SRCP1 were generated previously by Stephanie Santarriaga. SRCP1 for bacterial expression in pET47b(+), pGEX-6P1, and pQE30 were generated previously by Oliver Newsom. The pFastBac1 Nterminal GST baculovirus expression vector was obtained from Addgene (#128058). The H3c cleavage site to pFastBac1 Nterminal GST was cloned in using EcoRI and XbaI restriction sites and the following primers: Forward primer: GAATTCAACTGGAAGTTCTGTTCCAGGGGCCCTCTAGA, reverse primer: TCTAGAGGGCCCCTGGAACAGAACTTCCAGTTGAATTC. The 6X-His tag to pFastBac1 Nterminal GST-H3c was cloned in using BamHI restriction site and the following primers: forward primer: CGGGATCCATGCATCACCATCACCATCACGGATCCCG, reverse primer: CGGGATCCGTGATGGTGATGGTGATGCATGGATCCCG.

SRCP1 (DDB\_G0293362) was previously generated (Santarriaga et al., 2018). The plasmid for mammalian expression encoding SRCP1<sup>61-89</sup> was generated and obtained from Blue Heron. Individual point mutants of SRCP1 and SRCP1<sup>61-80</sup> were generated using the

QuikChange Lightning Site-Directed Mutagenesis Kit (Agilent). The plasmid for mammalian expression encoding pEGFP huntingtin exon-1 with 74 glutamines ( $\text{GFP}^{\text{Htt}^{\text{ex1Q74}}}$ ) was acquired from Addgene (#40262) (Narain et al., 1999).

### ***Dictyostelium* Cell Culture, Transformation, and SRCP1 Pulldowns**

*Dictyostelium discoideum* AX4 cells were maintained in shaking cultures at 22°C in HL5 media (17.8 g peptone, 7.2 g yeast extract, 0.54 g  $\text{Na}_2\text{HPO}_4$ , 0.4 g  $\text{KH}_2\text{PO}_4$ , 130 mL B12/folic acid, 20 mL of 50% w/v glucose, carbenicillin 150 mg/mL, pH 6.5). Cells were maintained at a density no greater than  $6 \times 10^6$  cells/mL.

Transformations were performed via electroporation as described previously (Knecht & Pang, 1995). Briefly,  $5 \times 10^6$  cells were spun down at  $500 \times g$  for 5 min at 4°C. Cells were then washed three times with ice-cold H-50 buffer (20 mM HEPES, 50 mM KCl, 10 mM NaCl, 1 mM  $\text{MgSO}_4$ , 5 mM  $\text{NaHCO}_3$ , 1 mM  $\text{NaH}_2\text{PO}_4$ ), resuspended in 100 mL of ice-cold H-50 buffer, and combined with 10  $\mu\text{g}$  of DNA. Cell and DNA mixture was added to a pre-cooled 1 mm cuvette and electroporated at 0.85 kV/25 mF/time constant 0.6 ms twice with about 5 s between pulses. Cells were then incubated on ice for 5 min and added to 10 mL of HL5 media on 10 cm plates. The selection drug G-418 (GIBCO by Life Technologies) was added at 10 mg/mL the following day and included in media going forward.

For both nickel (GFP) and FLAG pulldowns,  $1 \times 10^8$  cells transfected with either empty vector or SRCP1 were spun down at  $500 \times g$  for 5 min at 4°C. Cells were then

washed three times with ice-cold PBS and lysed in 1 mL NETN with protease inhibitor (GoldBio). Lysates were sonicated, spun down at  $20,000 \times g$  for 30 min at 4°C, and the supernatant was incubated on either nickel (GoldBio, for GFP-SRCP1) or Anti-FLAG-M2 (Sigma) beads for 1 h at 4°C. Beads were washed three times with ice-cold NETN. For elution, nickel beads were washed once with ice-cold NETN with 20 mM imidazole and eluted twice for 15 min in ice-cold NETN with 300 mM imidazole. Elution from FLAG beads was performed twice for 15 min with 150 ng/ $\mu$ L of 3x FLAG peptide in ice-cold NETN.

#### **Bacterial SRCP1 Expression and Purification**

SRCP1 in pET47b(+). BL21 cells were grown to an  $OD_{600}$  of 0.6 and induced with 1 mM IPTG (GoldBio) for 1.5 h at 37°C. Cells were spun down at 7,000 rpm (Thermo Scientific F9-6x1000 LEX rotor) and resuspended in Buffer A (50 mM Tris, pH 7.5, 1 M NaCl, 0.5% Triton X-100). Lysates were tumbled at 4°C for 30 min and spun down at  $20,000 \times g$  (Thermo Scientific F20-12x50 LEX rotor) for 10 min to separate soluble and insoluble fractions.

SRCP1 in pGEX-6P1. BL21 cells were grown to an  $OD_{600}$  of 0.6 and induced with 0.01 mM IPTG (GoldBio) for 6 h at 37°C. Cells were spun down at 7,000 rpm (Thermo Scientific F9-6x1000 LEX rotor) and resuspended in NETN or denaturing buffer (8 M urea, 500 mM NaCl, 20 mM sodium phosphate pH 8). Lysates were tumbled at 4°C (NETN) or

room temperature (denaturing) for 30 min and spun down at  $20,000 \times g$  (Thermo Scientific F20-12x50 LEX rotor) for 10 min to separate soluble and insoluble fractions.

### **Testing Solubility of SRCP1 in *E. coli* Lysate with Buffer Additives**

This protocol was adapted from a published method (Churion & Bondos, 2012). BL21 cells expressing SRCP1 in pGEX-6P1 were grown to an  $OD_{600}$  of 0.6 and induced with 0.01 mM IPTG (GoldBio) for 6 h at 37°C. Six 100  $\mu$ L aliquots of bacterial culture were spun down at  $20,000 \times g$  and cell pellets collected. Pellets were resuspended in 200  $\mu$ L of lysis buffer (50 mM Tris pH 8.0, 200 mM NaCl, 2 mg/mL lysozyme) and pipetted on ice for 5 min and then incubated without pipetting on ice for 5 min. Added 5  $\mu$ L of DNase (20 mg/mL stock) to each crude lysate, mixed by pipetting, and incubated on ice for another 5 min.

The 200  $\mu$ L aliquots of crude cell lysate were diluted to 2 mL in each test buffer (50 mM Tris pH 8.0, 200 mM NaCl, and selected additive). Additives included: 500 mM NaCl total, 10% glycerol, 0.5 M urea, 0.5 M arginine, or 1% IGEPAL. Lysates were tumbled at 4°C for 2 h and added to Centricon YM-100 filters (Amicon Bioseparations). Lysates were filtered through at  $1000 \times g$  according to manufacturer instructions. Aggregated protein caught by the filter was resuspended in 30  $\mu$ L MilliQ water. Both filtrate and insoluble fractions were ran on SDS-PAGE.

### **Cell-free SRCP1 Expression of SRCP1**

Performed expression experiment using the S30 T7 High-Yield Protein Expression System (Promega) according to the manufacturer's instructions. Reactions were prepared on ice, containing 1 µg DNA containing SRCP1, S30 Premix Plus, and T7 S30 extract and mixed thoroughly. Reactions were immediately incubated with constant shaking at 37°C for 1 h. Prior to SDS-PAGE, 5 µL of sample was diluted to 20 µL in TBS with RNase.

### **SF9 Insect Cell Culture, Baculovirus Generation, and Transfection**

To generate bacmid DNA for transformation, 1 ng of the pFastBac donor plasmid containing SRCP1 or SRCP1-like proteins were transformed into DH10Bac cells containing the bacmid, allowing the gene to be transduced into the bacmid. Positive colonies were selected by blue-white screening and insertion of the gene was verified by PCR using primers for pUC/M13 (Forward: CCCAGTCACGACGTTGTAAAACG, Reverse: AGCGGATAACAATTTACACAGG).

*Spodoptera frugiperda* 9 (SF9) cells were grown at 27°C and maintained in Grace's insect medium (Gibco) supplemented with 10% fetal bovine serum (Hyclone) and 1% antibiotic-antimycotic (Gibco). Cells maintained in spinner flasks were supplemented with 0.1% pluronic-F68 (Gibco) to minimize cell shearing. Cells density was kept below  $3 \times 10^6$  cell/mL. Cell viability was checked using trypan blue (Gibco).

To generate P0 stock baculovirus, SF9s were transfected with bacmid DNA using Expifectamine (Gibco) according to the manufacturer's protocol for cells containing antibiotics. Cells were incubated for 5 days at 27°C and the medium containing the P0

virus collected. The P1 viral amplification stock was generated by adding 10  $\mu$ L of P0 viral stock to  $1 \times 10^6$  cells in 2 mL supplemented Grace's insect medium. The cells were incubated for 5 days at 27°C in humid conditions and then the medium was collected. To produce the P2 working baculovirus stock, 10  $\mu$ L of P1 viral stock was added to  $1 \times 10^6$  cells in 2 mL supplemented Grace's insect medium. The cells were incubated for 5 days at 27°C in humid conditions and then the medium was collected. The P2 working stock was used for protein expression.

### **SRCP1 Protein Purification from SF9 cells**

Large-scale infections were performed in spinner or shaker flasks. To prevent cell shearing, 0.1% Pluronic-F68 (Gibco) was added to the cultures. SF9s at a cell density of  $\sim 2.0 \times 10^6$  cells/mL were infected with 700  $\mu$ L P2 virus per 50 mL of cell culture and incubated at 27°C for 48 h for maximum protein expression. Both GST and nickel purifications were carried out as described above in the section for bacterial SRCP1 purification.

### **Computational Modeling using Rosetta**

SRCP1's amino acid sequence was used to identify similar sequences to be used as templates for homology modeling. No homologous proteins were found, and coevolutionary data was insufficient to generate constraints for de novo modeling (Ovchinnikov et al., 2015). A rigorous methodology was constructed to generate and validate structural models of SRCP1 according to the latest protocols from the 12th Critical

Assessment of protein Structure Prediction (CASP) (Ovchinnikov et al., 2018). The first step of this process generated 100,000 models using the Rosetta Ab initio protocol as previously described (Barth et al., 2007; Simons et al., 1999). Each model was relaxed in torsion and cartesian space using the all-atom Rosetta energy function (Nivon et al., 2013), and this was repeated after hybridize refinement and molecular dynamics (MD)-based refinement. Next, models were clustered according to C $\alpha$  root-mean-square deviation (RMSD) using Calibur (Li & Ng, 2010). Top scoring models and models representing cluster centers were advanced to refinement. Similar to the low-resolution refinement protocol, the first step of refinement used 18 different ab initio models as inputs for separate hybridization runs that sampled the backbone of these models (Park et al., 2016). Models were once again relaxed, scored, and clustered, and 12 models were chosen for MD-based refinement. In this step, 10 nanoseconds of dynamic simulations were performed and independently repeated for a total of 5 times. The AMBER12SB forcefield was used with the TIP3P water model solvating the protein in a periodic boundary box (Ovchinnikov et al., 2018). Structures of each run are averaged and relaxed using Rosetta with hard positional restraints to backbone atoms (Mirjalili & Feig, 2013). RMSD from the original C $\alpha$  positions was calculated across the MD trajectory and root-mean-square fluctuation (RMSF) was calculated for each atom (Radom et al., 2018). Final models were ranked by ensemble averaged score, RMSD over time, and the percent of residues lower

than 1 Å RMSF. Of the 60 total MD runs, 13 were considered for final selection and further relaxed.

The model in Figure 25E was used to predict stabilizing and destabilizing mutations using Rosetta ddg\_monomer protocol row 16 (Kellogg et al., 2011). In this protocol all 20 amino acid side chains are substituted one at a time for each amino acid in the protein. The change in Rosetta energy is calculated compared to the unmutated model.

### **Mammalian Cell Culture and Transfection**

Human embryonic kidney 293 (HEK293) cells were grown at 37°C and 5.0% CO<sub>2</sub>. HEK293 cells were maintained in Dulbecco Modified Eagle's Medium (Gibco Life Technologies) supplemented with 10% fetal bovine serum (GE Life Sciences), 1% penicillin-streptomycin (Gibco Life Technologies), and 1% non-essential amino acids (Gibco Life Technologies). Transfections were performed as recommended by the manufacturer using Lipofectamine 2000 (Invitrogen by ThermoFisher Scientific). HEK293 cells were imaged by fluorescent microscopy with a 10x objective using the Evos FL Auto Imaging System. To harvest, HEK293s were washed twice with ice-cold PBS, lysed in 200 µL of ice-cold NETN buffer, and sonicated twice for 10 s.

### **SDS-PAGE and Western Blotting**

After sonication, protein concentration of the lysates was determined by BCA protein assay (ThermoFisher Scientific). Samples were prepared for loading by adding 4X Laemmli buffer and boiling for 4 min. Samples were ran on 12% SDS-polyacrylamide gels

and transferred onto Immunoblot PVDF membrane (BioRad) Membranes were blocked with 5% milk in TBS with 0.1% Tween (TBST) and incubated in primary antibody, also in 5% milk in TBST, overnight at 4°C. Membranes were washed with TBST three times for 10 min and incubated in secondary antibody for 30 min. Membranes were washed three times for 10 min with TBST and briefly incubated in buffer for enhanced chemiluminescence (50 mM Na<sub>2</sub>HPO<sub>4</sub>; 50 mM Na<sub>2</sub>CO<sub>3</sub>; 10 mM NaBO<sub>3</sub>·4 H<sub>2</sub>O; 250 mM luminol; 90 mM coumaric acid). Membranes were developed using a ChemiDoc MP Imaging System (BioRad).

Anti-RFP (Invitrogen by ThermoFisher Scientific, MA5-15257) and anti-GFP (Invitrogen by ThermoFisher Scientific, A-11122) were used at a 1:1000 dilution. Anti- $\beta$ -tubulin (DSHB, University of Iowa, E7) was used at a 1:100 dilution as a loading control. Peroxidase-conjugated mouse secondary antibody (Jackson ImmunoResearch Laboratories; 115-035-166) was used at a 1:5000 dilution.

### **Aggregation Kinetics of Htt<sup>ex1Q46</sup>**

Concentration-dependent Htt<sup>ex1Q46</sup> data was collected using our ThT assay described below. Data used for kinetic analysis of SRCP1<sup>61-80</sup> inhibition was acquired previously (Santarriaga et al., 2018) . Raw data was analyzed via the AmyloFit server (<https://amylofit.com/amylofitmain/fitter>) (Meisl et al., 2016). First, the data for Htt<sup>ex1Q46</sup> alone was analyzed by the half-time plotter to determine possible models. All data was

then analyzed using the “Nucleation Elongation, Unseeded”, “Fragmentation Dominated, Unseeded”, and “Secondary Nucleation Dominant, Unseeded” models.

### **Huntingtin<sup>ex1Q46</sup> purification**

Htt<sup>ex1Q46</sup> was purified as described previously (Santarriaga et al., 2018). Htt<sup>ex1Q46</sup> was grown in BL21 cells to an OD<sub>600</sub> of 0.6 and induced with 1 mM IPTG (GoldBio) overnight at 16°C. Cells were spun down at 7,000 rpm (Thermo Scientific F9-6x1000 LEX rotor) and resuspended in 15 mM Tris-HCl buffer, pH 8.0. Lysozyme was added for lysis, and cells were tumbled at 4°C for 45 min. Lysates were spun down at 12,000 rpm (Thermo Scientific F20-12x50 LEX rotor) for 10 min and the supernatant added to 3mL of nickel beads (GoldBio) per 100 mL of lysate and tumbled for 4 h at 4°C. Beads were washed 3 times with 15 mM Tris-HCl, pH 8.0 and 3 more times with wash buffer (50 mM Tris-HCl, pH 8.0, 150 mM NaCl, 1 mM PMSF, 1mM EDTA). Protein was eluted off beads by tumbling overnight at 4°C in 25 mL wash buffer with 250 mM imidazole.

### **Thio-polyQ45 purification**

Thio-polyQ45 was grown in BL21 cells to an OD<sub>600</sub> of 0.6 and induced with 1 mM IPTG (GoldBio) overnight at 16°C. Cells were spun down at 7,000 rpm (Thermo Scientific F9-6x1000 LEX rotor) and resuspended in Buffer A (50 mM Tris, pH 7.5, 1 M NaCl, 0.5% Triton X-100). Lysozyme was added for lysis, and cells were tumbled at 4°C for 30 min. Lysates were spun down at 12,000 rpm (Thermo Scientific F20-12x50 LEX rotor) for 10 min

and the supernatant added to 500  $\mu$ L of nickel beads (GoldBio) per 1 L of cells and tumbled for 3 h at 4°C. Beads were washed 3 times with Buffer A, 3 more times with Buffer B (50 mM Tris, pH 7.5, 1 M NaCl, 20 mM imidazole), and 3 more times with Buffer C (50 mM Tris, pH 7.5, 150 mM NaCl, 20 mM imidazole). Protein was eluted off beads by tumbling overnight at 4°C in 5 mL Buffer C with 300 mM imidazole. Protein was dialyzed into ThT assay buffer (20 mM Tris-HCl pH 8.0, 50 mM NaCl, 2 mM CaCl<sub>2</sub>).

### **Ataxin-3<sup>Q55</sup> purification**

Ataxin-3<sup>Q55</sup> was purified as described previously (Scaglione et al., 2011). GST-ATXN3<sup>Q55</sup> was grown in BL21 cells to an OD<sub>600</sub> of 0.6 and induced with 1 mM IPTG (GoldBio) overnight at 16°C. Cells were spun down at 7,000rpm (Thermo Scientific F9-6x1000 LEX rotor) and resuspended in NETN buffer (50 mM Tris, pH 7.5, 150 mM NaCl, 0.5% IGEPAL CA-630) containing aprotinin (GoldBio), leupeptin (Alfa Aesar), PMSF (Grainger), and DTT (Sigma). For lysis, cells were tumbled at 4°C for 30 min and sonicated 3 times for 30 s. Lysates were spun down at 12,000 rpm (Thermo Scientific F20-12x50 LEX rotor) for 10 min and the supernatant was added to glutathione sepharose beads (GoldBio) and tumbled at 4°C for over 1 h. Beads were then washed 3 times with NETN and washed 3 more times with PBS. Protein was eluted off the beads by incubating with HRV 3c protease in PBS overnight at 4°C.

### **Thioflavin T Aggregation Assays**

Huntingtin<sup>ex1Q46</sup> and Thio-polyQ45

Aggregation assays were performed as previously described (Kakkar et al., 2016; Santarriaga et al., 2018). In buffer (20 mM Tris-HCl pH 8.0, 50 mM NaCl, 2 mM CaCl<sub>2</sub>), 25 μM or 15 μM thioredoxin-Htt<sup>ex1Q46</sup> was mixed with 10 μM Thioflavin-T (Sigma-Aldrich) and indicated molar ratios of each SRCP1 peptide (Peptide 2.0; 1:6, 1:3, and 1:1 ratios). Enterokinase (New England BioLabs) was added at 1.6 units/50 μL reaction to cleave the thioredoxin tag and initiate Htt<sup>ex1Q46</sup> aggregation. All samples were transferred in 50 μL aliquots to a flat, black 384-well plate (Thermo Scientific) and allowed to aggregate for 12 h at 37°C. Fluorescence was measured with excitation at 440 nm and emission at 480 nm every 15 min using a Tecan Spark plate reader.

#### Ataxin-3<sup>Q55</sup>

Aggregation assays were performed as previously described (Ellisdon et al., 2006; Reinke et al., 2011). In PBS, 10 μM ATXN3<sup>Q55</sup> was mixed with 20 μM Thioflavin-T (Sigma-Aldrich) and indicated molar ratios of SRCP1<sup>61-80</sup> (Peptide 2.0; 1:3 and 1:1 ratios). All samples were transferred in 50 μL aliquots to a flat, black 384-well plate (Thermo Scientific) and allowed to aggregate for 72 h at 37°C with shaking prior to each read. Fluorescence was measured with excitation at 440 nm and emission at 480 nm every 1 h using a Tecan Spark plate reader.

#### **Transmission Electron Microscopy (TEM) of Ataxin-3<sup>Q55</sup>**

For TEM, samples were prepared in PBS containing 10  $\mu$ M ATXN3<sup>Q55</sup> and indicated molar ratios of SRCP1<sup>61-80</sup> (Peptide 2.0; 1:3, and 1:1 ratios). Samples were allowed to incubate for 6 h at 37°C under quiescent conditions.

Following aggregation assays, 5  $\mu$ L droplets of each sample were added on top of freshly ionized 300 mesh Formvar/Carbon coated copper grids (Electron Microscopy Sciences) for 2 min to allow adsorption to the grid. Samples were wicked away from the edge of the grid surface and immediately stained with a 5  $\mu$ L droplet of negative stain (2% aqueous uranyl acetate solution, courtesy of Duke Shared Materials Instrumentation Facility). The stain was wicked away from the edge of the grid surface and allowed to air dry. The grids were imaged on a FEI Tecnai G<sup>2</sup> Twin TEM.

### **Quantification and Statistical Analysis**

ImageJ was used for the quantification of Western blots. The band of interest were measured for intensity and normalized to the intensity of the loading control band. Values were entered into GraphPad Prism and analyzed by one-way ANOVA for multiple comparisons. Differences were considered statistically significant at a P-value less than 0.05.

## 4. Determining the biological function of the *Dictyostelium* disaggregase Hsp101

SRCP1 is one protein native to *Dictyostelium* that suppresses aggregation of a polyQ-expanded Htt protein. Another *Dictyostelium* protein, heat shock protein (Hsp) 101 has previously been implicated in dissipating heat-induced foci formed by Htt<sup>ex1</sup> and a prion-forming domain (Malinovska et al., 2015). Here I investigated whether Hsp101 is utilized by *Dictyostelium* to rid cells of pre-formed aggregates.

Cells naturally remove misfolded or aggregated proteins through the use of protein quality control pathways (proteostasis). One critical aspect of proteostasis is the molecular chaperone system. This system utilizes different chaperone proteins to bind and refold proteins that have become misfolded. The major groups of chaperones are the holdases, foldases, and disaggregases. Holdases include the small heat shock proteins and Hsp40 chaperones. These proteins are responsible for binding misfolded proteins and prevent them from aggregating under stress conditions (Haslbeck, 2002; Jakob et al., 1993). The foldases include chaperones from the Hsp70 and Hsp90 families, which assist in protein refolding in an ATP-dependent manner (Mayer & Bukau, 2005; Pearl, 2016). Protein disaggregases, which include the Hsp100 proteins like yeast Hsp104, utilize ATP to extract monomeric proteins from larger aggregates (Parsell et al., 1994).

Hsp100 chaperone proteins, such as bacterial ClpB and yeast Hsp104, are members of the AAA+ ATPase superfamily, and are associated with many cellular activities

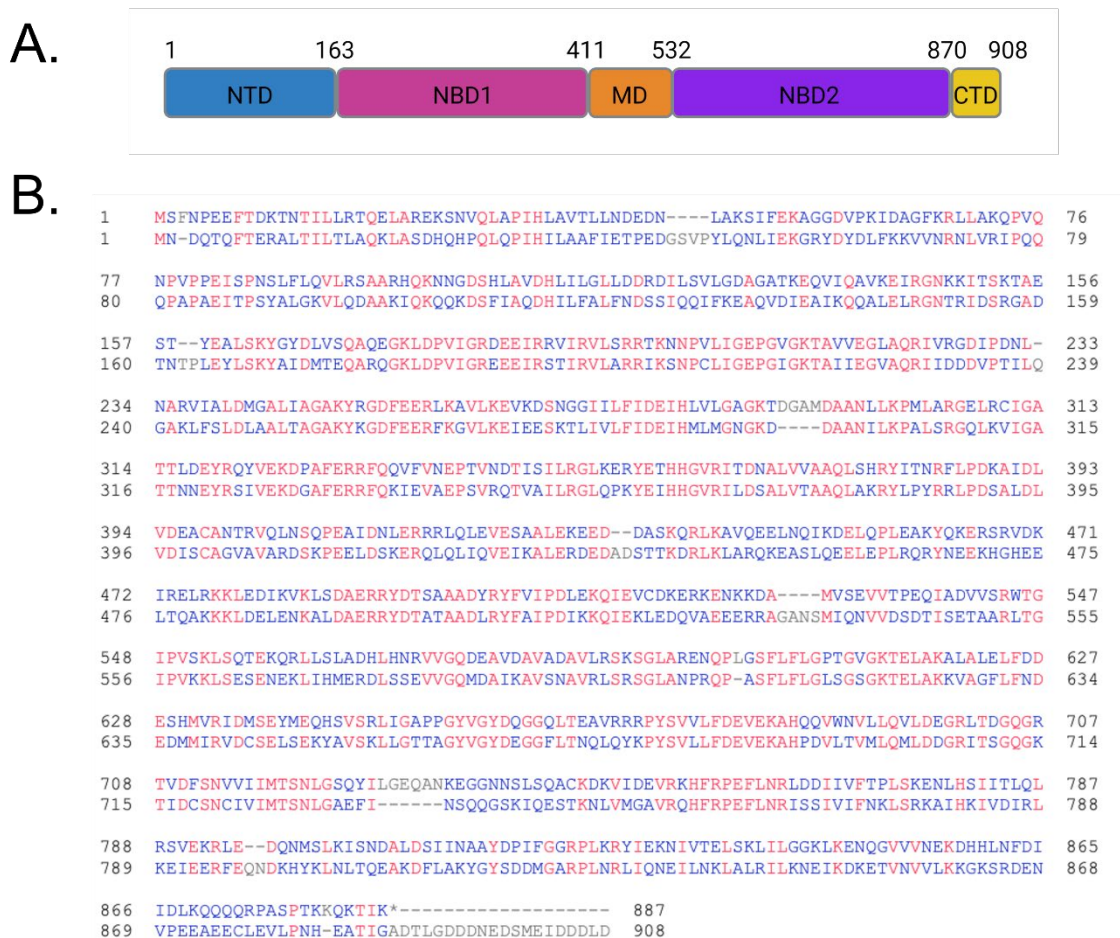


**Figure 35: Comparison of yeast Hsp104 and *Dictyostelium* Hsp101.**

(A) Schematic of the domain layout of yeast Hsp104. Hsp104 contains an N-terminal domain (NTD), two nucleotide-binding domains (NBDs), a middle domain (MD), and a short C-terminal domain (CTD). (Figure created in BioRender.) (B) Sequence alignment of *Dictyostelium* Hsp101 (top) and Hsp104 (bottom). Alignment was performed in NCBI COBALT with an identity threshold (Papadopoulos & Agarwala, 2007). Columns with no gaps are colored in either red, to indicate identical columns, or blue, to indicate less conserved columns.

(Hanson & Whiteheart, 2005; Neuwald et al., 1999; Zolkiewski et al., 2012). These proteins are required for cell survival under severe heat stress (Queitsch et al., 2000; Sanchez et al., 1992; Squires et al., 1991; Zolkiewski et al., 2012). Most notably, these chaperones have the

ability to disaggregate large protein aggregates into monomers which can then be refolded into functional proteins with the assistance of co-chaperones (Glover & Lindquist, 1998; Goloubinoff et al., 1999; Motohashi et al., 1999; Parsell et al., 1994; Zolkiewski, 1999; Zolkiewski et al., 2012).

The structure of the yeast disaggregase, Hsp104, is comprised of an N-terminal domain (NTD), two nucleotide-binding domains (NBD) separated by a middle domain (MD), and a short C-terminal domain (CTD) (Figure 35A) (Shorter & Southworth, 2019; Sweeny & Shorter, 2016). The NBDs are required for ATP hydrolysis that drives the disaggregation process of many higher-order protein structures (DeSantis et al., 2012; Glover & Lindquist, 1998; Klaips et al., 2014; Liu et al., 2011; Lo Bianco et al., 2008; Park et al., 2014; Parsell et al., 1994; Shorter & Lindquist, 2004, 2006, 2008; Shorter & Southworth, 2019; Zhao et al., 2017). The MD has been implicated in several functions including Hsp104-Hsp70 interaction and allosteric regulation of Hsp104 during substrate interaction and disaggregation (DeSantis et al., 2014; Gates et al., 2017; Haslberger et al., 2007; Heuck et al., 2016; Jackrel et al., 2014; Jackrel et al., 2015; Oguchi et al., 2012; Shorter & Southworth, 2019; Tariq et al., 2018). The CTD plays an essential role in the hexamerization of Hsp104 (Mackay et al., 2008). The mechanism by which Hsp104 disaggregates proteins is well-defined. First, an Hsp40 holdase will target an Hsp70 foldase to the protein aggregate and stimulate its ATPase activity (Faust et al., 2020; Jiang et al., 2019; Laufen et al., 1999; Lu & Cyr, 1998; Mogk et al., 2018; Yoo et al., 2022). Hsp70

then recruits and activates Hsp104, which threads substrate delivered by Hsp70 through Hsp104's hexameric ring and extracts the monomer from the aggregate to be refolded (Avellaneda et al., 2020; Carroni et al., 2014; Gates et al., 2017; Haslberger et al., 2007; Haslberger et al., 2008; Mogk et al., 2018; Rosenzweig et al., 2013; Seyffer et al., 2012; Yoo et al., 2022). This process is similar for other homologous Hsp100 disaggregases, such as bacterial ClpB.

*Dictyostelium discoideum* expresses a protein homologous to Hsp104, Hsp101. Hsp101 shares 65% similarity and 44% identity with Hsp104 (Figure 35B). Importantly, all key residues in both NBDs are conserved in Hsp101, with the exception of the glycine-alanine-arginine (GAR) motif at residues 824-826 in NBD2, which has been proposed to sense the nucleotide status and regulate CTD conformational changes during ATP hydrolysis (Grimminger-Marquardt & Lashuel, 2009; Mogk et al., 2003; Nicholls et al., 1991; Ogura & Wilkinson, 2001). The main structural difference between Hsp104 and Hsp101 is that Hsp101 is missing the short CTD (Figure 35B). Only one study has been done using Hsp101. It was observed that under heat stress, *Dictyostelium* expressing either mutant Htt or a prion protein formed foci of these proteins, and the foci dissipated during a recovery period (Malinowska et al., 2015). Overexpression of Hsp101 in *Dictyostelium* cells completely prevented the formation of foci under heat stress, and dominant negative variants of Hsp101 resulted in delayed dissipation of foci after heat stress (Malinowska et

al., 2015). These data suggest that Hsp101 acts as a disaggregase in *Dictyostelium*, however the true biological function of Hsp101 has not been determined.

Here I aimed to uncover Hsp101's function in *Dictyostelium*. I successfully generated viable Hsp101 *Dictyostelium* knockout strains using CRISPR-Cas9. I determined that these knockout strains both have an axenic growth defect that can be rescued by Hsp101 overexpression. I also found that a mutant Htt protein does not aggregate in the Hsp101 knockout under normal and heat stress conditions. Finally, to investigate Hsp101's intracellular interactors, I performed Hsp101 pulldowns in both Hsp101 knockout and rescue strains and performed quantitative mass spectrometry. Analysis of peptides identified in the screen showed that among the most upregulated proteins in the rescue strain were proteins involved the S phase kinase-associated protein 1 (Skp1)-cullin-F-box (SCF) complex, including cullins and F-box proteins, suggesting a potential role for Hsp101 in the SCF E3 ligase pathway.

#### ***4.1 Characterization of Dictyostelium Hsp101 knockout cells***

Until 2018, *Dictyostelium's* genome could not be efficiently edited using the clustered regularly interspaced short palindromic repeats (CRISPR)-associated protein 9 (Cas9) system. This is in-part due to the requirement of a flanking protospacer adjacent motif (PAM) for Cas9 to bind (Anders et al., 2014; Asano et al., 2021; Gasiunas et al., 2012; Jinek et al., 2012). PAMs consist of the sequence NGG, and drastically limit the binding sites in *Dictyostelium's* AT-rich genome (~78% AT content) (Eichinger et al., 2005) (Asano

et al., 2021; Muramoto et al., 2019). However, improved CRISPR tools, including an all-in-one *Dictyostelium*-specific vector encoding for your guide RNA, tRNA, and Cas9, as well as a mutated Cas9 to recognize a simpler PAM have been developed in the last 5 years and have greatly advanced the success of *Dictyostelium* genome editing by CRISPR-Cas9 (Asano et al., 2021; Muramoto et al., 2019). Therefore, at the time of the previous Hsp101 study CRISPR technology for *Dictyostelium* was not well-developed and dominant-negative Hsp101 variants were utilized instead.

I utilized the CRISPR-Cas9 system developed for *Dictyostelium* to generate an Hsp101 knockout (KO) cell line and investigate the function of Hsp101 in *Dictyostelium*. From my CRISPR screen, I was successful in generating two independent Hsp101 KO lines (KO3 and KO4) where the gene ended with a premature stop codon (Figure 36A). Using these KO strains, I wanted to determine if there were any phenotypes. *Dictyostelium* is a well-established model organism with many published protocols to probe gene function. I initially tested axenic growth, growth on a bacterial lawn, development, and spore germination phenotypes (Figure 36B-E). Of these, the only phenotype I observed was a defect in axenic growth in both KOs (Figure 36B). Because the observed phenotypes were the same between both KO strains, I chose to use Hsp101 KO4 for the remainder of my experiments.

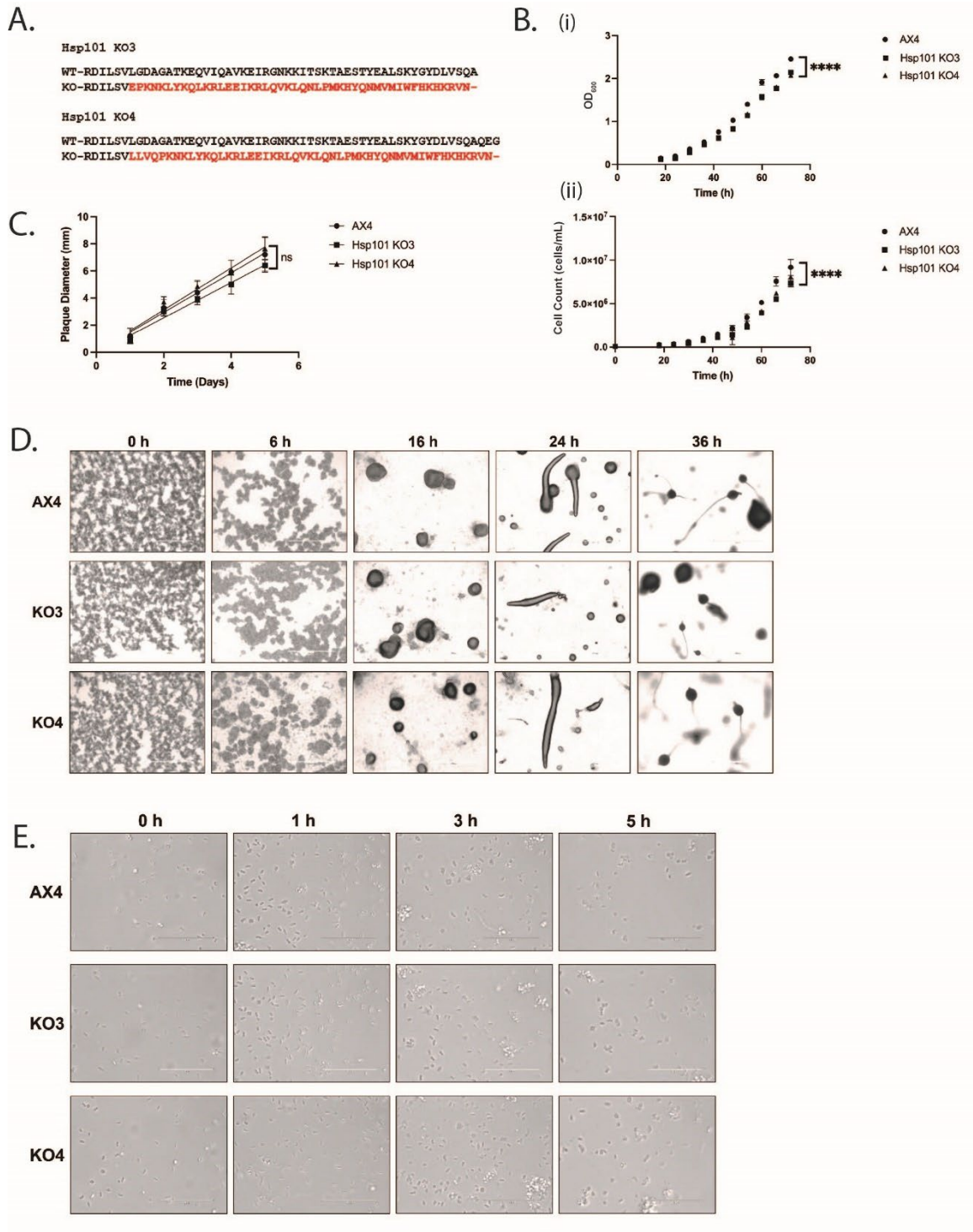
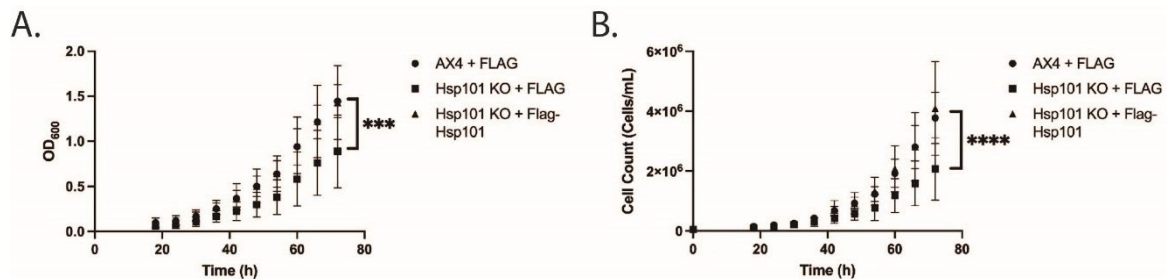


Figure 36: Hsp101 knockout cells have an axenic growth defect.

(A) Knockout (KO) *Dictyostelium discoideum* strains were generated using CRISPR/Cas9. The amino acid sequences of wildtype (WT) and mutant proteins are shown with mutated residues in red and (-) indicating a premature stop codon. (B) AX4 and Hsp101 KO strains were grown in shaker flasks for 72 h. Cell count or optical density (OD<sub>600</sub>) were taken every 6 h starting at 18 h of growth. Both KO strains had significant growth defects compared to AX4 (\*\*\*\*p<0.0001, n = 3) (C) AX4 and Hsp101 KO strains were plated with *K. aerogenes*. Once plaques appeared, the diameters were measured once daily for 5 days. No difference was observed in growth between AX4 and KO strains. (n = 3) (D) AX4 and Hsp101 KO strains were developed and imaged at the time points indicated. No difference in development was observed between the AX4 and KO strains. (n = 4, scale bar: 1 mm) (E) Spores from AX4 and Hsp101 KO strains were isolated and germinated. There was no difference in spore germination observed between strains (n = 3, scale bar: 100 μm).



**Figure 37: Overexpression of Hsp101 rescues the axenic growth defect.**

AX4 and Hsp101 KO strains expressing either pTxFLAG or FLAG-Hsp101 were grown in shaker flasks for 72 h. (A) Optical density (OD<sub>600</sub>) or (B) cell count was taken every 6 h starting at 18 h of growth. (\*\*p<0.001, \*\*\*\*p<0.0001, n = 3)

To determine if the growth phenotype was due to the lack of Hsp101, I overexpressed a FLAG-tagged version of Hsp101 in the Hsp101 KO strain and repeated the axenic growth assay. Overexpression of Hsp101 in the KO strain resulted in a rescue of the growth defect (Figure 37).

## ***4.2 Hsp101 does not act as a disaggregase in Dictyostelium's heat stress response***

While the lack of Hsp101 causes a growth defect under normal conditions, I was interested in determining if Hsp101 KO cells would be prone to protein aggregation. It has been previously shown that mutant Htt does not form foci with Hsp101 overexpression under heat stress and dominant negative Hsp101 mutants lead to prolonged clearance of foci (Malinowska et al., 2015). However, this has not been tested in a true knockout background.

I tested the aggregation of either mutant Htt exon 1 with 103 glutamines ( $\text{GFP}^{\text{Htt}^{\text{ex1Q103}}}$ ) or the native *Dictyostelium* prion protein  $\text{GFP}^{\text{eRF3}}$  (homologous to yeast Sup35) in either WT or KO cells under heat stress. GFP puncta indicating aggregates were not visible by microscopy in either AX4 or Hsp101 KO strains under normal and heat stress conditions (Figure 38A and B, microscopy performed by Felicia Williams). I also examined lysates by western blot and filter trap assay to determine the presence of insoluble  $\text{GFP}^{\text{Htt}^{\text{ex1Q103}}}$  or  $\text{GFP}^{\text{eRF3}}$ . SDS-PAGE revealed that  $\text{GFP}^{\text{Htt}^{\text{ex1Q103}}}$  did not form aggregates under heat stress in either AX4 or Hsp101 KO cells (Figure 38C and D). Surprisingly, aggregates were detected in the stacking gel for  $\text{GFP}^{\text{eRF3}}$  under normal and heat stress conditions in both cell types (Figure 38C). However, SDS insoluble species for eRF3 only appeared under heat stress conditions in the filter trap assay (Figure 38D). These results could suggest that eRF3 forms high molecular weight complexes in cells that

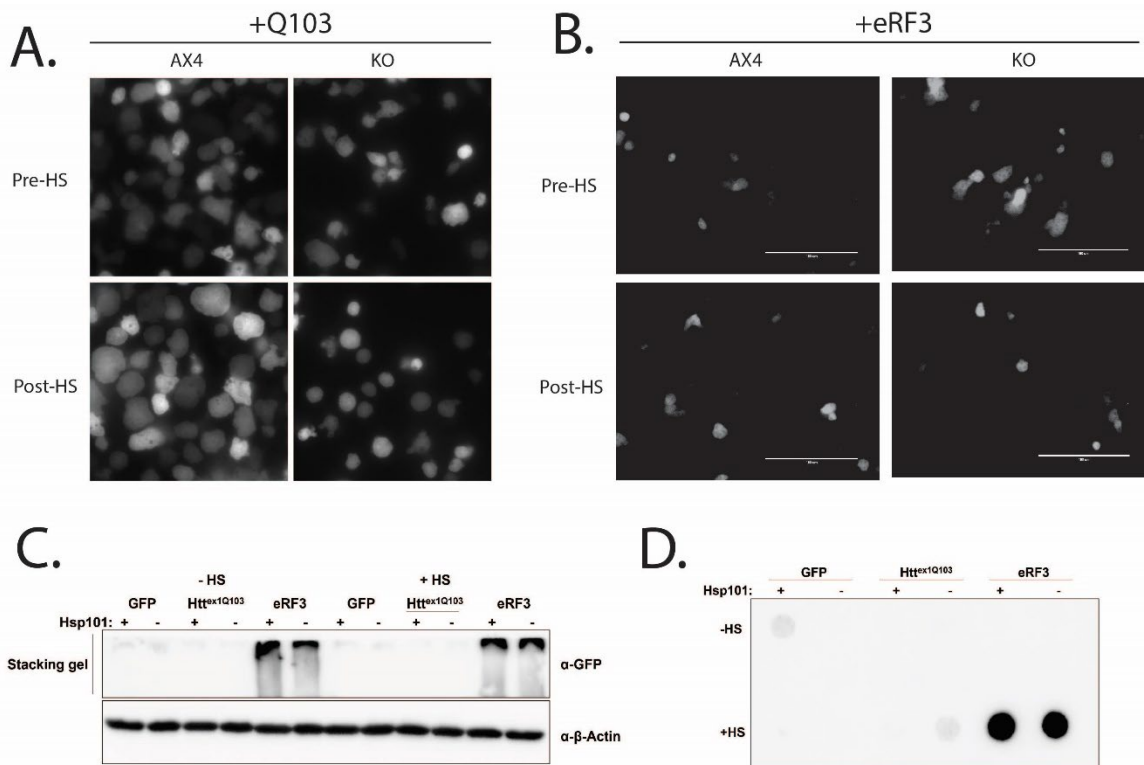


**Figure 38: Polyglutamine does not aggregate in Hsp101 KO cells, but eRF3 forms SDS-insoluble aggregates in WT and Hsp101 KO cells.**

(A) An expanded polyQ protein does not form puncta in *Dictyostelium*. AX4 *Dictyostelium* cells were electroporated with  $GFP^{Htt^{ex1Q103}}$  and imaged pre-heat stress (pre-HS) and 2 h post-heat stress (post-HS) at 30°C (performed by Felicia Williams). (B) The prion eRF3 does not form puncta in *Dictyostelium*. AX4 *Dictyostelium* cells were electroporated with  $GFP^{eRF3}$  and imaged pre-heat stress (pre-HS) and 2 h post-heat stress (post-HS) at 30°C (performed by Felicia Williams). (C) eRF3 forms aggregates in both WT and Hsp101 KO *Dictyostelium* strains. *Dictyostelium* lysates from (A) and (B) were subjected to SDS-PAGE and western blotted for GFP. Only the stacking gel is shown (n = 3). (D) Only heat-stressed *Dictyostelium* cells form SDS-insoluble aggregates. *Dictyostelium* lysates from (A) and (B) were subjected to filter trap assay and western blotted for GFP (n = 3).

become SDS insoluble under heat stress. However, Hsp101 does not play a role in polyQ or eRF3 insolubility, which does not agree with the previous dominant-negative data (Malinovska et al., 2015).

### ***4.3 Hsp101 is linked to many cellular pathways in Dictyostelium***

Because we determined that Hsp101 is not involved in keeping mutant Htt and eRF3 soluble under stress conditions, I next wanted to explore pathways in which Hsp101 was involved. To do this, I overexpressed either the pTxFLAG vector or Hsp101-FLAG in Hsp101 KO cells and performed FLAG pulldowns on cell lysates (Figure 39A). We performed quantitative mass spectrometry to identify proteins that were pulled down with Hsp101 (mass spectrometry and quantitation performed by Duke Proteomics and Metabolomics Core Facility, analysis performed by Matt Scaglione, Felicia Williams, and me). Initial gene ontology analysis revealed that Hsp101 pulled down many proteins involved in cellular metabolic processes and nucleotide binding (Figure 39B and C). This was not a surprising result as Hsp101 has canonical ATPase domains. Further analysis suggested that of the protein domains pulled down with Hsp101, the domains with the highest fold enrichment are associated with the SCF complex. These include cullins, cullin protein neddylation domains, leucine-rich repeats, motifs in proteasome subunits, and WD40 repeats (Figure 39D). Leucine-rich repeats and WD40 repeats are common motifs in certain types of F-box proteins. Interestingly, Hsp101 has been previously pulled down with the *Dictyostelium* F-box protein, FbxD (Sheikh et al., 2015). This suggests a role for Hsp101 in the SCF E3 ubiquitin ligase pathway.

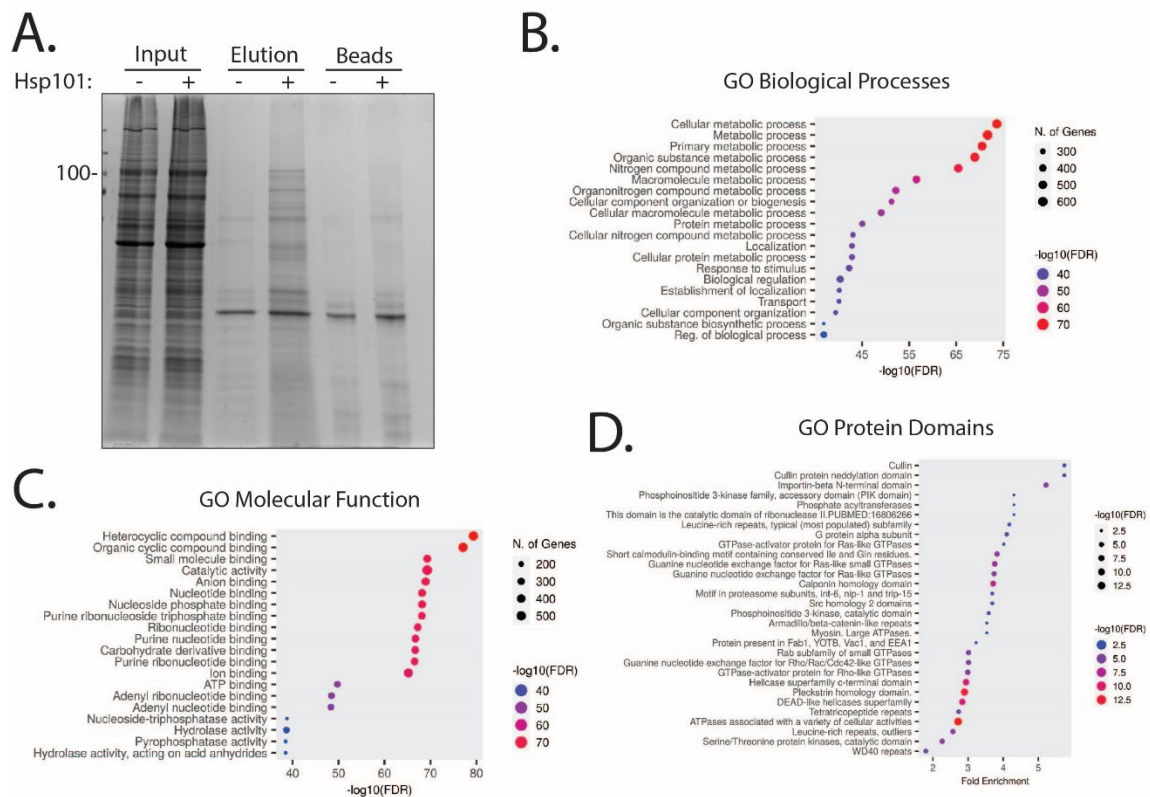


**Figure 39: Hsp101 is associated with components of the SCF E3 ubiquitin ligase pathway.**

(A) Hsp101 expressed in *Dictyostelium* pulls down numerous proteins. pTxFLAG or FLAG-Hsp101 were expressed in an Hsp101 KO *Dictyostelium* strain. FLAG pulldowns were performed on cell lysates and 1% input, elutions, and boiled beads were run on SDS-PAGE and stained with colloidal Coomassie stain (n = 4). Mass spectrometry was performed on all 4 samples. (B-D) Gene ontology analysis of mass spectrometry results reveal that Hsp101 interacts with members of the SCF E3 ubiquitin ligase pathway. Pictured are analyses for biological processes (B), molecular function (C), and protein domains (D), that Hsp101 interacts with in cells.

#### 4.4 Discussion

Here I attempted to uncover the biological function of the *Dictyostelium* AAA+ ATPase Hsp101. I was successful in developing Hsp101 KO *Dictyostelium* strains and

determined that the only major phenotype was an axenic growth defect (Figure 36). This defect was rescued by overexpression of Hsp101 (Figure 37). We also found that Hsp101 was dispensable for suppressing aggregation of both mutant Htt and the prion eRF3 in *Dictyostelium* (Figure 38). To better understand Hsp101's interactome, I performed pulldowns of Hsp101 from Hsp101 KO *Dictyostelium* lysate with or without Hsp101 and analyzed the results by mass spectrometry. Our data identified numerous components of the SCF ubiquitin ligase pathway that were enriched in the presence of Hsp101 (Figure 39). This suggests a potential role for Hsp101 in this pathway.

The only defect observed in the Hsp101 KO strains was a growth defect in axenic medium (Figure 36B). However, growth was the same as WT on a bacterial lawn (Figure 36C). This phenotype is consistent with defects in pinocytosis, but not phagocytosis. It could be possible that Hsp101 plays a role in macropinocytosis mechanisms. There are currently no data suggesting that Hsp101 or other AAA+ ATPases is involved in macropinocytosis. However, this growth defect could implicate its direct or indirect role on these processes.

My investigation of Hsp101's role in proteostasis revealed that lack of Hsp101 does not result in accumulation of either mutant Htt protein or a native *Dictyostelium* prion protein (Figure 38). These data suggest that Hsp101 is not involved in maintaining or disaggregating misfolded proteins in *Dictyostelium*. We did observe, however, that the prion protein eRF3 was forming high molecular weight species in both WT and Hsp101

KO strains that only formed SDS-insoluble species under heat stress (Figure 38C and D). While this phenomenon is not dependent on Hsp101, it was a surprising observation. eRF3 is homologous to the yeast prion Sup35, but it does not contain the aggregation-prone polyQ/N rich region found in Sup35. It is interesting that eRF3 aggregates while we see no aggregation from a mutant polyQ protein. It is necessary to further investigate the behavior of eRF3 and other prions in *Dictyostelium* biology to better understand this phenomenon.

To gain further insight into the biological role of Hsp101, I performed FLAG pulldowns in Hsp101 KO cells expressing either pTxFLAG or FLAG-Hsp101 to learn more about its interactome. From our screen, we got thousands of proteins that were upregulated with Hsp101 overexpression. One group of proteins with the highest fold enrichment caught our interest: cullins and other SCF complex-associated proteins (Figure 39).

The SCF complex is a part of the UPS that is involved in many cellular processes including transcription factor, cell cycle, DNA damage response, and growth factor receptor regulation (Ardley & Robinson, 2005; Bosu & Kipreos, 2008; Chung & Delleire, 2015; de Bie & Ciechanover, 2011; Gilberto & Peter, 2017; Kim et al., 2022; Li & Jin, 2012; Qi & Ronai, 2015; Schwechheimer & Villalobos, 2004; Serrano et al., 2018; Vodermaier, 2004; Willems et al., 2004). This complex is made up of four components: Skp1, a ubiquitin ligase, a cullin protein, and an F-box protein (Frescas, 2008; Xie et al., 2019; N. Zheng et

al., 2002). Cullin proteins (CulA-E in *Dictyostelium*) act as a scaffold for Skp1 and the E3 ligase (Kim et al., 2022; Zimmerman et al., 2010). Prior to SCF complex assembly, the cullin is bound to Cand1, preventing Skp1 recruitment (Dubiel et al., 2013; Kim et al., 2022; Liu et al., 2018; Pierce et al., 2013; J. Zheng et al., 2002). To activate assembly, the cullin gets neddylated, which allows Skp1 to bind to the N-terminus and Cand1 is displaced (Kim et al., 2022; Liu et al., 2002; J. Zheng et al., 2002). At this point, the ubiquitin ligase (Rbx1 in *Dictyostelium*) can bind the C-terminus of the cullin and an F-box protein is recruited to Skp1 (Xie et al., 2019). F-box proteins confer substrate selectivity to the SCF complex and there are three types: WD repeat proteins, leucine-rich proteins, and F-box only proteins (Xie et al., 2019; Zimmerman et al., 2010). Both WD40 repeat domains and leucine-rich repeat domains were enriched in our screen, suggesting Hsp101 interacts with F-box proteins as well as cullins (Figure 39D). In addition, Hsp101 was previously found to interact with the F-box protein FbxD in *Dictyostelium* (Sheikh et al., 2015).

The dissociation of the SCF complex is not as well-studied. However, it is known that the cullin is deneddylated by the COP9 signalosome and that there is a AAA+ ATPase involved in the dissociation process (Kim et al., 2022; Rao et al., 2020). In yeast, this is Cdc48/p97 (Jentsch & Rumpf, 2007). In *Dictyostelium*, it is unclear how SCF complex dissociation comes about. *Dictyostelium* has a homolog of p97, but our mass spectrometry data point to Hsp101, another AAA+ ATPase, interacting with SCF complex components. This suggests that Hsp101 could be the source of ATP to initiate disassembly.

## ***4.5 Materials and Methods***

### **Expression constructs**

Hsp101 (DDB\_G0291314) was PCR amplified from *Dictyostelium* cDNA and cloned into pTxFLAG (Dictybase) using XbaI and XhoI.

### ***Dictyostelium* culture and transformation**

*Dictyostelium* AX4 or KO cells were maintained in 10 cm petri dishes at 22°C in HL5 medium. Cells were sub-cultured to maintain a density no greater than  $4 \times 10^6$  cells/ml.

Transformations were performed as previously described (Knecht & Pang, 1995). Briefly,  $5 \times 10^6$  cells were washed with H-50 buffer (20 mM HEPES, 50 mM KCl, 10 mM NaCl, 1 mM MgSO<sub>4</sub>, 5 mM NaHCO<sub>3</sub>, 1 mM NaH<sub>2</sub>PO<sub>4</sub>; pH adjusted to 7.0 with HCl/NaOH). Cells were electroporated in a 1-mm cuvette (0.85 kV/25  $\mu$ F, 0.6 ms, twice with 5 s in between). Cells were selected with 10  $\mu$ g/ml G-418 for 1 week (Pang et al., 1999).

### **Hsp101 Knockout by CRISPR-Cas9**

Gene knockout was conducted by CRISPR-Cas9 as previously described (Sekine et al., 2018). Three small guide RNAs (sgRNA) specific to Hsp101 were designed using CRISPR RGEN Tools Cas-designer and checked for off-target sites using the CRISPR RGEN Tools Cas-OFFinder (Table 3) (Bae et al., 2014; Sekine et al., 2018). sgRNAs were cloned into the pTM1285 vector (acquired from the *Dictyostelium* Stock Center) using BpI (New England Biolabs) (Sekine et al., 2018).

**Table 3: Primers used for sgRNA cloning into pTM1285.**

Gene ID	Gene Name	Primer	Sequence
DDB_G0291314	Hsp101	sgRNA-1 sense(+)	AGCAACAATTAGCACCAATACATT
		sgRNA-1 antisense	AAACAATGTATTGGTGCTAATTGT
		sgRNA-2 sense(+)	AGCAGATGTACCAAAAATTGATGC
		sgRNA-2 antisense	AAACGCATCAATTTTGGTACATC
		sgRNA-3 sense(+)	AGCATTATCAGTATTGGGAGATGC
		sgRNA-3 antisense	AAACGCATCTCCCAATACTGATAA

To conduct gene knockout, WT AX4 cells were electroporated with each pTM1285-sgRNA construct using the standard protocol described on Dictybase (Pang et al., 1999). Briefly,  $5 \times 10^6$  AX4 cells were spun down at  $500 \times g$  and washed twice in ice-cold H50 buffer (20 mM HEPES, 50 mM KCl, 10 mM NaCl, 1 mM MgSO<sub>4</sub>, 5 mM NaHCO<sub>3</sub>, 1 mM NaH<sub>2</sub>PO<sub>4</sub>). Cells were resuspended in 100  $\mu$ L ice-cold H50 buffer and combined with 10  $\mu$ g of pTM1285-sgRNA. Cell and DNA mixture was added to a pre-cooled 1 mm cuvette and electroporated at 0.85 kV/25 mF/time constant 0.6 ms twice with about 5 s between pulses. Cells were then incubated on ice for 5 min and added to 10 mL of HL5 media on 10 cm plates. G-418 (Gibco) was added to the plates 8-16 h post-electroporation at 10  $\mu$ g/mL. After 72 h of selection, the cells were collected and were plated on SM agar plates with *Klebsiella aerogenes* bacterial lawns. Plates were incubated at room temperature for 5

days, after which clonal isolates were picked and transferred to 96-well plates containing HL5 media.

Once sufficient growth was observed in the 96-well plates, cells were transferred to larger 24-well plates. Once cells were confluent, they were collected from each well and pelleted by centrifugation at  $500 \times g$  for five minutes. Media was removed from cell pellets and pellets were lysed with 15  $\mu\text{L}$  of lysis buffer (50 mM KCl, 10 mM Tris pH 8.3, 2.5 mM  $\text{MgCl}_2$ , 0.45% IGEPAL CA360, 0.45% Tween 20, 1  $\mu\text{L}$  of 20  $\mu\text{g}/\text{mL}$  proteinase K per 25  $\mu\text{L}$  lysis buffer) prior to heat inactivation of proteinase K at  $95^\circ\text{C}$  for one minute (Charette & Cosson, 2004). To screen for the generation of indels by CRISPR, a small region surrounding the sgRNA target site for each gene was PCR-amplified and ran on a 4.5% agarose gel. Clonal isolates whose PCR products appeared to differ in size when compared to WT were cloned into the pCR4-TOPO vector using the TOPO TA Cloning Kit for Sequencing (ThermoFisher) and sent for Sanger sequencing using the M13 reverse sequencing primer. Mutations that resulted in a frameshift mutation that was not a multiple of three were considered to be knockouts.

Primers used for screening are shown in Table 4. Ideally, the amplified region would cover the 100 bp flanking the cut site on either side to produce an amplicon approximately 200 bp in length. However, in locations where PCR primers are not easily designed, amplicons of up to 400 bp are also suitable to assess indel generation.

**Table 4: Primers used for screening of indel generation by CRISPR-Cas9**

Gene Name	Primer	Sequence
Hsp101	Screening-Rv-1	CTGGATTTTGAACAGGTTGTTTGG
	Screening-Fw-1	ATGTCATTTAATCCAGAAGAATTTACTGATAAAACA
	Screening-Rv-2	CTGGATTTTGAACAGGTTGTTTGG
	Screening-Fw-2	ACAATTAGCACCAATACATTAGCA
	Screening-Rv-3	AACCATATTTTGATAATGCTTCATAGGTAG
	Screening-Fw-3	GGT GAT TCT CAT TTA GCA GTT GAC C

### ***Dictyostelium* Growth Assays**

#### Axenic Growth

Prior to the experiment, AX4 and Hsp101 KO strains were maintained in shaker flasks at 22°C in HL5 medium. Cells were subcultured to maintain a density no greater than  $4 \times 10^6$  cells/ml. For axenic growth assays, flasks were subcultured to have  $5 \times 10^4$  cells/mL. Cell count and optical density were taken every 6 h starting after 18 h of growth.

#### Growth on Bacterial Lawns

For growth on bacteria, AX4 or Hsp101 KO cells were washed and collected in ice-cold PBS. Cells were counted and serial diluted to have either 100 or 200 cells in 100  $\mu$ L PBS. Cells were added to 200  $\mu$ L of *Klebsiella aerogenes* and immediately plated on SM agarose plates. Plates were incubated inverted at 22°C and checked daily for plaques. Once plaques appeared, their diameter was measured every day for 5 days.

### ***Dictyostelium* Development**

To induce development,  $1 \times 10^8$  cells were washed three times with developmental buffer (5 mM Na<sub>2</sub>HPO<sub>4</sub>, 5 mM KH<sub>2</sub>PO<sub>4</sub>, 1 mM CaCl<sub>2</sub>, 2 mM MgCl<sub>2</sub>; pH adjusted to 6.5

with HCl/NaOH) and grown up on KK2 agarose plates at 22°C (Fey et al., 2007). Cells were developed for various time points and imaged using the Evos FL Auto Imaging System.

### ***Dictyostelium* Spore Germination**

AX4 or Hsp101 KO cells were developed for 3 days. For spore isolation, developed cells were harvested, resuspended in 1 ml of 10 mM MES (pH adjusted to 6.5 with HCl or NaOH), and vortexed for 1 min. An additional 4 ml of buffer was added to cells and they were vortexed again for 1 min. Cell suspensions were passed through a 114 Whatman filter paper (Chiew et al., 1985). Spores were then resuspended at a density of  $1.5 \times 10^6$  cells/ml in HL5 medium to induce germination and images were taken at various time points using the EVOS FL Auto Imaging System.

### ***Dictyostelium* Heat Stress Assays**

AX4 or Hsp101 KO cells expressing either GFP,  $\text{GFP}^{\text{Htt}^{\text{ex1Q103}}}$ , or  $\text{GFP}^{\text{eRF3}}$  were grown to confluency in a 10 cm petri dish. Prior to heat stress cells were imaged on either using the EVOS FL Auto Imaging System (cells expressing  $\text{GFP}^{\text{eRF3}}$ ) or a Deltavision microscope with a 60x/1.42 N.A. objective (cell expressing  $\text{GFP}^{\text{Htt}^{\text{ex1Q103}}}$ ). Cells were then heat stressed in a 30°C water bath for 2 h and immediately imaged post-heat stress. Samples not used for imaging were washed in ice cold PBS and lysed in 200  $\mu\text{L}$  RIPA buffer (50 mM Tris, pH 8.0, 150 mM NaCl, 0.1% (w/v) SDS, 0.5% (w/v) sodium deoxycholate, 1% (v/v) IGEPAL CA-630) supplemented with a 1:100 dilution of protease inhibitor cocktail (Millipore-

Sigma). Protein concentration was determined by BCA Assay (ThermoFisher Scientific) and 20 µg protein were prepared for either SDS-PAGE or filter trap assay.

SDS-PAGE: Gradient SDS-PAGE gels ran with 20 µg protein supplemented with 4X Laemmli buffer that had been boiled for 4 min. Gels were transferred onto PVDF membrane (BioRad) for western blotting.

Filter Trap Assay: Twenty micrograms of protein were diluted to 90 µL in RIPA buffer and then 10 µL of 10% SDS was added. Samples were diluted to 1 mL with 1% SDS in PBS and filtered through a 0.2 mm cellulose acetate membrane (Sterlitech). Samples were washed with 1 mL of 1% SDS in PBS and subjected to western blot.

Western Blot: Membranes were blocked with 5% milk in TBS with 0.1% Tween (TBST) for 1 h. Membranes were then incubated with Anti-GFP (Invitrogen by ThermoFisher Scientific; A11122; used at 1:1000), washed three times for 10 min with TBST, incubated with peroxidase-conjugated rabbit secondary antibody (Jackson ImmunoResearch Laboratories; 111-035-045; used at 1:5000), and washed again three times for 10 min with TBST. Membranes were then incubated with enhanced chemiluminescence buffer (50 mM Na<sub>2</sub>HPO<sub>4</sub>; 50 mM Na<sub>2</sub>CO<sub>3</sub>; 10 mM NaBO<sub>3</sub>•4H<sub>2</sub>O; 250 mM luminol; 90 mM coumaric acid) and developed using ChemiDoc MP Imaging System (BioRad)

## **FLAG pulldowns**

Hsp101 KO cells expressing either pTXFLAG or FLAG-Hsp101 were grown to confluency in 15 cm petri dishes. Cells were lysed in 1.5 mL RIPA buffer (50 mM Tris, pH 8.0, 150 mM NaCl, 0.1% (w/v) SDS, 0.5% (w/v) sodium deoxycholate, 1% (v/v) IGEPAL CA-630) supplemented with a 1:100 dilution of protease inhibitor cocktail (Millipore-Sigma) and incubated on 50  $\mu$ L of ANTI-FLAG M2 affinity gel beads (Millipore-Sigma) for 3 h at 4°C. Beads were washed 3 times in ice cold TBS and proteins were eluted by incubating at room temperature in 50  $\mu$ L of 0.1 M glycine, pH 2.0 for 5 min. Samples were then neutralized with 10  $\mu$ L of 0.5 M Tris, pH 7.5, 150 mM NaCl. Pulldown was verified by QC colloidal Coomassie staining (BioRad) before being sent off for mass spectrometry analysis.

## **Mass Spectrometry and Gene Ontology**

### Sample Preparation:

Samples were spiked with undigested bovine casein at a total of either 1 or 2 pmol as an internal quality control standard. Samples were next supplemented with 6.3  $\mu$ L of 20% SDS, a final concentration of 1.2% phosphoric acid and 796  $\mu$ L of S-Trap (Protifi) binding buffer (90% MeOH/100mM TEAB). Proteins were trapped on the S-Trap micro cartridge, digested using 20 ng/ $\mu$ L sequencing grade trypsin (Promega) for 1 hr at 47°C, and eluted using 50 mM TEAB, followed by 0.2% FA, and lastly using 50% ACN/0.2% FA.

All samples were then lyophilized to dryness. Samples were resolubilized using 120  $\mu$ L of 1% TFA/2% ACN with 12.5 fmol/ $\mu$ L yeast ADH.

#### LC-MS/MS Analysis:

Quantitative LC/MS/MS was performed on 3  $\mu$ L (25% of total sample) using an MClass UPLC system (Waters Corp) coupled to a Thermo Orbitrap Fusion Lumos high resolution accurate mass tandem mass spectrometer (Thermo) equipped with a FAIMSPro device via a nanoelectrospray ionization source. Briefly, the sample was first trapped on a Symmetry C18 20 mm  $\times$  180  $\mu$ m trapping column (5  $\mu$ L/min at 99.9/0.1 v/v water/acetonitrile), after which the analytical separation was performed using a 1.8  $\mu$ m Acquity HSS T3 C18 75  $\mu$ m  $\times$  250 mm column (Waters Corp.) with a 90-min linear gradient of 5 to 30% acetonitrile with 0.1% formic acid at a flow rate of 400 nanoliters/minute (nL/min) with a column temperature of 55C. Data collection on the Fusion Lumos mass spectrometer was performed for three different compensation voltages (-40v, -60v, -80v). Within each CV, a data-dependent acquisition (DDA) mode of acquisition with a r = 120,000 (@ m/z 200) full MS scan from m/z 375 – 1500 with a target AGC value of 4e5 ions was performed. MS/MS scans were acquired in the ion trap in Rapid mode with a target AGC value of 1e4 and max fill time of 35 ms. The total cycle time for each CV was 0.66s, with total cycle times of 2 sec between like full MS scans. A 20s dynamic exclusion was employed to increase depth of coverage. The total analysis cycle time for each injection was approximately 2 hours.

### Quantitative Data Analysis:

Following UPLC-MS/MS analyses, data were imported into Proteome Discoverer 2.5 (Thermo Scientific Inc.). In addition to quantitative signal extraction, the MS/MS data was searched against the TrEMBL D. discoideum database (downloaded in Nov 2019) and a common contaminant/spiked protein database (bovine albumin, bovine casein, yeast ADH, etc.), and an equal number of reversed-sequence “decoys” for false discovery rate determination. Sequest with Infernyx enabled (v 2.5, Thermo PD) was utilized to produce fragment ion spectra and to perform the database searches. Database search parameters included variable modification on Met (oxidation). Search tolerances were 2ppm precursor and 0.8Da product ion with full trypsin enzyme rules. Peptide Validator and Protein FDR Validator nodes in Proteome Discoverer were used to annotate the data at a maximum 1% protein false discovery rate based on q-value calculations. Note that peptide homology was addressed using razor rules in which a peptide matched to multiple different proteins was exclusively assigned to the protein has more identified peptides. Protein homology was addressed by grouping proteins that had the same set of peptides to account for their identification. A master protein within a group was assigned based on % coverage.

Prior to imputation, a filter was applied such that a peptide was removed if it was not measured in at least 2 unique samples (50% of a single group). After that filter, any missing data missing values were imputed using the following rules; 1) if only one single

signal was missing within the group of three, an average of the other two values was used or 2) if two out of three signals were missing within the group of three, a randomized intensity within the bottom 2% of the detectable signals was used. To summarize to the protein level, all peptides belonging to the same protein were summed into a single intensity. These protein levels were then subjected to a normalization in which the top and bottom 10 percent of the signals were excluded and the average of the remaining values was used to normalize across all samples. These normalized protein level intensities are what were used for the remainder of the analysis.

Gene ontology was performed by ShinyGO 0.76.3 on November 10, 2022. FDR cutoff was 0.05 and pathway size was 2-2000 with redundancy removed.

### **Statistical Analysis**

For growth curve analysis, values were entered into GraphPad Prism and analyzed by group analysis, two-way ANOVA for multiple comparisons. Differences were considered statistically significant at a P-value less than 0.05.

## 5. Conclusion

Here, I wanted to further explore the protein quality control pathways of the social amoeba *Dictyostelium discoideum* with regards to its resistance to protein aggregation. I began by showing that SRCP1 prevents polyQ aggregation by a sequence in its C-terminus, SRCP1<sup>61-80</sup>. I also determined that *in vitro* SRCP1<sup>61-80</sup> only delays aggregation, and polyQ aggregates formed in the presence of SRCP1<sup>61-80</sup> have a different morphology than aggregates without SRCP1<sup>61-80</sup>.

To investigate the molecular function of SRCP1, I next wanted to gain insight into its structure. I exhausted many methods to purify recombinant SRCP1 but was unsuccessful due to its insolubility. This was most likely due to SRCP1 being intrinsically disordered. I instead turned to computational modeling to predict key structural aspects of SRCP1. Our modeling predicted that SRCP1 is a largely disordered protein with the functional region consistently predicted to be structured as a  $\beta$ -hairpin, and this is supported by NMR analysis. I was able to determine that SRCP1<sup>61-80</sup> prevents polyQ aggregation at the secondary nucleation step of the aggregation process and that it most likely binds to a region of huntingtin exon 1 other than the polyQ region, such as the N-terminal domain. Finally, I determined that SRCP1<sup>61-80</sup> is sufficient to suppress polyQ aggregation in human cells as well as another polyQ protein, ataxin-3.

Another protein that has been implicated in preventing protein aggregation in *Dictyostelium* is Hsp101. I wanted to explore the biological role of Hsp101 within

*Dictyostelium*. I discovered that KO of Hsp101 caused only a slight growth defect in axenic medium. We performed experiments in the Hsp101 KO strain to determine if Hsp101 was responsible for disaggregating proteins in *Dictyostelium*. In the absence of Hsp101, we did not observe the accumulation or disaggregation of polyQ or prion proteins occurring, suggesting an alternative role for Hsp101 in *Dictyostelium*. I followed this with an Hsp101 pulldown to gain insight into the Hsp101 interactome. While its interactome is widespread, some of the highest fold enrichments in protein domains were in proteins associated with the SCF ubiquitin ligase pathway. This could implicate a role for Hsp101 within this pathway, perhaps as source of ATP hydrolysis for the dissociation of the SCF complex.

### ***5.1 Determining the role of other SRCP1 domains and SRCP1-like proteins***

While we understand the function of SRCP1<sup>61-80</sup>, the purpose of the remaining 68 amino acids remains unclear. According to our modeling predictions, the rest of SRCP1, specifically the N-terminus, is highly dynamic and disordered. This is most likely the reason I was unable to purify recombinant SRCP1 for structural studies. We also know that the N-terminus of SRCP1 is dispensable in the context of suppressing polyQ aggregation. However, we do not know if this region of the protein plays any other role in *Dictyostelium*.

Continuing studies on SRCP1 should focus on elucidating the purpose of its N-terminus. One hypothesis is that the N-terminus functions as a “cap” to prevent SRCP1 from binding to more than one polyQ protein. We have previously shown that SRCP1 targets proteins to the proteasome for degradation, a pathway that is for smaller debris (Santarriaga et al., 2018). This implicates that SRCP1 does not target large aggregates, nor does it co-aggregate with aggregation-prone proteins. Additionally, polyQ aggregates formed after 72 h in the presence of the SRCP1 peptide have a different morphology than polyQ aggregates alone. This suggests that the peptide delays aggregation, but over time integrates into the polyQ aggregates, forming mixed amyloid. We have not observed co-aggregation of polyQ and SRCP1 in cells, especially since SRCP1 is rapidly degraded. Future experimentation should utilize *in vitro* TEM experiments to determine if SRCP1<sup>61-80</sup> does form mixed amyloid with polyQ. It would also be interesting to compare full-length SRCP1 to SRCP1<sup>61-80</sup> in cells to investigate whether the lack of the N-terminus would cause co-aggregation with polyQ. Additionally, it would be beneficial to study if SRCP1<sup>61-80</sup> is rapidly degraded in cells, or if it is degraded more slowly and there is an accumulation of soluble polyQ.

If SRCP1 does form amyloid, it is possible that *Dictyostelium* utilizes it for a biological purpose (functional amyloid). While amyloid is better known to have pathogenic consequences in humans, many organisms have been found to use amyloid for functional purposes. Functional amyloid appears in nature as structural components

in bacterial biofilms, fungal coats, spider silk, and insect and fish eggshells (Butko et al., 2001; Iconomidou et al., 2006; Kenney et al., 2002; Mackay et al., 2001; Pham et al., 2014; Podrabsky et al., 2001). In addition to *srcp1*, there are approximately 70 other *Dictyostelium*-specific genes with high sequence homology to SRCP1. The proteins have unknown function, although it is possible that they could function in a similar manner to SRCP1 by helping suppress protein aggregation. There is little literature covering this family of genes, but one study suggests that they are upregulated during *Dictyostelium* development (Vicente et al., 2008). It was shown that a subset of genes from this family are upregulated around 10 h of development, and their promoter activity directed expression to pre-stalk cells (Vicente et al., 2008). I previously utilized dictyExpress to analyze the mRNA expression profile of all the SRCP1-like genes and found that the majority are expressed during development (Table 5). It is therefore feasible that *Dictyostelium* could use functional amyloid to help stabilize its developmental structures. It would be of interest to determine if these proteins are secreted at different points in development, and to also analyze development structure by an EM method to demonstrate whether functional amyloid is used within these structures, particularly the fruiting body's stalk.

**Table 5: SRCP1-like genes are upregulated during development.**

<b>Expression Time Point During Development</b>	<b>Number of Genes Expressed</b>
12 h	3
14 h	15
16 h	10
18 h	33
20 h	1
22 h	5
24 h	3
Low Expression During Development	8

## ***5.2 Elucidating Hsp101's function as an ATPase and a chaperone***

From my Hsp101 study, I did not observe a disaggregase function for this protein in cells. Using my Hsp101 KO cells, I determined that the only major phenotype was an axenic growth defect. This phenotype is commonly seen in strains that are defective in macropinocytosis, the process by which *Dictyostelium* consumes nutrients in axenic culture. Macropinocytosis is a well-studied event in *Dictyostelium*, and the mechanism and components are fairly established. There is one ATPase involved, the vacuolar ATPase (V-ATPase), which is responsible at the early stages of macropinocytosis for acidification of the endosomal lumen, initiating digestion (Clarke et al., 2002; Gotthardt et al., 2002; Vines & King, 2019). The V-ATPase is the most-studied component of macropinocytosis. It is composed of numerous subunits, the largest (VatM) of which is essential for cell viability (Liu & Clarke, 1996; Liu et al., 2002; Vines & King, 2019). Notably, it is not an AAA+ ATPase like Hsp101. Hsp101 KO does not cause a loss in cell viability, so it would not play a critical role in macropinocytosis. However, it could be acting indirectly in this

process. To investigate this, it would first be necessary to ascertain that the slow axenic growth is indeed due to a macropinocytosis defect. If so, the appropriate experiments should be carried out to elucidate the function that Hsp101 has in micropinocytosis, such as growth with heat-killed bacteria. If not, then further experiments should focus on the pathway affected that causes the growth impairment.

We did not see accumulated mutant Htt or eRF3 under heat stress conditions via microscopy in our Hsp101 KO strain, which has been previously observed using a Hsp101 dominant negative mutant (Malinovska et al., 2015). I did, however, observe that eRF3 accumulated in *Dictyostelium* via western blot analysis regardless of Hsp101 status. Future experiments should focus on looking at the prion properties of eRF3 in *Dictyostelium* and whether Hsp101 has an effect on eRF3, much like its yeast ortholog Hsp104 has on Sup35. This would include studying eRF3 persistence as a prion in daughter cells as well as clearance of eRF3 from the cell.

The other potential role for Hsp101 could be in the SCF complex ubiquitin pathway, as suggested by our mass spectrometry data. While this pathway is well-studied in other systems, it has not been widely investigated in *Dictyostelium*. One aspect of this pathway that has not been the primary focus of SCF complex research is the dissociation of the SCF complex. While assembly is initiated by neddylation of a cullin protein, deneddylation signals for dissociation but an energy source is also required (Kim et al., 2022; Rao et al., 2020). In yeast it has been shown that Cdc48/p97, another AAA+ ATPase

participates in the disassembly of the SCF complex (Jentsch & Rumpf, 2007). *Dictyostelium* has a p97 ortholog that could function similarly in the SCF complex dissociation. I have established here, however, that *Dictyostelium* orthologs of yeast proteins do not necessarily function the same, as Hsp101 does not seem to act as a disaggregase. It is possible that Hsp101 may act as the ATPase to dissociate the SCF complex in *Dictyostelium*. Validation experiments must be performed in order to confirm this. It will first be essential to verify that the SCF components that were identified in our screen do interact with Hsp101. Then it would be important to follow up with Hsp101 functional assays, both *in vitro* and in cells, to show that it is the driving force of SCF complex dissociation.

## 5.2 Conclusions

Here I investigated two proteins involved in *Dictyostelium's* proteostasis. I found that SRCP1's C-terminus is sufficient to suppress polyQ aggregation. I also showed that SRCP1 most likely has a  $\beta$ -hairpin structure at residues 61-80, consistent with the hypothesis that SRCP1 uses an amyloid-like region to bind to amyloid of aggregation-prone proteins. Additionally, I determined that SRCP1 inhibits aggregation at the secondary nucleation pathway, and its function is broadly applicable to other polyQ proteins. Finally, I explored the biological role of *Dictyostelium's* Hsp101 and demonstrated that it does not function as a disaggregase, as previously thought, but may function as a part of the SCF ubiquitin ligase pathway. This work has yielded more insight on *Dictyostelium's* proteostasis pathways, especially in how it has naturally overcome the

obstacle of protein aggregation. This model organism could be the key to unlocking new therapies to cure or even prevent protein aggregation diseases.

## Appendix – Contributions to other projects<sup>1</sup>

The below figures are experimental contributions I made to a project in the lab unrelated to my dissertation project.

For this project, I performed ubiquitination reactions to show that the E2 ubiquitin conjugating enzyme, UbcH5, was capable of ubiquitinating its substrate (either the Josephin domain of ataxin-3 (JD) or full-length ataxin-3 (ATXN3)) in the absence of a ubiquitin ligase, in this case C-terminus of Hsc70 interacting protein (CHIP).

---

<sup>1</sup> This section is adapted with permission from the published article:

Kanack, AJ, Vittal, V, Haver, HN, Keppel, T, Gundry, RL, Klevit, RE, Scaglione, KM. (2020) UbcH5 Interacts with Substrates to Participate in Lysine Selection with the E3 Ubiquitin Ligase CHIP. *Biochemistry*. 59(22):2078-2088. <https://doi.org/10.1021/acs.biochem.0c00084>.

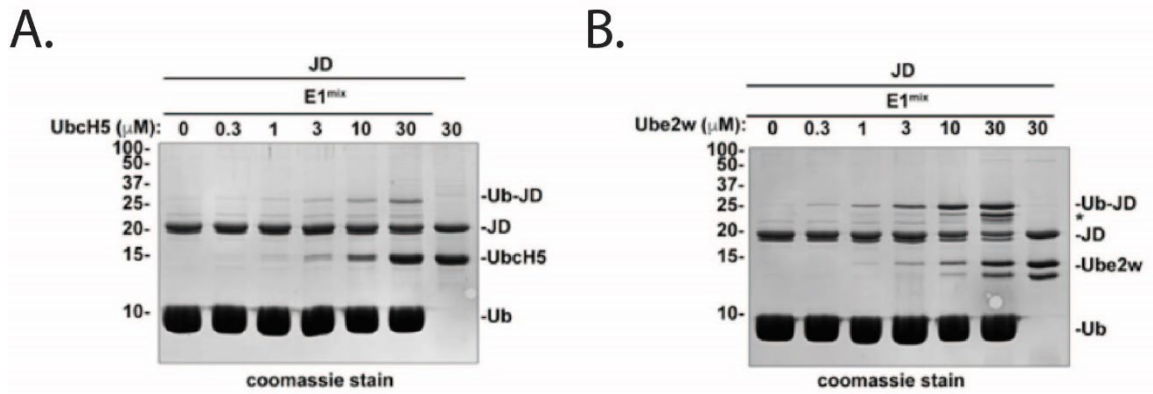


**Figure 40: Increased concentrations of an E2 ubiquitinating enzyme and substrate bypasses the need for and E3 ubiquitin ligase for *in vitro* ubiquitination assays.**

(A) Ubiquitination of JD by UbcH5. Ubiquitination assays using 20  $\mu$ M JD were performed with the indicated concentration of the E2 UbcH5c. Reactions were visualized by Coomassie stain. (B) Ubiquitination of JD by Ube2w. A similar reaction as in (A) but using the E2 Ube2w.

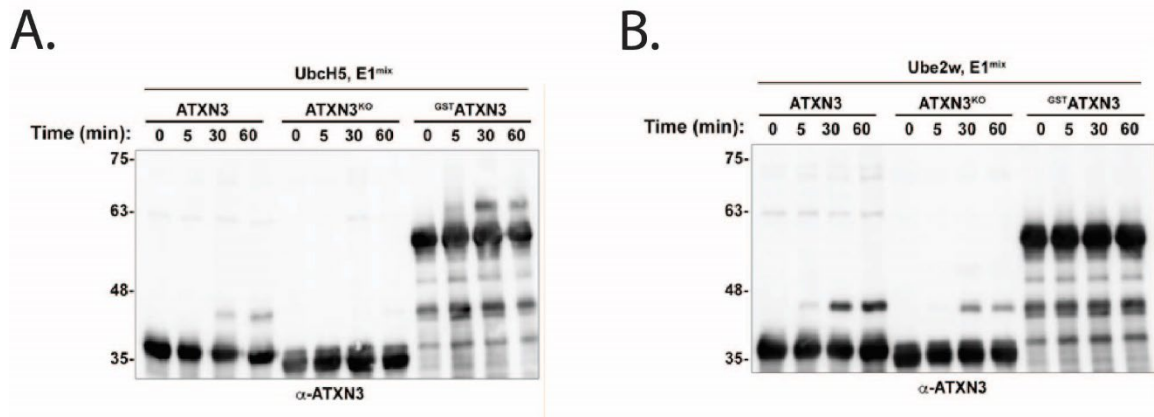


**Figure 41: Ube2w and UbcH5 retain substrate residue selectivity in the absence of CHIP.**

(A) UbcH5 ubiquitinates lysine residues in the absence of CHIP. E3 independent ubiquitination assays were performed with UbcH5 and either ATXN3, ATXN3<sup>KO</sup>, or G<sup>ST</sup>ATXN3 as the substrate. Samples were visualized by Western blot analysis.

(B) Ube2w ubiquitinates the N-termini, but not internal lysine residues in the absence of an E3. E3 independent ubiquitination assays were performed with Ube2w and either ATXN3, ATXN3<sup>KO</sup>, or G<sup>ST</sup>ATXN3 as the substrate. Samples were visualized by Western blot analysis.

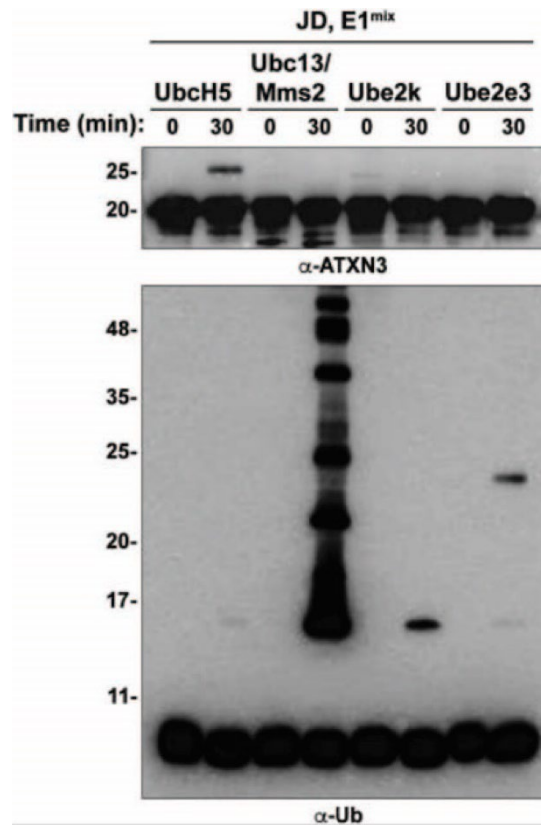


**Figure 42: UbcH5, but not other E2s, ubiquitinates the JD of ATXN3 in the absence of CHIP.**

E3 independent ubiquitination assays were performed utilizing the JD of ATXN3 were performed with either UbcH5, Ubc13/Mms2, Ube2k, or Ube2e3 as the E2. Samples were analyzed by Western blot with the indicated antibodies.

## Method

For E3 independent ubiquitination reactions, 5  $\mu\text{M}$  of indicated E2, 20  $\mu\text{M}$  of indicated substrate, and E1<sup>mix</sup> (100 nM Ube1, 250  $\mu\text{M}$  ubiquitin, 2.5 mM ATP, and 2.5 mM  $\text{MgCl}_2$ ) was used with reactions carried out for four hours in kinase buffer (50 mM Tris pH 7.5, 50 mM KCl, 0.2 mM DTT). All reactions were performed at 37°C. Reactions were stopped by addition of Laemmli buffer and boiling, followed by SDS-PAGE and visualization by either Coomassie stain or western blotting with the appropriate antibodies.

## References

- Adegbuyiro, A., Sedighi, F., Pilkington, A., Groover, S., & Legleiter, J. (2017). Proteins Containing Expanded Polyglutamine Tracts and Neurodegenerative Disease. *Biochemistry*, *56*(9), 1199-1217. <https://doi.org/10.1021/acs.biochem.6b00936>
- Anders, C., Niewoehner, O., Duerst, A., & Jinek, M. (2014). Structural basis of PAM-dependent target DNA recognition by the Cas9 endonuclease. *Nature*, *513*, 569-573. <https://doi.org/10.1038/nature13579>
- Andrews, B., Boone, C., Davis, T., & Fields, F. (2016). *Budding Yeast: A Laboratory Manual* (B. Andrews, C. Boone, T. Davis, & F. Fields, Eds.). Cold Spring Harbor Laboratory Press.
- Ardley, H., & Robinson, P. (2005). E3 ubiquitin ligases. *Essays Biochem*, *41*, 15-30. <https://doi.org/10.1042/bse0410015>
- Arosio, P., Vendruscolo, M., Dobson, C., & Knowles, T. (2014). Chemical kinetics for drug discovery to combat protein aggregation diseases. *Trends Pharmacol Sci*, *35*, 127-135. <https://doi.org/10.1016/j.tips.2013.12.005>
- Arrasate, M., Mitra, S., Schweitzer, E., Segal, M., & Finkbeiner, S. (2004). Inclusion body formation reduces levels of mutant huntingtin and the risk of neuronal death. *Nature*, *431*(7010), 805-810. <https://doi.org/10.1038/nature02998>
- Asano, Y., Yamashita, K., Hasegawa, A., Ogasawara, T., Iriki, H., & Muramoto, T. (2021). Knock-in and precise nucleotide substitution using near-PAMless engineered Cas9 variants in *Dictyostelium discoideum*. *Sci Rep*, *11*(11163). <https://doi.org/10.1038/s41598-021-89546-0>
- Austen, B., Paleologou, K., Ali, S., Qureshi, M., Allsop, D., & El-Agnaf, O. (2008). Designing Peptide Inhibitors for Oligomerization and Toxicity of Alzheimer's  $\beta$ -Amyloid Peptide. *Biochemistry*, *47*, 1984-1992. <https://doi.org/10.1021/bi701415b>
- Avellaneda, M., Franke, K., Sunderlikova, V., Bukau, B., Mogk, A., & Tans, S. (2020). Processive extrusion of polypeptide loops by a hsp100 disaggregase. *Nature*, *578*, 317-320. <https://doi.org/10.1038/s41586-020-1964-y>
- Bae, S., Park, J., & Kim, J. (2014). Cas-OFFinder: a fast and versatile algorithm that searches for potential off-target sites of Cas9 RNA-guided endonucleases. *Bioinformatics*, *30*, 1473-1475. <https://doi.org/10.1093/bioinformatics/btu048>

- Bakthisaran, R., Tangirala, R., & Rao, C. (2015). Small heat shock proteins: Role in cellular functions and pathology. *Biochim Biophys Acta*, 1854(4), 291-319. <https://doi.org/10.1016/j.bbapap.2014.12.019>
- Balbirnie, M., Grothe, R., & Eisenberg, D. (2001). An amyloid-forming peptide from the yeast prion Sup35 reveals a dehydrated  $\beta$ -sheet structure for amyloid. *PNAS*, 98(5), 2375-2380. <https://doi.org/10.1073/pnas.041617698>
- Barth, P., Schonbrun, J., & Baker, D. (2007). Toward high-resolution prediction and design of transmembrane helical protein structures. *PNAS*, 104(40), 15682–15687. <https://doi.org/10.1073/pnas.0702515104>
- Batelli, S., Albani, D., Rametta, R., Polito, L., Prato, F., Pesaresi, M., Negro, A., & Forloni, G. (2008). DJ-1 modulates alpha-synuclein aggregation state in a cellular model of oxidative stress: Relevance for Parkinson's disease and involvement of HSP70. *PLoS ONE*, 3.
- Batelli, S., Invernizzi, R., Negro, A., Calcagno, E., Rodilossi, S., Forloni, G., & Albani, D. (2015). The Parkinson's disease-related protein DJ-1 protects dopaminergic neurons in vivo and cultured cells from alpha-synuclein and 6-hydroxydopamine toxicity. *Neurodegen Dis*, 15, 13-23.
- Baumketner, A., & Shea, J.-E. (2006). Folding Landscapes of the Alzheimer Amyloid- $\beta$  Peptide. *J Mol Biol*, 362, 567-579. <https://doi.org/10.1016/j.jmb.2006.07.032>
- Belsare, K., Wu, H., Mondal, D., Bond, A., Castillo, E., Jin, J., Jo, H., Roush, A., Pilla, K., Sali, A., Condello, C., & DeGrado, W. (2022). Soluble TREM2 inhibits secondary nucleation of A $\beta$  fibrillization and enhances cellular uptake of fibrillar A $\beta$ . *PNAS*, 119(5). <https://doi.org/10.1073/pnas.2114486119>
- Bett, C., Serem, W., Fontenot, K., Hammer, R., & Garno, J. (2010). Effects of Peptides Derived from Terminal Modifications of the A $\beta$  Central Hydrophobic Core on A $\beta$  Fibrillization. *ACS Chem Neurosci*, 1, 661-678. <https://doi.org/10.1021/cn900019r>
- Bichet, P., Mollat, P., Capdevila, C., & Sarubbi, E. (2000). Endogenous Glutathione-Binding Proteins of Insect Cell Lines: Characterization and Removal from Glutathione S-Transferase (GST) Fusion Proteins. *Protein Expression and Purification*, 19, 197-201. <https://doi.org/10.1006/prep.2000.1239>
- Boatz, J., Piretra, T., Lasorsa, A., Matlahov, I., Conway, J., & van der Wel, P. (2020). Protofilament Structure and Supramolecular Polymorphism of Aggregation

- Mutant Huntingtin Exon 1. *J Mol Biol*, 432(16), 4722-4744.  
<https://doi.org/10.1016/j.jmb.2020.06.021>
- Bolton, D., & Bendheim, P. (2007). A modified host protein model of scrapie. *Ciba Foundation Symposium 135 - Novel Infectious Agents and the Central Nervous System*.  
<https://doi.org/10.1002/9780470513613.ch11>
- Bosgraaf, L., Russcher, H., Smith, J., Wessels, D., Soll, D., & van Haastert, P. (2002). A novel cGMP signalling pathway mediating myosin phosphorylation and chemotaxis in *Dictyostelium*. *EMBO J*, 21.
- Bosgraaf, L., & van Haastert, P. (2003). Roc, a Ras/GTPase domain in complex proteins. *Biochim Biophys Acta*, 1643, 5-10.
- Bosu, D., & Kipreos, E. (2008). Cullin-RING ubiquitin ligases: global regulation and activation cycles. *Cell Div*, 3(7). <https://doi.org/10.1186/1747-1028-3-7>
- Bozzaro, S., Bucci, C., & Steinert, M. (2008). Phagocytosis and host-pathogen interactions in *Dictyostelium* with a look at macrophages. *Int Rev Cell Mol Biol*, 271, 253-300.
- Bulone, D., Masino, L., Thomas, D., San Biagio, P., & Pastore, A. (2006). The Interplay between PolyQ and Protein Context Delays Aggregation by Forming a Reservoir of Protofibrils. *PLoS ONE*, 1(1), e111.  
<https://doi.org/10.1371/journal.pone.0000111>
- Butko, P., Buford, J., Goodwin, J., Stroud, P., McCormick, C., & Cannon, G. (2001). Spectroscopic Evidence for Amyloid-like Interfacial Self-Assembly of Hydrophobin Sc3. *Biochem Biophys Res Commun*, 280, 212-215.  
<https://doi.org/10.1006/bbrc.2000.4098>
- Cai, H., & Devreotes, P. (2011). Moving in the right direction: how eukaryotic cells migrate along chemical gradients. *Semin Cell Dev Biol*, 22, 834-841.
- Carroni, M., Kummer, E., Oguchi, Y., Wendler, P., Clare, D., Sinning, I., Kopp, J., Mogk, A., Bukau, B., & Saibil, H. (2014). Head-to-tail interactions of the coiled-coil domains regulate ClpB activity and cooperation with hsp70 in protein disaggregation. *eLife*, 3. <https://doi.org/10.7554/eLife.02481>
- Casella, R., Bigi, A., Cremades, N., & Cecchi, C. (2022). Effects of oligomer toxicity, fibril toxicity, and fibril spreading in synucleinopathies. *Cell Mol Life Sci*, 79, 174.  
<https://doi.org/10.1007/s00018-022-04166-9>

- Catazaro, J., Andrews, T., Milkovic, N., Lin, J., Lowe, A., Wilson, M., & Powers, R. (2018). (15)N CEST data and traditional model-free analysis capture fast internal dynamics of DJ-1. *Anal Biochem*, *542*, 24-28.
- Cecchi, C., & Stefani, M. (2013). The amyloid-cell membrane system. The interplay between the biophysical features of oligomers/fibrils and cell membrane defines amyloid toxicity. *Biophys Chem*, *182*, 30-43.  
<https://doi.org/10.1016/j.bpc.2013.06.003>
- Ceccon, A., Tugarinov, V., Torricella, F., & Clore, G. (2022). Quantitative NMR analysis of the kinetics of prenucleation oligomerization and aggregation of pathogenic huntingtin exon-1 protein. *PNAS*, *119*(29).  
<https://doi.org/10.1073/pnas.2207690119>
- Charette, S., & Cosson, P. (2004). Preparation of genomic DNA from *Dictyostelium discoideum* for PCR analysis. *Biotechniques*, *36*, 574-575.  
<https://doi.org/10.2144/04364BM01>
- Chattwood, A., & Thompson, C. (2011). Nongenetic heterogeneity and cell fate choice in *Dictyostelium discoideum*. *Dev Growth Differ*, *53*, 558-566.
- Chen, B., Retzlaff, M., Roos, T., & Frydman, J. (2011). Cellular Strategies of Protein Quality Control. *Cold Spring Harb Perspect Biol*, *3*(8).  
<https://doi.org/10.1101/cshperspect.a004374>
- Chen, S., Annesley, S., Jasim, R., & Fisher, P. (2021). The Parkinson's Disease-Associated Protein DJ-1 Protects *Dictyostelium* Cells from AMPK-Dependent Outcomes of Oxidative Stress. *Cells*, *10*(8). <https://doi.org/10.3390/cells10081874>
- Chen, S., Annesley, S., Jasim, R., Musco, V., Sanislav, O., & Fisher, P. (2017). The Parkinson's disease-associated protein DJ-1 plays a positive nonmitochondrial role in endocytosis in *Dictyostelium* cells. *Dis Model Mech*, *10*, 1261-1271.  
<https://doi.org/10.1242/dmm.028084>
- Cheng, P.-N., Liu, C., Zhao, M., Eisenberg, D., & Nowick, J. (2012). Amyloid  $\beta$ -Sheet Mimics that Antagonize Amyloid Aggregation and Reduce Amyloid Toxicity. *Nat Chem*, *4*(11), 927-933. <https://doi.org/10.1038/nchem.1433>
- Chiew, Y., Reimers, J., & Wright, B. (1985). Steady state models of spore cell metabolism in *Dictyostelium discoideum*. *J Biol Chem*, *260*(28), 15325-15331.  
[https://doi.org/10.1016/S0021-9258\(18\)95739-X](https://doi.org/10.1016/S0021-9258(18)95739-X)

- Chisholm, R., & Firtel, R. (2004). Insights into morphogenesis from a simple developmental system. *Nat Rev Mol Cell Biol*, 5, 531-541.
- Chisholm, R., Gaudet, P., Just, E., Pilcher, K., Fey, P., Merchant, S., & Kibbe, W. (2006). dictyBase, the model organism database for Dictyostelium discoideum. *Nucleic Acids Res*, 34(Database issue), D423-427. <https://doi.org/10.1093/nar/gkj090>
- Chung, D., & Dellaire, G. (2015). The role of the COP9 signalosome and neddylation in DNA damage signaling and repair. *Biomolecules*, 5, 2388-2416. <https://doi.org/10.3390/biom5042388>
- Chunna, A., & Pu, X. (2017). Role of DJ-1 in Fertilization. *Adv Exp Med Biol*, 1037, 61-66.
- Churion, K., & Bondos, S. (2012). Identifying Solubility-Promoting Buffers for Intrinsically Disordered Proteins Prior to Purification. In V. Uversky & A. Dunker (Eds.), *Intrinsically Disordered Protein Analysis: Methods and Experimental Tools* (Vol. 2). Springer Science+Business Media. [https://doi.org/10.1007/978-1-4614-3704-8\\_28](https://doi.org/10.1007/978-1-4614-3704-8_28)
- Ciechanover, A. (1994). The ubiquitin-proteasome proteolytic pathway. *Cell*, 79(1), 13-21. [https://doi.org/10.1016/0092-8674\(94\)90396-4](https://doi.org/10.1016/0092-8674(94)90396-4).
- Clarke, M., Kohler, J., Arana, Q., Liu, T., Heuser, J., & Gerisch, G. (2002). Dynamics of the vacuolar H<sup>+</sup>-ATPase in the contractile vacuole complex and the endosomal pathway of Dictyostelium cells. *J Cell Sci*, 115, 2893-2905. <https://doi.org/10.1242/jcs.115.14.2893>
- Cohen, F., Pan, K., Huang, Z., Baldwin, M., Fletterick, R., & Prusiner, S. (1994). Structural clues to prion replication. *Science*, 264(5158), 530-531. <https://doi.org/10.1126/science.7909169>
- Cohen, S., Vendruscolo, M., Welland, M., Dobson, C., Terentjev, E., & Knowles, T. (2011). Nucleated polymerization with secondary pathways. I. Time evolution of the principal moments. *J Chem Phys*, 135. <https://doi.org/10.1063/1.3608916>
- Come, J., Fraser, P., & Lansbury Jr, P. (1993). A kinetic model for amyloid formation in the prion diseases: importance of seeding. *PNAS*, 90(13), 5959-5963. <https://doi.org/10.1073/pnas.90.13.5959>
- Cook, C., Stetler, C., & Petrucelli, L. (2012). Disruption of Protein Quality Control in Parkinson's Disease. *Cold Spring Harb Perspect Med*, 2(5). <https://doi.org/10.1101/cshperspect.a009423>

- Crick, S., Ruff, K., Garai, K., & Pappu, R. (2013). Unmasking the roles of N- and C-terminal flanking sequences from exon 1 of huntingtin as modulators of polyglutamine aggregation. *PNAS*, *110*(50), 20075-20080. <https://doi.org/10.1073/pnas.1320626110>
- Cuervo, A., & Wong, E. (2014). Chaperone-mediated autophagy: roles in disease and aging. *Cell Res*, *24*(1), 92-104. <https://doi.org/10.1038/cr.2013.153>
- Cupo, R., & Shorter, J. (2020). Skd3 (human ClpB) is a potent mitochondrial protein disaggregase that is inactivated by 3-methylglutaconic aciduria-linked mutations. *eLife*, *9*. <https://doi.org/10.7554/eLife.55279>
- Dawson, T., Golde, T., & Lagier-Tourenne, C. (2018). Animal models of neurodegenerative diseases. *Nat Neurosci*, *21*, 1370-1379. <https://doi.org/10.1038/s41593-018-0236-8>
- de Bie, P., & Ciechanover, A. (2011). Ubiquitination of E3 ligases: self-regulation of the ubiquitin system via proteolytic and non-proteolytic mechanisms. *Cell Death Differ*, *18*, 1393-1402. <https://doi.org/10.1038/cdd.2011.16>
- De Strooper, B., Annaert, W., Cupers, P., Saftig, P., Craessaerts, K., Mumm, J., Schroeter, E., Schrijvers, V., Wolfe, M., Ray, W., Goate, A., & Kopan, R. (1999). A presenilin-1-dependent g-secretase-like protease mediates release of Notch intracellular domain. *Nature*, *398*, 518-522.
- De Strooper, B., Iwatsubo, T., & Wolfe, M. (2012). Presenilins and g-Secretase: Structure, Function, and Role in Alzheimer Disease. *Cold Spring Harb Perspect Med*, *2*. <https://doi.org/10.1101/cshperspect.a006304>
- De Strooper, B., Saftig, P., Craessaerts, K., Vanderstichele, H., Guhde, G., Annaert, W., Von Figura, K., & Van Leuven, F. (1998). Deficiency of presenilin-1 inhibits the normal cleavage of amyloid precursor protein. *Nature*, *391*, 387-390.
- DeSantis, M., Leung, E., Sweeny, E., Jackrel, M., Cushman-Nick, M., Neuhaus-Follini, A., Vashist, S., Sochor, M., Knight, M., & Shorter, J. (2012). Operational plasticity enables hsp104 to disaggregate diverse amyloid and nonamyloid clients. *Cell*, *151*(4), 778-793.
- DeSantis, M., Sweeny, E., Snead, D., Leung, E., Go, M., Gupta, K., Wendler, P., & Shorter, J. (2014). Conserved distal loop residues in the Hsp104 and ClpB middle domain contact nucleotide-binding domain 2 and enable Hsp70-dependent

protein disaggregation. *J Biol Chem*, 289, 848-867.  
<https://doi.org/10.1074/jbc.M113.520759>

- Dias, V., Junn, E., & Maral Mouradian, M. (2013). The Role of Oxidative Stress in Parkinson's Disease. *J Parkinsons Dis*, 3(4), 461-491. <https://doi.org/10.3233/JPD-130230>
- Diogenes, M., Dias, R., Rombo, D., Miranda, H., Maiolino, F., Guerreiro, P., Nasstrom, T., Franquelim, H., Oliverira, L., Castanho, M., Lannfelt, L., Bergstrom, J., Ingelsson, M., Quintas, A., Sebastiao, A., Lopes, L., & Outeiro, T. (2012). Extracellular alpha-synuclein oligomers modulate synaptic transmission and impair LTP via NMDA-receptor activation. *J Neurosci*, 32(34), 11750-11762. <https://doi.org/10.1523/JNEUROSCI.0234-12.2012>
- Dubiel, D., Gierisch, M., Huang, X., Dubiel, W., & Naumann, M. (2013). CAND1-dependent control of cullin 1-RING Ub ligases is essential for adipogenesis. *Biochim Biophys Acta*, 1833, 1078-1084. <https://doi.org/10.1016/j.bbamcr.2013.01.005>
- Dupuis, N., Wu, C., Shea, J.-E., & Bowers, M. (2009). Human Islet Amyloid Polypeptide Monomers Form Ordered  $\beta$ -hairpins: A Possible Direct Amyloidogenic Precursor. *JACS*, 131(51), 18283-18292. <https://doi.org/10.1021/ja903814q>
- Eberhard, D., & Lammert, E. (2017). The Role of the Antioxidant Protein DJ-1 in Type 2 Diabetes Mellitus. *Adv Exp Med Biol*, 1037, 173-186.
- Ebrahimi-Fakhari, D., Saidi, L.-J., & Wahlster, L. (2013). Molecular chaperones and protein folding as therapeutic targets in Parkinson's disease and other synucleinopathies. *Acta Neuropathol Comm*, 1(79). <https://doi.org/10.1186/2051-5960-1-79>
- Eichinger, L., Pachebat, J., Glöckner, G., Rajandream, M., Sucgang, R., Berriman, M., Song, J., Olsen, R., Szafranski, K., Xu, Q., Tunggal, B., Kummerfeld, S., Madera, M., Konfortov, B., Rivero, F., Bankier, A., Lehmann, R., Hamlin, N., Davies, R., . . . Kuspa, A. (2005). The genome of the social amoeba *Dictyostelium discoideum*. *Nature*, 435, 43-57.
- Ellisdon, A., Pearce, M., & Bottomley, S. (2007). Mechanisms of Ataxin-3 Misfolding and Fibril Formation: Kinetic Analysis of a Disease-associated Polyglutamine Protein. *J Mol Biol*, 368(2), 595-605. <https://doi.org/10.1016/j.jmb.2007.02.058>

- Ellisdon, A., Thomas, B., & Bottomley, S. (2006). The Two-stage Pathway of Ataxin-3 Fibrillogenesis Involves a Polyglutamine-independent Step. *J Biol Chem*, 281(25), 16888-16896. <https://doi.org/10.1074/jbc.M601470200>
- Emborg, M. (2017). Nonhuman Primate Models of Neurodegenerative Disorders. *ILAR Journal*, 58(2), 190-201. <https://doi.org/10.1093/ilar/ilx021>
- Eskici, G., & Gur, M. (2013). Computational design of new Peptide inhibitors for amyloid Beta ( $\alpha\beta$ ) aggregation in Alzheimer's disease: application of a novel methodology. *PLoS ONE*, 8(6). <https://doi.org/10.1371/journal.pone.0066178>
- Esler, W., Kimberly, W., Ostaszewski, B., Diehl, T., Moore, C., Tsai, J., Rahmati, T., Xia, W., Selkoe, D., & Wolfe, M. (2000). Transition-state analogue inhibitors of  $\gamma$ -secretase bind directly to presenilin-1. *Nat Cell Biol*, 2, 428-434.
- Faust, O., Abayev-Avraham, M., Wentink, A., Maurer, M., Nillegoda, N., London, N., Bukau, B., & Rosenzweig, R. (2020). HSP40 proteins use class-specific regulation to drive HSP70 functional diversity. *Nature*, 287, 489-494. <https://doi.org/10.1038/s41586-020-2906-4>
- Fernando, S., Allan, C., Mroczek, K., Pearce, X., Sanislav, O., Fisher, P., & Annesley, S. (2020). Cytotoxicity and Mitochondrial Dysregulation Caused by  $\alpha$ -Synuclein in *Dictyostelium discoideum*. *Cells*, 9(10). <https://doi.org/10.3390/cells9102289>
- Fey, P., Kowal, A., Gaudet, P., Pilcher, K., & Chisholm, R. (2007). Protocols for growth and development of *Dictyostelium discoideum*. *Nat Protoc*, 2, 1307-1316. <https://doi.org/10.1038/nprot.2007.178>
- Fradinger, E., Monien, B., Urbanc, B., Lomakin, A., Tan, M., Li, H., Spring, S., Condron, M., Cruz, L., Xie, C., Benedek, G., & Bitan, G. (2008). C-terminal peptides coassemble into  $A\beta_{42}$  oligomers and protect neurons against  $A\beta_{42}$ -induced neurotoxicity. *PNAS*, 105, 14175-14180.
- Francione, L., Annesley, S., Carilla-Latorre, S., Escalante, R., & PR, F. (2011). The *Dictyostelium* model for mitochondrial disease. *Semin Cell Dev Biol*, 22, 120-130.
- Franco, A., Velasco-Careros, L., Alvarez, N., Orozco, N., Moro, F., Prado, A., & Muga, A. (2021). Unzipping the Secrets of Amyloid Disassembly by the Human Disaggregase. *Cells*, 10(10). <https://doi.org/10.3390/cells10102745>

- Frescas, D. P., M. (2008). Deregulated proteolysis by the F-box proteins SKP2 and beta-TrCP: tipping the scales of cancer. *Nat Rev Cancer*, 8, 438-449.  
<https://doi.org/10.1038/nrc2396>
- Gajdusek, D. (1996). Infectious amyloids: subacute spongiform encephalopathies as transmissible cerebral amyloidoses. In B. Fields, D. Knipe, & P. Howley (Eds.), *Virology* (3 ed.). Lippincott-Raven Publishers.
- Gales, L., Cortes, L., Almeida, C., Melo, C., do Carmo Costa, M., Maciel, P., Clarke, D., Damas, A., & Macedo-Ribeiro, S. (2005). Towards a Structural Understanding of the Fibrillization Pathway in Machado-Joseph's Disease: Trapping Early Oligomers of Non-expanded Ataxin-3. *J Mol Biol*, 353(3), 642-654.  
<https://doi.org/10.1016/j.jmb.2005.08.061>
- Gama Sosa, M., De Gasperi, R., & Elder, G. (2012). Modeling human neurodegenerative diseases in transgenic systems. *Hum Genet*, 131, 535-563.  
<https://doi.org/10.1007/s00439-011-1119-1>
- Gao, X., Carroni, M., Nussbaum-Krammer, C., Mogk, A., Nillegoda, N., Szlachcic, A., Lys Guilbride, D. S., HR, Mayer, M., & Bukau, B. (2015). Human Hsp70 Disaggregase Reverses Parkinson's-Linked  $\alpha$ -Synuclein Amyloid Fibrils. *Mol Cell*, 59(5), 781-793. <https://doi.org/10.1016/j.molcel.2015.07.012>
- Gasiunas, G., Barrangou, R., Horvath, P., & Siksnys, V. (2012). Cas9-crRNA ribonucleoprotein complex mediates specific DNA cleavage for adaptive immunity in bacteria. *Science*, 337, 816-821.  
<https://doi.org/10.1126/science.1225829>
- Gates, S., Yokom, A., Lin, J., Jackrel, M., Sweeny, E., Mack, K., Chuang, E., Torrente, M., Su, M., Shorter, J., & Southworth, D. (2017). Ratchet-like polypeptide translocation mechanism of the AAA+ disaggregase Hsp104. *Science*, 357, 273-279. <https://doi.org/10.1126/science.aan1052>
- Gazit, E. (2005). Mechanisms of amyloid fibril self-assembly and inhibition: Model short peptides as a key research tool. *FEBS Journal*, 272, 5971-5978.  
<https://doi.org/10.1111/j.1742-4658.2005.05022.x>
- Giasson, B., Murray, I., Trojanowski, J., & Lee, V.-Y. (2001). A Hydrophobic Stretch of 12 Amino Acid Residues in the Middle of  $\alpha$ -Synuclein Is Essential for Filament Assembly. *J Biol Chem*, 276(4), 2380-2386. <https://doi.org/10.1074/jbc.M008919200>

- Gilberto, S., & Peter, M. (2017). Dynamic ubiquitin signaling in cell cycle regulation. *J Cell Biol*, 216, 2259-2271. <https://doi.org/10.1083/jcb.201703170>
- Giusti, C., Tresse, E., Luciani, M., & Golstein, P. (2008). Autophagic cell death: analysis in *Dictyostelium*. *Biochim Biophys Acta*, 1793, 1422-1431.
- Glover, J., & Lindquist, S. (1998). Hsp104, Hsp70, and Hsp40: A novel chaperone system that rescues previously aggregated proteins. *Cell*, 94(1), 73-82.
- Goloubinoff, P., Mogk, A., Zvi, A., Tomoyasu, T., & Bukau, B. (1999). Sequential mechanism of solubilization and refolding of stable protein aggregates by a bichaperone network. *PNAS*, 96(24), 13732-13737. <https://doi.org/10.1073/pnas.96.24.13732>
- Gorner, K., Holtorf, E., Waak, J., Pham, T., Vogt-Weisenhorn, D., Wurst, W., Haass, C., & Kahle, P. (2007). Structural determinants of the C-terminal helix-kink-helix motif essential for protein stability and survival promoting activity of DJ-1. *J Biol Chem*, 282, 13680-13691.
- Gotthardt, D., Warnatz, H., Henschel, O., Bruckert, F., Schleicher, M., & Soldati, T. (2002). High-resolution dissection of phagosome maturation reveals distinct membrane trafficking phases. *Mol Biol Cell*, 13(10), 3508-3520. <https://doi.org/10.1091/mbc.e02-04-0206>
- Grimminger-Marquardt, V., & Lashuel, H. (2009). Structure and function of the molecular chaperone Hsp104 from yeast. *Biopolymers*, 93(3), 252-276. <https://doi.org/10.1002/bip.21301>
- Gu, Y., Sanjo, N., Chen, F., Hasegawa, H., Petit, A., Ruan, X., Li, W., Shier, C., Kawarai, T., Schmitt-Ulms, G., Westaway, D., St. George-Hyslop, P., & Fraser, P. (2004). The presenilin proteins are components of multiple membrane-bound complexes that have different biological activities. *J Biol Chem*, 279(30), 31329-31336.
- Guerin, N., & Larochelle, D. (2002). A user's guide to restriction enzyme-mediated integration in *Dictyostelium*. *J Muscle Res Cell Motil*, 23, 597-604. <https://doi.org/10.1023/A:1024494704863>
- Haass, C., Kaether, C., Sisodia, S., & Thinakaran, G. (2012). Trafficking and proteolytic processing of APP. *Cold Spring Harb Perspect Med*, 2(5). <https://doi.org/10.1101/cshperspect.a006270>

- Halverson, K., Fraser, P., Kirschner, D., & Lansbury Jr, P. (1990). Molecular determinants of amyloid deposition in Alzheimer's disease: conformational studies of synthetic beta-protein fragments. *Biochemistry*, 29(11), 2639-2644. <https://doi.org/10.1021/bi00463a003>
- Han, W., & Wu, Y.-D. (2005). A Strand-Loop-Strand Structure Is a Possible Intermediate in Fibril Elongation: Long Time Simulations of Amyloid- $\beta$  Peptide. *JACS*, 127, 15408-15416. <https://doi.org/10.1021/ja051699h>
- Hanson, P., & Whiteheart, S. (2005). AAA+ proteins: have engine, will work. *Nat Rev Mol Cell Biol*, 6(7), 519-529. <https://doi.org/10.1038/nrm1684>
- Harris, D. (1999). Cellular Biology of Prion Diseases. *Clinical Microbiology Reviews*, 12(3), 429-444. <https://doi.org/10.1128/CMR.12.3.429>
- Hartl, F., Bracher, A., & Hayer-Hartl, M. (2011). Molecular chaperones in protein folding and proteostasis. *Nature*, 475, 324-332. <https://doi.org/10.1038/nature10317>
- Hartl, F., & Hayer-Hartl, M. (2002). Molecular chaperones in the cytosol: from nascent chain to folded protein. *Science*, 295(5561), 1852-1858. <https://doi.org/10.1126/science.1068408>
- Harwood, A. (2008). *Dictyostelium* development: a prototypic Wnt pathway? *Methods Mol Biol*, 469, 21-32.
- Haslbeck, M. (2002). sHsps and their role in the chaperone network. *Cell Mol Life Sci*, 59(10), 1649-1657. <https://doi.org/10.1007/pl00012492>
- Haslberger, T., Weibezahn, J., Zahn, R., Lee, S., Tsai, F., Bukau, B., & Mogk, A. (2007). M domains couple the ClpB threading motor with the DnaK chaperone activity. *Mol Cell*, 25, 247-260. <https://doi.org/10.1016/j.molcel.2006.11.008>
- Haslberger, T., Zdanowicz, A., Brand, I., Kirstein, J., Turgay, K., Mogk, A., & Bukau, B. (2008). Protein disaggregation by the AAA+ chaperone ClpB involves partial threading of looped polypeptide segments. *Nat Struct Mol Biol*, 15, 641-650. <https://doi.org/10.1038/nsmb.1425>
- Haver, H., Wedemeyer, M., Butcher, E., Peterson, F., Volkman, B., & Scaglione, K. (2023). Mechanistic Insight into the Suppression of Polyglutamine Aggregation by SRCP1. *ACS Chem Biol*, 18(3), 549-560. <https://doi.org/10.1021/acscchembio.2c00893>

- Henning-Knetchel, A., Kumar, S., Wallin, C., Krol, S., Warmlander, S., Jarvet, J., Esposito, G., Kirmizialtin, S., Graslund, A., Hamilton, A., & Magzoub, M. (2020). Designed Cell-Penetrating Peptide Inhibitors of Amyloid-beta Aggregation and Cytotoxicity. *Cell Reports Phys Sci*, 1(2). <https://doi.org/10.1016/j.xcrp.2020.100014>
- Heuck, A., Schitter-Sollner, S., Suskiewicz, M., Kurzbauer, R., Kley, J., Schleiffer, A., Rombaut, P., Herzog, F., & Clausen, T. (2016). Structural basis for the disaggregase activity and regulation of Hsp104. *eLife*, 5. <https://doi.org/10.7554/eLife.21516>
- Hocking, T. (2017). *directlabels: Direct Labels for Multicolor Plots*. In (Version R package version 20170331)
- Hope, J., Morton, L., Farquhar, C., Multhaup, G., Beyreuther, K., & Kimberlin, R. (1986). The major polypeptide of scrapie-associated fibrils (SAF) has the same size, charge distribution and N-terminal protein sequence as predicted for the normal brain protein (PrP). *EMBO J*, 5(10), 2591-2597.
- Hopping, G., Kellock, J., Caughey, B., & Daggett, V. (2013). Designed Trpzip-3  $\beta$ -Hairpin Inhibits Amyloid Formation in Two Different Amyloid Systems. *ACS Med Chem Lett*, 4(9), 824-828. <https://doi.org/10.1021/ml300478w>
- Huggins, K., Bisaglia, M., Bubacco, L., Tatarek-Nossol, M., Kapurniotu, A., & Andersen, N. (2011). Designed Hairpin Peptides Interfere with Amyloidogenesis Pathways: Fibril Formation and Cytotoxicity Inhibition, Interception of the Preamyloid State. *Biochemistry*, 50(38), 8202-8212. <https://doi.org/10.1021/bi200760h>
- Hutton, M., & Hardy, J. (1997). The Presenilins and Alzheimer's Disease. *Hum Mol Genet*, 6(10), 1639-1646. <https://doi.org/10.1093/hmg/6.10.1639>
- Iconomidou, V., Chryssikos, G., Gionis, V., Galanis, A., Cordopatis, P., Hoenger, A., & Hamodrakas, S. (2006). Amyloid Wbril formation propensity is inherent into the hexapeptide tandemly repeating sequence of the central domain of silkworm chorion proteins of the A-family. *J Struct Biol*, 156, 480-488. <https://doi.org/10.1016/j.jsb.2006.08.011>
- Insall, R. (2005). The Dictyostelium genome: the private life of a social model revealed? *Genome Biol*, 6(6). <https://doi.org/10.1186/gb-2005-6-6-222>
- Jackrel, M., DeSantis, M., Martinez, B., Castellano, L., Stewart, R., Caldwell, K., Caldwell, G., & Shorter, J. (2014). Potentiated Hsp104 variants antagonize diverse

- proteotoxic misfolding events. *Cell*, 156, 170-182.  
<https://doi.org/10.1016/j.cell.2013.11.047>
- Jackrel, M., Yee, K., Tariq, A., Chen, A., & Shorter, J. (2015). Disparate mutations confer therapeutic gain of Hsp104 function. *ACS Chem Biol*, 10, 2672-2679.  
<https://doi.org/10.1021/acscchembio.5b00765>
- Jain, D., Jain, R., Eberhard, D., Eglinger, J., Bugliani, M., Piemonti, L., Marchetti, P., & Lammert, E. (2012). Age- and diet-dependent requirement of DJ-1 for glucose homeostasis in mice with implications for human type 2 diabetes. *J Mol Cell Biol*, 4, 221-230.
- Jakob, U., Gaestel, M., Engel, K., & Buchner, J. (1993). Small heat shock proteins are molecular chaperones. *J Biol Chem*, 268(3), 1517-1520.  
[https://doi.org/10.1016/S0021-9258\(18\)53882-5](https://doi.org/10.1016/S0021-9258(18)53882-5)
- Jaleel, M., Nichols, R., Deak, M., Campbell, D., Gillardon, F., Knebel, A., & Alessi, D. (2007). LRRK2 phosphorylates moesin at threonine-558: characterization of how Parkinson's disease mutants affect kinase activity. *Biochem J*, 405(2), 307-317.  
<https://doi.org/10.1042/BJ20070209>
- Jayaraman, M., Kodali, R., Sahoo, B., Thakur, A., Mayasundari, A., Mishra, R., Peterson, C., & Wetzel, R. (2012). Slow Amyloid Nucleation via  $\alpha$ -Helix-Rich Oligomeric Intermediates in Short Polyglutamine-Containing Huntingtin Fragments. *J Mol Biol*, 415(5), 881-899. <https://doi.org/10.1016/j.jmb.2011.12.010>
- Jentsch, S., & Rumpf, S. (2007). Cdc48 (p97): a "molecular gearbox" in the ubiquitin pathway? *Trends Biochem Sci*, 32(1), 6-11. <https://doi.org/10.1016/j.tibs.2006.11.005>
- Jha, A., Kumar, M., Gopi, H., & Paknikar, K. (2018). Inhibition of  $\beta$ -Amyloid Aggregation through a Designed  $\beta$ -Hairpin Peptide. *Langmuir*, 34, 1591-1600.  
<https://doi.org/10.1021/acs.langmuir.7b03617>
- Jiang, Y., Rossi, P., & Kalodimos, C. (2019). Structural basis for client recognition and activity of hsp40 chaperones. *Science*, 365, 1313-1319.  
<https://doi.org/10.1126/science.aax1280>
- Jinek, M., Chylinski, K., Fonfara, I., Hauer, M., Doudna, J., & Charpentier, E. (2012). A programmable dual-RNA-guided DNA endonuclease in adaptive bacterial immunity. *Science*, 337(6096), 816-821. <https://doi.org/10.1126/science.1225829>

- Jumper, J., Evans, R., Pritzel, A., Green, T., Figurnov, M., Ronneberger, O., Tunyasuvunakool, K., Bates, R., Zidek, A., Potapenko, A., Bridgland, A., Meyer, C., Kohl, S., Ballard, A., Cowie, A., Romera-Paredes, B., Nikolov, S., Jain, R., Adler, J., . . . Hassabis, D. (2021). Highly accurate protein structure prediction with AlphaFold. *Nature*, 596, 583-589. <https://doi.org/10.1038/s41586-021-03819-2>
- Kakkar, V., Månsson, C., de Mattos, E., Bergink, S., van der Zwaag, M., van Waarde, M., Kloosterhuis, N., Melki, R., Cruchten, R., Al-Karadaghi, S., Arosio, P., Dobson, C., Knowles, T., Bates, G., van Deursen, J., Linse, S., van de Sluis, B., Emanuelsson, C., & Kampinga, H. (2016). The S/T-Rich Motif in the DNAJB6 Chaperone Delays Polyglutamine Aggregation and the Onset of Disease in a Mouse Model. *Mol Cell*, 62(2), 272-283. <https://doi.org/10.1016/j.molcel.2016.03.017>
- Kalia, S., Kalia, L., & McLean, P. (2010). Molecular Chaperones as Rational Drug Targets for Parkinson's Disease Therapeutics. *CNS Neurol Disord Drug Targets*, 9(6), 741-753. <https://doi.org/10.2174/187152710793237386>
- Kar, K., Baker, M., Lengyel, G., Hoop, C., Kodali, R., Byeon, I.-J., Horne, W., van der Wel, P., & Wetzel, R. (2017). Backbone Engineering within a Latent  $\beta$ -Hairpin Structure to Design Inhibitors of Polyglutamine Amyloid Formation. *J Mol Biol*, 429(2), 308-323. <https://doi.org/10.1016/j.jmb.2016.12.010>
- Karpinar, D., Baliija, M., Kugler, S., Opazo, F., Rezaei-Ghaleh, N., Wender, N., Kim, H.-Y., Taschenberger, G., Falkenburger, B., Heise, H., Kumar, A., Riedel, D., Fichtner, L., Voigt, A., Braus, G., Giller, K., Becker, S., Herzig, A., Baldus, M., . . . Zweckstetter, M. (2009). Pre-fibrillar alpha-synuclein variants with impaired beta-structure increase neurotoxicity in Parkinson's disease models. *EMBO J*, 28(20), 3256-3268. <https://doi.org/10.1038/emboj.2009.257>
- Kaushik, S., & Cuervo, A. (2015). Proteostasis and aging. *Nat Med*, 21(12), 1406-1415. <https://doi.org/10.1038/nm.4001>
- Kaushik, S., & Cuervo, A. (2018). The coming of age of chaperone-mediated autophagy. *Nat Rev Mol Cell Biol*, 19(6), 365-381. <https://doi.org/10.1038/s41580-018-0001-6>
- Kawate, T., Tsuchiya, B., & Iwaya, K. (2017). Expression of DJ-1 in Cancer Cells: Its Correlation with Clinical Significance. *Adv Exp Med Biol*, 1037, 45-59.
- Kellogg, E., Leaver-Fay, A., & Baker, D. (2011). Role of conformational sampling in computing mutation-induced changes in protein structure and stability. *Proteins*:

*Structure, Function and Bioinformatics*, 79(3), 830-838.  
<https://doi.org/10.1002/prot.22921>

- Kelly, J. (1996). Alternative conformations of amyloidogenic proteins govern their behavior. *Curr Opin Struct Biol*, 6(1), 11-17. [https://doi.org/10.1016/s0959-440x\(96\)80089-3](https://doi.org/10.1016/s0959-440x(96)80089-3)
- Kelly, J. (1997). Amyloid fibril formation and protein misassembly: a structural quest for insights into amyloid and prion diseases. *Structure*, 5(5), 595-600.  
[https://doi.org/10.1016/s0969-2126\(97\)00215-3](https://doi.org/10.1016/s0969-2126(97)00215-3)
- Kenney, J., Knight, D., Wise, M., & Vollrath, F. (2002). Amyloidogenic nature of spider silk. *Eur J Biochem*, 269, 4159-4163. <https://doi.org/10.1046/j.1432-1033.2002.03112.x>
- Kessin, R. (2001). *Dictyostelium - Evolution, cell biology, and the development of multicellularity*. Cambridge University Press.
- Kim, R., Smith, P., Aleyasin, H., Hayley, S., Mount, M., Pownall, S., Wakeham, A., You-Ten, A., Kalia, S., Horne, P., Westaway, D., Lozano, A., Anisman, H., Park, D., & Mak, T. (2005). Hypersensitivity of DJ-1-deficient mice to 1-methyl-4-phenyl-1,2,3,6-tetrahydropyridine (MPTP) and oxidative stress. *PNAS*, 102, 5215-5220.
- Kim, W., Mathavarajah, S., & Huber, R. (2022). The Cellular and Developmental Roles of Cullins, Neddylation, and the COP9 Signalosome in *Dictyostelium discoideum*. *Front Physiol*, 13. <https://doi.org/10.3389/fphys.2022.827435>
- Kim, Y., Hipp, M., Bracher, A., Hayer-Hartl, M., & Hartl, F. (2013). Molecular chaperone functions in protein folding and proteostasis. *Annu Rev Biochem*, 82, 323-355.  
<https://doi.org/10.1146/annurev-biochem-060208-092442>
- Kinumi, T., Kimata, J., Taira, T., Ariga, H., & Niki, E. (2004). Cysteine-106 of DJ-1 is the most sensitive cysteine residue to hydrogen peroxide-mediated oxidation in vivo in human umbilical vein endothelial cells. *Biochem Biophys Res Commun*, 317, 722-728.
- Kiss, R., Zhu, M., Jojart, B., Czajlik, A., Solti, K., Forizs, B., Nagy, E., Zsila, F., Beke-Somfai, T., & Toth, G. (2017). Structural features of human DJ-1 in distinct Cys106 oxidative states and their relevance to its loss of function in disease. *biochim Biophys Acta Gen Subj*, 1861, 2619-2629.

- Klaips, C., Hochstrasser, M., Langlois, C., & Serio, T. (2014). Spatial quality control bypasses cell-based limitations on proteostasis to promote prion curing. *eLife*, 3. <https://doi.org/10.7554/eLife.04288>
- Klein, W., Krafft, G., & Finch, C. (2001). Targeting small A $\beta$  oligomers: the solution to an Alzheimer's disease conundrum? *Trends Neurosci*, 24(4), 219-224. [https://doi.org/10.1016/S0166-2236\(00\)01749-5](https://doi.org/10.1016/S0166-2236(00)01749-5)
- Knecht, D., & Pang, K. (1995). Electroporation of *Dictyostelium discoideum*. In J. Nickoloff (Ed.), *Electroporation Protocols for Microorganisms* (Vol. 47, pp. 321-330). Humana Press. <https://doi.org/10.1385/0-89603-310-4:321>
- Kortholt, A., Gilsbach, B., & van Haastert, P. (2012). Dictyostelium discoideum: A Model System to Study LRRK2-Mediated Parkinson Disease. In D. J. (Ed.), *Mechanisms in Parkinson's Disease - Models and Treatments*. InTech.
- Kroemer, G., Mariño, G., & Levine, B. (2010). Autophagy and the integrated stress response. *Mol Cell*, 40(2), 280-293. <https://doi.org/10.1016/j.molcel.2010.09.023>
- Kuspa, A. (2006). Restriction Enzyme-Mediated Integration (REMI) Mutagenesis. In L. Eichinger & F. Rivero (Eds.), *Dictyostelium discoideum Protocols* (Vol. 346, pp. 201-209). Humana Press. <https://doi.org/10.1385/1-59745-144-4:201>
- Kwon, Y., & Ciechanover, A. (2017). The Ubiquitin Code in the Ubiquitin-Proteasome System and Autophagy. *Trends Biochem Sci*, 42(11), 873-886. <https://doi.org/10.1016/j.tibs.2017.09.002>
- Kyte, J., & Doolittle, R. (1982). A simple method for displaying the hydropathic character of a protein. *J Mol Biol*, 157(1), 105-132. [https://doi.org/10.1016/0022-2836\(82\)90515-0](https://doi.org/10.1016/0022-2836(82)90515-0)
- La Spada, A., & Taylor, J. (2003). Polyglutamines placed into context. *Neuron*, 38, 681-684. [https://doi.org/10.1016/s0896-6273\(03\)00328-3](https://doi.org/10.1016/s0896-6273(03)00328-3).
- Labbadia, J., & Morimoto, R. (2015). The biology of proteostasis in aging and disease. *Annu Rev Biochem*, 84, 435-464. <https://doi.org/10.1146/annurev-biochem-060614-033955>
- Lambert, M., Barlow, A., Chromy, B., Edwards, C., Freed, R., Liosatos, M., Morgan, T., Rozovsky, I., Trommer, B., Viola, K., Wals, P., Zhang, C., Finch, C., Krafft, G., & Klein, W. (1998). Diffusible, nonfibrillar ligands derived from A $\beta$ <sub>1-42</sub> are potent

- central nervous system neurotoxins. *PNAS*, 95(11), 6448-6453.  
<https://doi.org/10.1073/pnas.95.11.6448>
- Laufen, T., Mayer, M., Beisel, C., Klostermeier, D., Mogk, A., Reinstein, J., & Bukau, B. (1999). Mechanism of regulation of hsp70 chaperones by DnaJ cochaperones. *PNAS*, 96, 5452-5457. <https://doi.org/10.1073/pnas.96.10.5452>
- Li, H., Monien, B., Fradinger, E., Urbanc, B., & Bitan, G. (2010). Biophysical Characterization of A $\beta$ 42 C-Terminal Fragments: Inhibitors of A $\beta$ 42 Neurotoxicity. *Biochemistry*, 49, 1259-1267. <https://doi.org/10.1021/bi902075h>
- Li, J., & Jin, J. (2012). CRL ubiquitin ligases and DNA damage response. *Front Oncol*, 2(29). <https://doi.org/10.3389/fonc.2012.00029>
- Li, S., & Ng, Y. (2010). Calibur: a tool for clustering large numbers of protein decoys. *BMC Bioinformatics*, 11(25). <https://doi.org/10.1186/1471-2105-11-25>
- Li, Y., Xu, M., Lai, M., Huang, Q., Castro, J., DiMuzio-Mower, J., Harrison, T., Lellis, C., Nadin, A., Neduvelil, J., Register, R., Sardana, M., Shearman, M., Smith, A., Shi, X., Yin, K., Shafer, J., & Gardell, S. (2000). Photoactivated g-secretase inhibitors directed to the active site covalently label presenilin 1. *Nature*, 405, 689-694.
- Liebman, S., & Meredith, S. (2010). Protein folding: Sticky N17 speeds huntingtin pile-up. *Nat Chem Biol*, 6, 7-8. <https://doi.org/10.1038/nchembio.279>
- Liu, J., Furukawa, M., Matsumoto, T., & Xiong, Y. (2002). NEDD8 modification of CUL1 dissociates p120(CAND1), an inhibitor of CUL1-SKP1 binding and SCF ligases. *Mol Cell*, 10, 1511-1518. [https://doi.org/10.1016/s1097-2765\(02\)00783-9](https://doi.org/10.1016/s1097-2765(02)00783-9)
- Liu, T., & Clarke, M. (1996). The vacuolar proton pump of Dictyostelium discoideum: molecular cloning and analysis of the 100 kDa subunit. *J Cell Sci*, 109(5), 1041-1051. <https://doi.org/10.1242/jcs.109.5.1041>
- Liu, T., Mirschberger, C., Chooback, L., Arana, Q., Sacco, Z., MacWilliams, H., & Clarke, M. (2002). Altered expression of the 100 kDa subunit of the Dictyostelium vacuolar proton pump impairs enzyme assembly, endocytic function and cytosolic pH regulation. *J Cell Sci*, 115, 489-497. <https://doi.org/10.1242/jcs.115.9.1907>
- Liu, X., Reitsma, J., Mamrosh, J., Zhang, Y., Straube, R., & Deshaies, R. (2018). Cand1-mediated adaptive exchange mechanism enables variation in F-box protein expression. *Mol Cell*, 69, 773-786. <https://doi.org/10.1016/j.molcel.2018.01.038>

- Liu, Y., Han, Y., Song, J., Wang, Y., Jing, Y., Shi, Q., Tian, C., Wang, Z., Li, C., Han, J., & Dong, X. (2011). Heat shock protein 104 inhibited the fibrillization of prion peptide 106–126 and disassembled prion peptide 106–126 fibrils in vitro. *Int J Biochem Cell Biol*, 43, 768-774. <https://doi.org/10.1016/j.biocel.2011.01.022>
- Lo Bianco, C., Shorter, J., Régulier, E., Lashuel, H., Iwatsubo, T., Lindquist, S., & Aebischer, P. (2008). Hsp104 antagonizes  $\alpha$ -synuclein aggregation and reduces dopaminergic degeneration in a rat model of Parkinson disease. *J Clin Invest*, 118, 3087-3097. <https://doi.org/10.1172/JCI35781>
- Lopes, F., Bristot, I., Da Motta, L., Parsons, R., & Klamt, F. (2017). Mimicking Parkinson's disease in a dish: merits and pitfalls of the most commonly used dopaminergic *in vitro* models. *Neuromol Med*, 19, 241-255. <https://doi.org/10.1007/s12017-017-8454-x>
- Lu, Z., & Cyr, D. (1998). Protein folding activity of hsp70 is modified differentially by the hsp40 co-chaperones sis1 and ydj1. *J Biol Chem*, 273, 27824-27830. <https://doi.org/10.1074/jbc.273.43.27824>
- Lue, L.-F., Kuo, Y.-M., Roher, A., Brachova, L., Shen, Y., Sue, L., Beach, T., Kurth, J., Rydel, R., & Rogers, J. (1999). Soluble Amyloid  $\beta$  Peptide Concentration as a Predictor of Synaptic Change in Alzheimer's Disease. *Am J Pathol*, 155(3), 853-862. [https://doi.org/10.1016/S0002-9440\(10\)65184-X](https://doi.org/10.1016/S0002-9440(10)65184-X)
- Luecke, I., Lin, G., Santarriaga, S., Scaglione, K., & Ebert, A. (2021). Viral vector gene delivery of the novel chaperone protein SRCP1 to modify insoluble protein in *in vitro* and *in vivo* models of ALS. *Gene Ther*. <https://doi.org/doi.org/10.1038/s41434-021-00276-4>
- Mackay, J., Matthews, J., Winefield, R., Mackay, L., Haverkamp, R., & Templeton, M. (2001). The Hydrophobin EAS Is Largely Unstructured in Solution and Functions by Forming Amyloid-Like Structures. *Structure*, 9, 83-91.
- Mackay, R., Helsen, C., Tkach, J., & Glover, J. (2008). The C-terminal extension of *Saccharomyces cerevisiae* Hsp104 plays a role in oligomer assembly. *Biochemistry*, 47(7), 1918-1927. <https://doi.org/10.1021/bi701714s>
- Malgieri, G., & Eliezer, D. (2008). Structural effects of Parkinson's disease linked DJ-1 mutations. *Protein Sci*, 17, 855-868.
- Malinowska, M., Palm, S., Gibson, K., Verbavatz, J., & Alberti, S. (2015). *Dictyostelium discoideum* has a highly Q/N-rich proteome and shows an unusual resilience to

protein aggregation. *PNAS*, 112(20), E2620-E2629.  
<https://doi.org/https://doi.org/10.1073/pnas>

- Maniak, M. (2003). Fusion and fission events in the endocytic pathway of *Dictyostelium*. *Traffic*, 4, 1-5.
- Marchal, S., Shehi, E., Harricane, M.-C., Fusi, P., Heitz, F., Tortora, P., & Lange, R. (2003). Structural Instability and Fibrillar Aggregation of Non-expanded Human Ataxin-3 Revealed under High Pressure and Temperature. 278(34), 31554-31563.  
<https://doi.org/10.1074/jbc.M304205200>
- Masino, L., Nicastro, G., Menon, R., Dal Piaz, F., Calder, L., & Pastore, A. (2004). Characterization of the Structure and the Amyloidogenic Properties of the Josephin Domain of the Polyglutamine-containing Protein Ataxin-3. *J Mol Biol*, 344(4), 1021-1035. <https://doi.org/10.1016/j.jmb.2004.09.065>
- Mayer, M., & Bukau, B. (2005). Hsp70 chaperones: cellular functions and molecular mechanism. *Cell Mol Life Sci*, 62(6), 670-684. <https://doi.org/10.1007/s00018-004-4464-6>
- McClellan, A., Tam, S., Kaganovich, D., & Frydman, J. (2005). Protein quality control: chaperones culling corrupt conformations. *Nat Cell Biol*, 7(8), 736-741.  
<https://doi.org/10.1038/ncb0805-736>
- McLean, C., Cherny, R., Fraser, F., Fuller, S., Smith, M., Vbeyreuther, K., Bush, A., & Masters, C. (2001). Soluble pool of A $\beta$  amyloid as a determinant of severity of neurodegeneration in Alzheimer's disease. *Annals of Neurology*, 46(6), 860-866.  
[https://doi.org/10.1002/1531-8249\(199912\)46:6<860::AID-ANA8>3.0.CO;2-M](https://doi.org/10.1002/1531-8249(199912)46:6<860::AID-ANA8>3.0.CO;2-M)
- McLoughlin, H., Moore, L., & Paulson, H. (2020). Pathogenesis of SCA3 and implications for other polyglutamine diseases. *Neurobiol Dis*, 134, 104635.  
<https://doi.org/10.1016/j.nbd.2019.104635>
- McMains, V., Myre, M., Kreppel, L., & Kimmel, A. (2010). Dictyostelium possesses highly diverged presenilin/g-secretase that regulates growth and cell-fate specification and can accurately process human APP: a system for functional studies of the presenilin/g-secretase complex. *Dis Model Mech*, 3, 581-594.  
<https://doi.org/10.1242/dmm.004457>
- Meisl, G., Kirkegaard, J., Arosio, P., Michaels, T., Vendruscolo, M., Dobson, C., Linse, S., & Knowles, T. (2016). Molecular mechanisms of protein aggregation from global

fitting of kinetic models. *Nat Protoc*, 11(2), 252-272.  
<https://doi.org/10.1038/nprot.2016.010>

Meulener, M., Whitworth, A., Armstrong-Gold, C., Rizzu, P., Heutink, P., Wes, P., Pallanck, L., & Bonini, N. (2005). *Drosophila* DJ-1 mutants are selectively sensitive to environmental toxins associated with Parkinson's disease. *Curr Biol*, 15, 1572-1577.

Miller-Fleming, L., Giorgini, F., & Outeiro, T. (2008). Yeast as a model for studying human neurodegenerative disorders. *Biotechnol J*, 3, 325-338.  
<https://doi.org/10.1002/biot.200700217>

Mirjalili, V., & Feig, M. (2013). Protein Structure Refinement through Structure Selection and Averaging from Molecular Dynamics Ensembles. *J. Chem. Theory Comput.*, 9(2), 1294-1303. <https://doi.org/10.1021/ct300962x>

Mogk, A., Bukau, B., & Kampinga, H. (2018). Cellular handling of protein aggregates by disaggregation machines. *Mol Cell*, 69, 214-226.  
<https://doi.org/10.1016/j.molcel.2018.01.004>

Mogk, A., Schlieker, C., Strub, C., Rist, W., Weibezahn, J., & Bukau, B. (2003). Roles of Individual Domains and Conserved Motifs of the AAA+ Chaperone ClpB in Oligomerization, ATP Hydrolysis, and Chaperone Activity. *JBC*, 278(20), 17615-17624. <https://doi.org/10.1074/jbc.M209686200>

Motohashi, K., Watanabe, Y., Yohda, M., & Yoshida, M. (1999). Heat-inactivated proteins are rescued by the DnaK·J·GrpE set and ClpB chaperones. *PNAS*, 96(13), 7184-7189. <https://doi.org/10.1073/pnas.96.13.7184>

Mucke, L. (2012). Neurotoxicity of amyloid b-protein: Synaptic and network dysfunction. *Cold Spring Harb Perspect Med*, 2(7).  
<https://doi.org/10.1101/cshperspect.a006338>

Muramoto, T., Iriki, H., Watanabe, J., & Kawata, T. (2019). Recent Advances in CRISPR/Cas9-Mediated Genome Editing in *Dictyostelium*. *Cells*, 8(46).  
<https://doi.org/10.3390/cells8010046>

Myre, M. (2012). Clues to g-secretase, huntingtin and Hirano body normal function using the model organism *Dictyostelium discoideum*. *J Biomed Sci*, 19.

- Myre, M., Lumsden, A., Thompson, M., Wasco, W., Macdonald, M., & Gusella, J. (2011). Deficiency of huntingtin has pleiotropic effects in the social amoeba *Dictyostelium discoideum*. *PLOS Genet*, 7.
- Narain, Y., Wyttenbach, A., Rankin, J., Furlong, R., & Rubinsztein, D. (1999). A molecular investigation of true dominance in Huntington's disease. *J Med Genet*, 36(10), 739-746. <https://doi.org/10.1136/jmg.36.10.739>
- Neddenriep, B., Calciano, A., Conti, D., Suave, E., Paterson, M., Bruno, E., & Moffet, D. (2011). Short Peptides as Inhibitors of Amyloid Aggregation. *Open Biotechnol J*, 5, 39-46. <https://doi.org/10.2174/1874070701105010039>
- Neuwald, A., Aravind, L., Spouge, J., & Koonin, E. (1999). AAA+: A class of chaperone-like ATPases associated with the assembly, operation, and disassembly of protein complexes. *Genome Res*, 9(1), 27-43. <https://doi.org/10.1101/gr.9.1.27>
- Nicholls, A., Sharp, K., & Honig, B. (1991). Protein Folding and Association: Insights From the Interfacial and Thermodynamic Properties of Hydrocarbons. *Proteins: Structure, Function, and Bioinformatics*, 11(4), 239-328. <https://doi.org/10.1002/prot.340110407>
- NINDS. (2017). Huntington's Disease: Hope through Research. *NIH Publication No. 17-NS-19*.
- Nivon, L., Moretti, R., & Baker, D. (2013). A Pareto-Optimal Refinement Method for Protein Design Scaffolds. *PLOS ONE*, 8(4). <https://doi.org/10.1371/journal.pone.0059004>
- O'Brien, R., & Wong, P. (2011). Amyloid Precursor Protein Processing and Alzheimer's Disease. *Annu Rev Biochem*, 34, 185-204. <https://doi.org/10.1146/annurev-neuro-061010-113613>
- Oguchi, Y., Kummer, E., Seyffer, F., Berynskyy, M., Anstett, B., Zahn, R., Wade, R., Mogk, A., & Bukau, B. (2012). A tightly regulated molecular toggle controls AAA+ disaggregase. *Nat Struct Mol Biol*, 19, 1338-1346. <https://doi.org/10.1038/nsmb.2441>
- Ogura, T., & Wilkinson, A. (2001). AAA+ superfamily ATPases: common structure-diverse function. *Genes to Cells*, 6(7), 575-652. <https://doi.org/10.1046/j.1365-2443.2001.00447.x>

- Ohta, E., Kubo, M., & Obata, F. (2010). Prevention of intracellular degradation of I2020T mutant LRRK2 restores its protectivity against apoptosis. *Biochem Biophys Res Commun*, 391, 242-247.
- Orner, B., Liu, L., Murphy, R., & Kiessling, L. (2006). Phage Display Affords Peptides that Modulate  $\beta$ -Amyloid Aggregation. *JACS*, 128, 11882-11889.  
<https://doi.org/10.1021/ja0619861>
- Ottolini, D., Cali, T., Negro, A., & Brini, M. (2013). The Parkinson disease-related protein DJ-1 counteracts mitochondrial impairment induced by the tumour suppressor protein p53 by enhancing endoplasmic reticulum-mitochondria tethering. *Hum Mol Genet*, 22, 2152-2168.
- Ovchinnikov, S., Kim, D., Wang, R., Liu, Y., DiMaio, F., & Baker, D. (2015). Improved de novo structure prediction in CASP11 by incorporating coevolution information into Rosetta. *Proteins: Structure, Function and Bioinformatics*, 84(S1), 67-75.  
<https://doi.org/10.1002/prot.24974>
- Ovchinnikov, S., Park, H., Kim, D., DiMaio, F., & Baker, D. (2018). Protein structure prediction using Rosetta in CASP12. *Proteins: Structure, Function and Bioinformatics*, 86, 113-121. <https://doi.org/10.1002/prot.25390>
- Pang, K., Lynes, M., & Knecht, D. (1999). Variables controlling the expression level of exogenous genes in *Dictyostelium*. *Plasmid*, 41, 187-197.  
<https://doi.org/10.1006/plas.1999.1391>
- Papadopoulos, J., & Agarwala, R. (2007). COBALT: constraint-based alignment tool for multiple protein sequences. *Bioinformatics*, 23(9), 1073-1079.  
<https://doi.org/10.1093/bioinformatics/btm076>
- Park, H., DiMaio, F., & Baker, D. (2016). CASP11 refinement experiments with ROSETTA. *Proteins*, 84, 314-322. <https://doi.org/10.1002/prot.24862>
- Park, J.-S., Davis, R., & Sue, C. (2018). Mitochondrial Dysfunction in Parkinson's Disease: New Mechanistic Insights and Therapeutic Perspectives. *Curr Neurol Neurosci Rep*, 18(5). <https://doi.org/10.1007/s11910-018-0829-3>
- Park, Y., Zhao, X., Yim, Y., Todor, H., Ellerbrock, R., Reidy, M., Eisenberg, E., Masison, D., & Greene, L. (2014). Hsp104 overexpression cures *Saccharomyces cerevisiae* [PSI<sup>+</sup>] by causing dissolution of the prion seeds. *Eukaryot Cell*, 13, 635-647.  
<https://doi.org/10.1128/EC.00300-13>

- Parsell, D., Kowal, A., Singer, M., & Lindquist, S. (1994). Protein disaggregation mediated by heat-shock protein Hsp104. *Nature*, 372(6505), 475-478.
- Paulson, H. (2007). Dominantly Inherited Ataxias: Lessons Learned from Machado-Joseph Disease/Spinocerebellar Ataxia Type 3. *Semin Neurol*, 27(2), 133-142. <https://doi.org/10.1055/s-2007-971172>
- Pearl, L. (2016). Review: The HSP90 molecular chaperone—an enigmatic ATPase. *Biopolymers*, 105(8), 594-607. <https://doi.org/10.1002/bip.22835>
- Pham, C., Kwan, A., & Sunde, M. (2014). Functional amyloid: widespread in Nature, diverse in purpose. *Essays Biochem*, 56, 207-219. <https://doi.org/10.1042/bse0560207>
- Picconi, B., Piccoli, G., & Calabresi, P. (2012). Synaptic Dysfunction in Parkinson's Disease. In M. Kreutz & C. Sala (Eds.), *Synaptic Plasticity. Adv Exp Med Biol* (Vol. 970, pp. 553-572). Springer. [https://doi.org/10.1007/978-3-7091-0932-8\\_24](https://doi.org/10.1007/978-3-7091-0932-8_24)
- Pierce, N., Lee, J., Liu, X., Sweredoski, M., Graham, R., Larimore, E., Rome, M., Zheng, N., Clurman, B., Hess, S., Shan, S., & Deshaies, R. (2013). Cand1 promotes assembly of new SCF complexes through dynamic exchange of F-box proteins. *Cell*, 153(1), 206-215. <https://doi.org/10.1016/j.cell.2013.02.024>
- Podrabsky, J., Carpenter, J., & Hand, S. (2001). Survival of water stress in annual fish embryos: dehydration avoidance and egg envelope amyloid fibers. *Am J Physiol Regulatory Integrative Comp Physiol*, 280, R123-R131.
- Poirier, M., Li, H., Macosko, J., Cai, S., Amzel, M., & Ross, C. (2002). Huntingtin Spheroids and Protofibrils as Precursors in Polyglutamine Fibrilization. *J Biol Chem*, 277(43), 41032-41037. <https://doi.org/10.1074/jbc.M205809200>
- Qi, J., & Ronai, Z. (2015). Dysregulation of ubiquitin ligases in cancer. *Drug Resist Updat*, 23, 1-11. <https://doi.org/10.1016/j.drup.2015.09.001>
- Queitsch, C., Hong, S.-W., Vierling, E., & Lindquist, S. (2000). Heat Shock Protein 101 Plays a Crucial Role in Thermotolerance in Arabidopsis. *Plant Cell*, 12(4), 479-492. <https://doi.org/10.1105/tpc.12.4.479>
- Radom, F., Plückthun, A., & Paci, E. (2018). Assessment of ab initio models of protein complexes by molecular dynamics. *PLOS Computational Biology*. <https://doi.org/10.1371/journal.pcbi.1006182>

- Ramsey, C., & Giasson, B. (2010). L10p and P158DEL DJ-1 mutations cause protein instability, aggregation, and dimerization impairments. *J Neurosci Res*, *88*, 3111-3124.
- Rao, F., Lin, H., & Su, Y. (2020). Cullin-RING ligase regulation by the COP9 signalosome: structural mechanisms and new physiologic players. *Adv Exp Med Biol*, *1217*, 47-60. [https://doi.org/10.1007/978-981-15-1025-0\\_4](https://doi.org/10.1007/978-981-15-1025-0_4)
- Reinke, A., Abulwerdi, G., & Gestwicki, J. (2011). Quantifying Prefibrillar Amyloids in vitro by Using a "Thioflavin-Like" Spectroscopic Method. *Chembiochem*, *11*(13), 1889-1895. <https://doi.org/10.1002/cbic.201000358>
- Rivero, F. (2008). Endocytosis and the actin cytoskeleton in *Dictyostelium discoideum*. *Int Rev Cell Mol Biol*, *267*, 343-397.
- Rockabrand, E., Slepko, N., Pantalone, A., Nukala, V., Kazantsev, A., Marsh, J., Sullivan, P., Steffan, J., Sensi, S., & Thompson, L. (2007). The first 17 amino acids of Huntingtin modulate its sub-cellular localization, aggregation and effects on calcium homeostasis. *Hum Mol Genet*, *16*(1), 61-77. <https://doi.org/10.1093/hmg/ddl440>
- Rosenbusch, K., Oun, A., Sanislav, O., Lay, S., Keizer-Gunnink, I., Annesley, S., Fisher, P., Dolga, A., & Kortholt, A. (2021). A Conserved Role for LRRK2 and Roco Proteins in the Regulation of Mitochondrial Activity. *Front Cell Dev Biol*, *9*. <https://doi.org/10.3389/fcell.2021.734554>
- Rosenzweig, R., Moradi, S., Zarrine-Afsar, A., Glover, J., & Kay, L. (2013). Unraveling the mechanism of protein disaggregation through a ClpB-DnaK interaction. *Science*, *339*, 1080-1083. <https://doi.org/10.1126/science.1233066>
- Ross, C., & Poirier, M. (2004). Protein aggregation and neurodegenerative diseases. *Nat Med*, *10*(Suppl 7), S10-S17. <https://doi.org/10.1038/nm1066>
- Ross, C., & Tabrizi, S. (2011). Huntington's disease: from molecular pathogenesis to clinical treatment. *The Lancet Neurology*, *10*(1), 83-98. [https://doi.org/10.1016/S1474-4422\(10\)70245-3](https://doi.org/10.1016/S1474-4422(10)70245-3)
- Rui, Q., Ni, H., Li, D., Gao, R., & Chen, G. (2018). The Role of LRRK2 in Neurodegeneration of Parkinson Disease. *Curr Neuropharm*, *16*, 1348-1357. <https://doi.org/10.2174/1570159X16666180222165418>

- Saibil, H. (2013). Chaperone machines for protein folding, unfolding and disaggregation. *Nat Rev Mol Cell Biol*, 14(10), 630-342. <https://doi.org/10.1038/nrm3658>
- Sajjad, M., Green, E., Miller-Fleming, L., Hands, S., Herrera, F., Campesan, S., Khoshnan, A., Outeiro, T., Giorgini, F., & Wyttenbach, A. (2014). DJ-1 modulates aggregation and pathogenesis in models of Huntington's disease. *Hum Mol Genet*, 23, 755-766.
- Sanchez, I., Mahlke, C., & Yuan, J. (2003). Pivotal role of oligomerization in expanded polyglutamine neurodegenerative disorders. *Nature*, 421, 373-379. <https://doi.org/10.1038/nature01301>
- Sanchez, Y., Taulien, J., Borkovich, K., & Lindquist, S. (1992). Hsp104 is required for tolerance to many forms of stress. *EMBO J*, 11(6), 2357-2364. <https://doi.org/10.1002/j.1460-2075.1992.tb05295.x>
- Santarriaga, S., Haver, H., Kanack, A., Fikejs, A., Sison, S., Egner, J., Bostrom, J., Seminary, E., Hill, R., Link, B., Ebert, A., & Scaglione, K. (2018). SRCP1 Conveys Resistance to Polyglutamine Aggregation. *Mol Cell*, 71, 216-228.
- Santarriaga, S., Petersen, A., Ndukwe, K., Brandt, A., Gerges, N., Scaglione, J., & Scaglione, K. (2015). The Social Amoeba *Dictyostelium discoideum* Is Highly Resistant to Polyglutamine Aggregation. *JBC*, 290(42), 25571-25578.
- Sato, T., Kienlen-Campard, P., Ahmed, M., Liu, W., Li, H., Elliott, J., Aimoto, S., Constantinescu, S., Octave, J.-N., & Smith, S. (2006). Inhibitors of Amyloid Toxicity Based on  $\beta$ -sheet Packing of A $\beta$ 40 and A $\beta$ 42. *Biochemistry*, 45, 5503-5516. <https://doi.org/10.1021/bi052485f>
- Saunders, H., Gilis, D., Rومان, M., Dehouck, Y., Robertson, A., & Bottomley, S. (2011). Flanking domain stability modulates the aggregation kinetics of a polyglutamine disease protein. *Protein Sci*, 20(10), 1675-1681. <https://doi.org/10.1002/pro.698>
- Scaglione, K., Zavodsky, E., Todi, S., Patury, S., Xu, P., Rodriguez-Lebron, E., Fischer, S., Konen, J., Djarmati, A., Peng, J., Gestwicki, J., & Paulson, H. (2011). Ube2w and Ataxin-3 Coordinately Regulate the Ubiquitin Ligase CHIP. *Mol Cell*, 43(4), 599-612. <https://doi.org/10.1016/j.molcel.2011.05.036>
- Scherzinger, E., Sittler, A., Schweiger, K., & Wanker, E. (1999). Self-assembly of polyglutamine-containing huntingtin fragments into amyloid-like fibrils: Implications for Huntington's disease pathology. *PNAS*, 96(8), 4604-4609. <https://doi.org/10.1073/pnas.96.8.4604>

- Schwechheimer, C., & Villalobos, L. (2004). Cullin-containing E3 ubiquitin ligases in plant development. *Curr Opin Plant Biol*, 7, 677-686.  
<https://doi.org/10.1016/j.molcel.2010.08.030>
- Sekine, R., Kawata, T., & Muramoto, T. (2018). CRISPR/Cas9 mediated targeting of multiple genes in *Dictyostelium*. *Sci Rep*, 8. <https://doi.org/10.1038/s41598-018-26756-z>
- Serrano, I., Campos, L., & Rivas, S. (2018). Roles of E3 ubiquitin-ligases in nuclear protein homeostasis during plant stress responses. *Front Plant Sci*, 9(139).  
<https://doi.org/10.3389/fpls.2018.00139>
- Seyffer, F., Kummer, E., Oguchi, Y., Kumar, M., Zahn, R., Sourjik, V., Bukau, B., & Mogk, A. (2012). Hsp70 proteins bind hsp100 regulatory M domains to activate AAA+ disaggregase at aggregate surfaces. *Nat Struct Mol Biol*, 19, 1347-1355.  
<https://doi.org/10.1038/nsmb.2442>
- Sheikh, M., Xu, Y., van der Wel, H., Walden, P., Hartson, S., & West, C. (2015). Glycosylation of Skp1 promotes formation of Skp1/Cullin-1/F-box protein complexes in *Dictyostelium*. *Mol Cell Proteomics*, 14, 66-80.  
<https://doi.org/10.1074/mcp.M114.044560>
- Shim, S.-H., Gupta, R., Ling, Y., Strasfeld, D., Raleigh, D., & Zanni, M. (2009). Two-dimensional IR spectroscopy and isotope labeling defines the pathway of amyloid formation with residue-specific resolution. *PNAS*, 106(16), 6614-6619.  
<https://doi.org/10.1073/pnas.0805957106>
- Shorter, J., & Lindquist, S. (2004). Hsp104 catalyzes formation and elimination of self-replicating Sup35 prion conformers. *Science*, 304, 1793-1797.  
<https://doi.org/10.1126/science.1098007>
- Shorter, J., & Lindquist, S. (2006). Destruction or potentiation of different prions catalyzed by similar Hsp104 remodeling activities. *Mol Cell*, 23, 425-438.  
<https://doi.org/10.1016/j.molcel.2006.05.042>
- Shorter, J., & Lindquist, S. (2008). Hsp104, Hsp70 and Hsp40 interplay regulates formation, growth and elimination of Sup35 prions. *EMBO J*, 27, 2712-2724.  
<https://doi.org/10.1038/emboj.2008.194>

- Shorter, J., & Southworth, D. (2019). Spiraling in Control: Structures and Mechanisms of the Hsp104 Disaggregase. *Cold Spring Harb Perspect Biol*, 11(8).  
<https://doi.org/10.1101/cshperspect.a034033>
- Simons, K., Ruczinski, I., Kooperberg, C., Fox, B., Bystroff, C., & Baker, D. (1999). Improved recognition of native-like protein structures using a combination of sequence. *Proteins*, 34(1), 82-95. [https://doi.org/10.1002/\(SICI\)1097-0134\(19990101\)34:1<82::AID-PROT7>3.0.CO;2-A](https://doi.org/10.1002/(SICI)1097-0134(19990101)34:1<82::AID-PROT7>3.0.CO;2-A)
- Sinnige, T., Yu, A., & Morimoto, R. (2020). Challenging Proteostasis: Role of the Chaperone Network to Control Aggregation-Prone Proteins in Human Disease. In M. Mendillo, D. Pincus, & R. Scherz-Shouval (Eds.), *HSF1 and Molecular Chaperones in Biology and Cancer* (Vol. 1243, pp. 53-68). Springer, Cham.  
[https://doi.org/10.1007/978-3-030-40204-4\\_4](https://doi.org/10.1007/978-3-030-40204-4_4)
- Slanzi, A., Iannoto, G., Rossi, B., Zenaro, E., & Constantin, G. (2020). *In vitro* Models of Neurodegenerative Diseases. *Front Cell Dev Biol*, 8.  
<https://doi.org/10.3389/fcell.2020.00328>
- Smith, N., & Wilson, M. (2017). Structural Biology of the DJ-1 Superfamily. *Adv Exp Med Biol*, 1037, 5-24.
- Squires, C., Pedersen, S., Ross, B., & Squires, C. (1991). ClpB is the Escherichia coli heat shock protein F84.1. *J Bacteriol*, 173(14), 4254-4262.  
<https://doi.org/10.1128/jb.173.14.4254-4262.1991>
- Stefanis, L. (2012). Alpha-Synuclein in Parkinson's disease. *Cold Spring Harb Perspect Med*, 2. <https://doi.org/10.1101/cshperspect.a009399>
- Struhl, G., & Greenwald, I. (1999). Presenilin is required for activity and nuclear access of Notch in *Drosophila*. *Nature*, 398, 522-525.
- Sun, Y., & MacRae, T. (2005). Small heat shock proteins: molecular structure and chaperone function. *Cell Mol Life Sci*, 62(21), 2460-2476.  
<https://doi.org/10.1007/s00018-005-5190-4>
- Sunde, M., Serpell, L., Fraser, P., Pepys, M., & Blake, C. (1997). Common core structure of amyloid fibrils by synchrotron X-ray diffraction. *J Mol Biol*, 273(3), 729-739.  
<https://doi.org/10.1006/jmbi.1997.1348>
- Surcel, A., Kee, Y., Luo, T., & Robinson, D. (2010). Cytokinesis through biochemical-mechanical feedback loops. *Semin Cell Dev Biol*, 21, 866-873.

- Suresh, S., Verma, V., Sateesh, S., Clement, J., & Manjithaya, R. (2018). Neurodegenerative diseases: model organisms, pathology and autophagy. *J Genet*, 97(3), 679-701. <https://doi.org/10.1007/s12041-018-0955-3>
- Swaney, K., Huang, C., & Devreotes, P. (2010). Eukaryotic chemotaxis: a network of signaling pathways controls motility, directional sensing, and polarity. *Annu Rev Biophys*, 39, 265-289.
- Sweeny, E., & Shorter, J. (2016). Mechanistic and Structural Insights into the Prion-Disaggregase Activity of Hsp104. *J Mol Biol*, 428, 1870-1885. <https://doi.org/10.1016/j.jmb.2015.11.016>
- Taira, T., Saito, Y., Iki, T., Iguchi-Ariga, S., Takahashi, K., & Ariga, H. (2004). DJ-1 has a role in antioxidative stress to prevent cell death. *EMBO Rep*, 5, 213-218.
- Tam, S., Spiess, C., Auyeung, W., Joachimiak, L., Chen, B., Poirier, M., & Frydman, J. (2009). The Chaperonin TRiC Blocks a Huntingtin Sequence Element that Promotes the Conformational Switch to Aggregation. *Nat Struct Mol Biol*, 16(12), 1279-1285. <https://doi.org/10.1038/nsmb.1700>
- Tanaka, K., & Matsuda, N. (2014). Proteostasis and neurodegeneration: The roles of proteasomal degradation and autophagy. *Biochim Biophys Acta*, 1843(1), 197-204. <https://doi.org/10.1016/j.bbamcr.2013.03.012>
- Tariq, A., Lin, J., Noll, M., Torrente, M., Mack, K., Murillo, O., Jackrel, M., & Shorter, J. (2018). Potentiating Hsp104 activity via phosphomimetic mutations in the middle domain. *FEMS Yeast Res*, 18. <https://doi.org/10.1093/femsyr/foy042>
- Taylor, R., & Benjamin, I. (2005). Small heat shock proteins: a new classification scheme in mammals. *J Mol Cell Cardiol*, 38(3), 433-444. <https://doi.org/10.1016/j.yjmcc.2004.12.014>
- Team, R. C. (2016). *R: A Language and Environment for Statistical Computing*. In R Foundation for Statistical Computing. <https://www.R-project.org/>
- Terry, R., Masliah, E., Salmon, D., Butters, N., DeTeresa, R., Hill, R., Hansen, L., & Katzman, R. (1991). Physical basis of cognitive alterations in Alzheimer's disease: Synapse loss is the major correlate of cognitive impairment. *Annals of Neurology*, 30(4), 572-580. <https://doi.org/10.1002/ana.410300410>
- Thakur, A., Jayaraman, M., Mishra, R., Thakur, M., Chellgren, V., Byeon, I.-J., Anjum, D., Kodali, R., Creamer, T., Conway, J., Gronenborn, A., & Wetzel, R. (2009).

- Polyglutamine disruption of the huntingtin exon 1 N terminus triggers a complex aggregation mechanism. *Nat Struct Mol Biol*, 16(4), 380-389.  
<https://doi.org/10.1038/nsmb.1570>
- Totzeck, F., Andrade-Navarro, M., & Mier, P. (2017). The Protein Structure Context of PolyQ Regions. *PLoS ONE*, 12(1). <https://doi.org/10.1371/journal.pone.0170801>
- Tsigelny, I., Crews, L., Desplats, P., Shaked, G., Sharikov, Y., Mizuno, H., Spencer, B., Rockenstein, E., Trejo, M., Platoshyn, O., Yuan, J.-J., & Masliah, E. (2008). Mechanisms of Hybrid Oligomer Formation in the Pathogenesis of Combined Alzheimer's and Parkinson's Diseases. *PLoS ONE*, 3.  
<https://doi.org/10.1371/journal.pone.0003135>
- van Ham, T., Breitling, R., Swertz, M., & Nollen, E. (2009). Neurodegenerative diseases: Lessons from genome-wide screens in small model organisms. *EMBO Mol Med*, 1, 360-370. <https://doi.org/10.1002/emmm.200900051>
- Varadi, M., Anyango, S., Deshpande, M., Nair, S., Natassia, C., Yordanova, G., Yuan, D., Stroe, O., Wood, G., Laydon, A., Zidek, A., Green, T., Tunyasuvunakool, K., Petersen, S., Jumper, J., Clancy, E., Green, R., Vora, A., Lutfi, M., . . . Velankar, S. (2021). AlphaFold Protein Structure Database: massively expanding the structural coverage of protein-sequence space with high-accuracy models. *Nucleic Acids Res*, 50(D1), D439-444. <https://doi.org/10.1093/nar/gkab1061>
- Vicente, J., Galardi-Castilla, M., Escalante, R., & Sastre, L. (2008). Structural and functional studies of a family of Dictyostelium discoideum developmentally regulated, prestalk genes coding for small proteins. *BMC Microbiol*, 8.  
<https://doi.org/10.1186/1471-2180-8-1>
- Vines, J., & King, J. (2019). The endocytic pathways of Dictyostelium discoideum. *Int J Dev Biol*, 63, 461-471. <https://doi.org/10.1387/ijdb.190236jk>
- Vodermaier, H. (2004). APC/C and SCF: controlling each other and the cell cycle. *Curr Biol*, 14, R787-R796. <https://doi.org/10.1016/j.cub.2004.09.020>
- Voisine, C., Pedersen, J., & Morimoto, R. (2010). Chaperone networks: Tipping the balance in protein folding diseases. *Neurobiol Dis*, 40(1), 12-20.  
<https://doi.org/10.1016/j.nbd.2010.05.007>
- Volles, M., Lee, S.-J., Rochet, J.-C., Shtilerman, M., Ding, T., Kessler, J., & Lansbury, P. (2001). Vesicle Permeabilization by Protofibrillar  $\alpha$ -Synuclein: Implications for

- the Pathogenesis and Treatment of Parkinson's Disease. *Biochemistry*, 40(26), 7812-7819. <https://doi.org/10.1021/bi0102398>
- von Bergen, M., Friedhoff, P., Biernat, J., & Mandelkow, E. (2000). Assembly of  $\tau$  protein into Alzheimer paired helical filaments depends on a local sequence motif (<sup>306</sup>VQIVYK<sup>311</sup>) forming  $\beta$  structure. *PNAS*, 97(10), 5129-5134. <https://doi.org/10.1073/pnas.97.10.5129>
- Wagenfeld, A., Yeung, C., Strupat, K., & Cooper, T. (1998). Shedding of a rat epididymal sperm protein associated with infertility induced by ornidazole and alpha-chlorohydrin. *Biol Reprod*, 58, 1257-1265.
- Wagner, A., Politi, A., Ast, M., Bravo-Rodriguez, K., Baum, K., Buntru, A., Stempel, N., Brusendorf, L., Hanig, C., Boeddrich, A., Plassmann, S., Klockmeier, K., Ramirez-Anguita, J., Sanchez-Garcia, E., Wolf, J., & Wanker, E. (2018). Self-assembly of Mutant Huntingtin Exon-1 Fragments into Large Complex Fibrillar Structures Involves Nucleated Branching. *J Mol Biol*, 430(12), 1725-1744. <https://doi.org/10.1016/j.jmb.2018.03.017>
- Walsh, D., Klyubin, I., Fadeeva, J., Cullen, W., Anwyl, R., Wolfe, M., Rowan, M., & Selkoe, D. (2002). Naturally secreted oligomers of amyloid  $\beta$  protein potently inhibit hippocampal long-term potentiation in vivo. *Nature*, 416, 535-539. <https://doi.org/10.1038/416535a>
- Wang, Y., Steimle, P., Ren, Y., Ross, C., Robinson, D., Egelhoff, T., Sesaki, H., & Iijima, M. (2011). *Dictyostelium* huntingtin controls chemotaxis and cytokinesis through the regulation of myosin II phosphorylation. *Mol Biol Cell*, 22, 2270-2281.
- Wang, Z., Zhang, Y., Zhang, S., Guo, Q., Tan, Y., Wang, X., Xiong, R., Ding, J., & Chen, S. (2011). DJ-1 can inhibit microtubule associated protein 1 B formed aggregates. *Mol Neurodegener*, 6.
- Wanker, E., Scherzinger, E., Heiser, V., Sittler, A., Eickhoff, H., & Lehrach, H. (1999). Membrane filter assay for detection of amyloid-like polyglutamine-containing protein aggregates. In R. Wetzel (Ed.), *Methods in Enzymology* (Vol. 309, pp. 375-386). Academic Press. [https://doi.org/10.1016/S0076-6879\(99\)09026-6](https://doi.org/10.1016/S0076-6879(99)09026-6)
- Wetzel, R. (1994). Mutations and off-pathway aggregation of proteins. *Trends Biotechnol*, 12(5), 193-198. [https://doi.org/10.1016/0167-7799\(94\)90082-5](https://doi.org/10.1016/0167-7799(94)90082-5)
- Wickham, H. (2016). *scales: Scale Functions for Visualization*. In <https://cran.r-project.org/web/packages/scales/index.html>.

- Wickham, H. (2017). *tidyverse: Easily Install and Load "Tidyverse" Packages*. In (Version R package version 111)
- Willems, A., Schwab, M., & Tyer, M. (2004). A hitchhiker's guide to the cullin ubiquitin ligases: SCF and its kin. *Biochim Biophys Acta*, *16955*, 133-170. <https://doi.org/10.1016/j.bbamcr.2004.09.027>
- Williams, A., & Paulson, H. (2008). Polyglutamine neurodegeneration: protein misfolding revisited. *Trends Neurosci*, *31*(10), 521-528. <https://doi.org/10.1016/j.tins.2008.07.004>
- Williams, J. (2006). Transcriptional regulation of *Dictyostelium* pattern formation. *EMBO Rep*, *7*, 694-698.
- Wilson, M. (2011). The role of cysteine oxidation in DJ-1 function and dysfunction. *Antioxid Redox Signal*, *15*, 111-122.
- Wilson, M., Collins, J., Hod, Y., Ringe, D., & Petsko, G. (2003). The 1.1-Å resolution crystal structure of DJ-1, the protein mutated in autosomal recessive early onset Parkinson's disease. *PNAS*, *100*, 9256-9261.
- Winner, B., Jappelli, R., Maji, S., Desplats, P., Boyer, L., Aigner, S., Hetzer, C., Loher, T., Vilar, M., Campioni, S., Tzitzilonis, C., Soragni, A., Jessberger, S., Mira, H., Consiglio, A., Pham, E., Masliah, E., Gage, F., & Riek, R. (2011). In vivo demonstration that alpha-synuclein oligomers are toxic. *PNAS*, *108*(10), 4194-4199. <https://doi.org/10.1073/pnas.1100976108>
- Wolfe, M., Xia, W., Ostaszewski, B., Diehl, T., Kimberly, W., & Selkoe, D. (1999b). Two transmembrane aspartates in presenilin-1 required for presenilin endoproteolysis and g-secretase activity. *Nature*, *398*, 513-517.
- Xie, J., Jin, Y., & Wang, G. (2019). The role of SCF ubiquitin-ligase complex at the beginning of life. *Reprod Biol Endocrinol*, *17*. <https://doi.org/10.1186/s12958-019-0547-y>
- Yamin, G., Ruchala, P., & Teplow, D. (2009). A Peptide Hairpin Inhibitor of Amyloid  $\beta$ -Protein Oligomerization and Fibrillogenesis. *Biochemistry*, *48*, 11329-11331. <https://doi.org/10.1021/bi901325g>
- Yoo, H., Bard, J., Pilipenko, E., & Drummond, D. (2022). Chaperones directly and efficiently disperse stress-triggered biomolecular condensates. *Mol Cell*, *82*(4), 741-755.e711. <https://doi.org/10.1016/j.molcel.2022.01.005>

- Yu, A., Fox, S., Cavallini, A., Kerridge, C., O'Neill, M., Wolak, J., Bose, S., & Morimoto, R. (2019). Tau protein aggregates inhibit the protein-folding and vesicular trafficking arms of the cellular proteostasis network. *J Biol Chem*, 294(19), 7917-7930. <https://doi.org/10.1074/jbc.RA119.007527>
- Zhao, X., Rodriguez, R., Silberman, R., Ahearn, J., Saidha, S., Cummins, K., Eisenberg, E., & Greene, L. (2017). Heat shock protein 104 (Hsp104)-mediated curing of [PSI<sup>+</sup>] yeast prions depends on both [PSI<sup>+</sup>] conformation and the properties of the Hsp104 homologs. *J Biol Chem*, 292, 8630-8641. <https://doi.org/10.1074/jbc.M116.770719>
- Zheng, J., Yang, X., Harrell, J., Ryzhikov, S., Shim, E., Lykke-Andersen, K., Wei, N., Sun, H., Kobayashi, R., & Zhang, H. (2002). CAND1 Binds to Unneddylated CUL1 and Regulates the Formation of SCF Ubiquitin E3 Ligase Complex. *Mol Cell*, 10(6), 1519-1526. [https://doi.org/10.1016/s1097-2765\(02\)00784-0](https://doi.org/10.1016/s1097-2765(02)00784-0)
- Zheng, N., Schulman, B., Song, L., Miller, J., Jeffrey, P., Wang, P., Chu, C., Koepf, D., Elledge, S., Pagano, M., Conaway, R., Conaway, J., Harper, J., & Pavletich, N. (2002). Structure of the Cul1-Rbx1-Skp1-Fbx<sup>Skp2</sup> SCF ubiquitin ligase complex. *Nature*, 416, 703-709. <https://doi.org/10.1038/416703a>
- Zimmerman, E., Schulman, B., & Zheng, N. (2010). Structural assembly of cullin-RING ubiquitin ligase complexes. *Curr Opin Struct Biol*, 20, 714-721. <https://doi.org/10.1016/j.sbi.2010.08.010>
- Zolkiewski, M. (1999). ClpB cooperates with DnaK, DnaJ, and GrpE in suppressing protein aggregation. A novel multi-chaperone system from Escherichia coli. *J Biol Chem*, 274(40), 28083-28086. <https://doi.org/10.1074/jbc.274.40.28083>
- Zolkiewski, M., Zhang, T., & Nagy, M. (2012). Aggregate reactivation mediated by the Hsp100 chaperones. *Arch Biochem Biophys*, 520(1), 1-6. <https://doi.org/10.1016/j.abb.2012.01.012>
- Zondler, L., Miller-Fleming, L., Repici, M., Gonçalves, S., Tenreiro, S., Rosado-Ramos, R., Betzer, C., Straatman, K. J., HP, Giorgini, F., & Outeiro, T. (2014). DJ-1 interactions with alpha-synuclein attenuate aggregation and cellular toxicity in models of Parkinson's disease. *Cell Death Dis*, 5.

## Biography

Holly earned her Bachelor of Science degree in Chemistry with a Biochemistry concentration from St. Norbert College in May 2016. In August 2016 she began graduate school at the Medical College of Wisconsin and joined Dr. Matt Scaglione's laboratory in May 2017. Holly transferred into Duke University's Molecular Genetics and Microbiology graduate program when Dr. Scaglione accepted a faculty position. Since starting graduate school, she has contributed as an author to the following publications: "SRCP1 Conveys Resistance to Polyglutamine Aggregation" (2018); "UbcH5 Interacts with Substrates to Participate in Lysine Selection with the E3 Ubiquitin Ligase CHIP" (2020); "*Dictyostelium discoideum* as a Model for Investigating Neurodegenerative Diseases" (2021); "Mechanistic insight into the suppression of polyglutamine aggregation by SRCP1" (2023).